The Pennsylvania State University

The Graduate School

STRUCTURE-FUNCTION CHANGES IN LATE STAGES OF TENDON DEVELOPMENT AND ITS SENSITIVITY TO MUSCULOSKELETAL ACTIVITY

A Dissertation in

Bioengineering

by

Benjamin E. Peterson

Submitted in Partial Fulfillment of
the Requirements
for the Degree of

Doctor of Philosophy

December 2022

The dissertation of Benjamin E. Peterson was reviewed and approved by the following:

Spencer E. Szczesny
Assistant Professor of Biomedical Engineering
Dissertation Advisor
Chair of Committee

Esther Gomez
Associate Professor of Chemical Engineering & Biomedical Engineering

Gregory Lewis
Associate Professor of Orthopaedics and Rehabilitation

Claire Thomas
Associate Professor of Biology and Biochemistry and Molecular Biology

Paula Murphy
Special Member
Professor in Developmental Biology
University of Dublin, Trinity College Dublin

Daniel Hayes
Department Head – Biomedical Engineering
Dorothy Foehr Huck and J. Lloyd Huck Chair in
Nanotherapeutics and Regenerative Medicine

Abstract

Tendons are essential connective tissues that transmit forces between muscle and bone, ultimately enabling locomotion. These load-bearing capabilities are initially acquired during embryonic and neonatal stages of development as the tissue undergoes the coordinated synthesis and deposition of collagen. While significant progress has been made over the last three decades to unravel this process, there are still several critical questions that remain unanswered. More specifically, during lates stages of chick development there is a near-spontaneous transformation in the load bearing capabilities of embryonic tendons. Prior work has suggested that this transformation is mediated by changes in collagen fibril lengths in vivo. Despite this, no study has directly investigated how changes in the collagenous ultrastructure facilitate this transformation in mechanical capabilities. Prior work has further suggested that this transformation may be mediated via musculoskeletal activity during development. Indeed, while muscle activity has been correlated with gross changes in tendon mass, it's still unclear how musculoskeletal stimulation drives this transformation in load-bearing capabilities during development. Addressing these unresolved questions is essential to elucidating the biological mechanisms that govern the development of functional loading-bearings.

As such, the primary objective of this dissertation is to investigate the multiscale mechanical microenvironment during standard physiological development, determine the gross role of musculoskeletal activity, and probe the structural elements that enable the functional load-bearing capabilities of tendon during late stages of development. Initial work was conducted in mature rat tail tendons to establish the relationship between fibril continuity and multiscale mechanical behavior. We demonstrated that we could increase interfibrillar loading behavior by artificially inducing fibril continuity, establishing that the multiscale strain behavior can be utilized to indirectly evaluate changes in relative collagen fibril lengths in developmental systems. Utilizing these techniques in chick embryos, we observed that an increase in the macroscale modulus with development is accompanied by than an increase in the interfibrillar loading, consistent with an increase in collagen fibril lengths. Suggesting that collagen fibril fusion (i.e., lengthening) drives the

transformation in developing tendons. Ensuing studies leveraged paralysis agents to probe the role of muscle activity in mediating this developmental response. After immobilization, there was a decrease in macroscale modulus and interfibrillar loading capabilities, suggesting that the transformation in tendon's load-bearing capabilities is mediated by mechanobiological activity. However, recent work has suggested that crosslinking may contribute to the maturation in the structure-function behavior during tendon development and be dependent on musculoskeletal activity. Thus, subsequent work leveraged a crosslinking inhibitor to investigate the role of intermolecular crosslinks in tendon development. Interestingly, the absence of crosslinks significantly impaired the macroscale and multiscale loading capabilities of the embryonic tissue, highlighting the importance of crosslinks in tendon development. However, thermodynamic and solubility behavior suggested that immobilized tissue had minimal changes in the relative crosslinking, indicating that paralysis is dominantly impairing fibril fusion (i.e., fibril lengthening) events in vivo.

To validate these findings, subsequent work aimed to use serial-block face microscopy to track three-dimensional changes within the collagenous ultrastructure. To overcome preexisting limitations in the field, we leveraged deep learning neural networks for the automatic segmentation of collagen fibrils with over 95% accuracy. Two-dimensional characterization showed a progressive increase in collagen fibril lengths with development, further suggesting that fibril fusion behavior is mediating changes in loading capabilities. Current attempts at automated tracking of fibrils in three-dimensional space have proved difficult and on-going work aims to address current pitfalls. While still in-progress, this is one of the few studies that has successfully leveraged deep learning strategies to study changes within the collagenous ultrastructure.

Collectively, these data suggest that fibril fusion behavior enables the functional transformation in load-bearing capabilities during late stages of tendon development and is mediated by mechanobiological activity. This information provides valuable insight into the multiscale structure-function relationships of developing tendon and the biological mechanisms required to produce robust load-bearing tendon.

Table of Contents

List of Tables

List of Figures

List of Abbreviations:

5-DTAF - Dichlorotriazinylaminofluorescein

AGEs - Advanced glycation end-productions

BAPN - β-aminopropionitrile

COL – Collagen

deH-HLNL - Dehydro-hydroxylysine-norleucine

deH-LNL - Dehydro-lysinonorleucine

DMB - Decamethonium bromide

ECM – Extracellular Matrix

EDS - Ehlers-Danlos syndrome

EGF - Epidermal growth factor

GAGs – Glycosaminoglycans

GL – Gauge Length

GPCs - Golgi-to-Plasma membrane carriers

HBSS- Hank's Balanced Salt Solution

HLKNL - Hydroxylysino-ketonorleucine

LKNL - Lysino-ketonorleucine

LOX - Lysyl-Oxidase

LOXL - Lysyl-Oxidase Like

LP-Pyr / HP - Hydroxylysl-pyridinoline

L-Pyr / LP - Lysyl-pyridinoline

PB - Pancuronium bromide

PBLs – Photo Bleached Lines

PBS – Phosphate-Buffered Saline

SBF-SEM - Serial-Block Face Scanning-Electron Microscopy

SCX - Scleraxis

SLRP – Small Leucine-Rich Proteoglycans

TGF-β – Transforming growth factor beta

UTS - Ultimate Tensile Strength

Acknowledgements

While everyone's Ph.D. experience is different, I think it's safe to say that the events of the Covid-19 pandemic have made the current generation of Ph.D. students' experiences *unique*. While the pandemic was cause for concern and anxiety for many, it wasn't without its silver lining. Through these additional trials and tribulations, many of my greatest friendships were formed and helped me become a more emphatic, compassionate person. There has also been a multitude of people that have been a constant source of mentorship, support, and inspiration over the last couple of years that played a key role in helping me get across the finish line.

First and foremost, I'd like to thank my advisor, Dr. Spencer Szczesny. You have been an amazing mentor (and borderline therapist) that took a risk on me early during my PhD. You've put up with a lot of my blunders over the years and I'll always feel indebted for the opportunity to work under your mentorship. Your patience, guidance, and commitment to your students have been instrumental in my decision to pursue a career in academia. Similarly, I'd like to thank Dr. Claire Thomas for all her advice and for letting me be a fly on the wall (pun intended) in your lab meetings. It's given me the opportunity to continuously learn new skills and explore new avenues of research.

Of course, I'd also like to thank everyone in the Szczesny Lab; Krishna, Lauren, Maria, and Maggs. Y'all have put up with an astounding amount of my sass over the last couple of years. You've been instrumental to my academic success and helping me maintain my sanity during some of those exceedingly long days in the lab. I'm so excited to see where your work takes you and have full confidence in everyone's future success.

It goes without saying that the love and support of my family has been a large motivator in my pursuit of science. Mom & Dad, you've both worked hard to give me all the tools to my success and, perhaps most importantly, you gave me the space to fail, learn, and find my own path. I'll always be extremely thankful and grateful for the opportunities that you've been able to provide me. The same for my amazing siblings (and new sister-in-law!), Sam, Rachel, and Colleen. Your persistent cheerleading has not gone unnoticed and been a constant source of motivation and strength.

Next, I want to make sure I take this opportunity to thank all my friends who've played such a pivotal role in shaping me as a person. From back in North Carolina; Rob, Eleanor, Alex, Sydney, Coleman, Addison, Coleman, Lea, and Claire. You all have been life-long friends, a constant source of support and inspiration, and helped me so much in making the decision to leave NC to chase new opportunities.

To everyone here at State College, there are almost too many of you to count, but I refuse to leave anyone out. In no particular order, Joe, Josh, Scott, Sailahari, Krishna, Haider, Lauren (Randolph & Paschall), Maria, Maggs, Gabbi, Elizabeth, Michael, Katie, Michael, Farnaz, Caroline, Janna, Sean, Alex, Brian, Connor, Stef, Andy, Leo, Alana, Brandon, Alyssa, Caleb, Logan, Andy, Kevin, Dotts, Wes, Judit, Sajid…plus anyone I may be blanking on at this very moment. I think it goes without saying that a PhD can be a stressful endeavor, and I really have no idea what I would have done without you all. I also want to give a plug to Voodoo Brewing for providing a rally point for our group and giving us space to kick back after long days in the lab.

Finally, I want to give one final shout out to Josh & Scott. You both have become some of my best friends, and I don't think I could have gotten through the Covid-19 lockdown without y'all. We've developed so many inside jokes that it's practically a second language. I have full confidence we're stay life-long friends and I'm excited to see what opportunities await us.

Funding Statement:

The material presented in this dissertation was supported by the National Institutes of Health (R21 AR075941) and the National Science Foundation (NSF2127527). The opinions, findings, and conclusions expressed in this dissertation are those of the author and do not necessarily reflect the views of the awarding agencies.

Chapter 1: Introduction & Background

1.1 Introduction

Tendon is a highly collagenous connective tissue that facilitates the transmission of force between muscles and bone, ultimately enabling locomotion. Upon injury, their characteristic high load-bearing capabilities are compromised and can coincide with weakness, pain, and a reduction in motility [1–3]. The resulting loss in quality of life is further exacerbated by tendons poor innate healing capacity. Clinical interventions vary depending on the degree of injury but show limited efficacy and present a high likelihood of future re-rupture [4]. These concerns have motivated the rise of tissue engineering and regenerative medicine strategies to augment/replace damaged or diseased tendons. However, the dynamic variables required to recapitulate the formation of functional tendon tissue are not fully understood and represents a critical gap in knowledge.

To this end, developmental systems have emerged as an invaluable resource to gain insight into the conditions required for functional tendon formation. Over the last three decades, substantial progress has been made in outlining the process of fibrillogenesis [5–13], which describes the multi-stage events of collagen synthesis, deposition, and self-assembly. Despite this progress, it is unclear how the progressive maturation of the collagenous extracellular matrix (ECM) dynamically alters the mechanical microenvironment within developing tendons. Tendon fibroblasts (tenocytes) are highly sensitive to external mechanical cues [14–17], suggesting that tendon development is heavily influenced by changes in the structure-function behavior within the maturing system. Nevertheless, there is a severe lack of understanding concerning

the multiscale mechanical environment of tendons during development. Establishing these fundamental structure-function relationships throughout tenogenesis is essential to elucidate the biological mechanisms which govern the formation of load-bearing tendons.

Prior work has shown that mechanical stimulation, generated by skeletal elongation and muscle contractions, may play a pivotal role in tendon formation [11, 18–20]. While musculoskeletal paralysis has shown to play a key role in the mediation of skeletogenesis and joint formation during development [21–24], it's contributions to tenogenesis is less clear. Intracellular myosin contractility has been shown to be critical in early stages of tendon development, enabling force transfer between neighboring cells via adherens junctions [11]. During later stages of maturation, muscle activity has been shown to be correlated to changes within tendon size [25]. Furthermore, embryonic motility rapidly increased in the periods preceding significant shifts in tendon macroscale mechanical capabilities, further suggesting that muscle activity plays a pivotal role in tenogenesis [18]. Despite these insights, it's unclear how external mechanical stimulation elicits mechanobiological signaling behavior within the developing system. Additionally, as a more robust organized extracellular matrix is established, it's unclear how alterations of the loading path through the tissue may result in divergent mechanobiological signaling activity. Investigating how musculoskeletal activity influences tenogenesis is a critical first step to establishing the role of mechanobiological activity in the formation of load-bearing tissue.

The objectives of this work are to investigate the multiscale mechanical microenvironment during standard physiological development, determine the gross role of musculoskeletal activity, and probe the specific structural elements that enable the

functional load-bearing capabilities of tendon during late stages of development. In this dissertation, I will outline the multiscale mechanical testing, developmental animal models, treatment regimes, and ultrastructural characterization utilized to accomplish these primary objectives.

In Chapter 2, I will establish the testing criteria for multiscale mechanical testing of small tissues. In which, I'll discuss how gauge length affects the multiscale mechanical behavior in mature tendons, establishing protocols for future embryonic tendon mechanical testing. In Chapter 3, I will discuss our work characterizing the multiscale mechanical behavior during late stages of tendon development and its implications on structure-function relationships in tenogenesis. Chapter 3 will continue to explore the role of muscle activity in development, utilizing paralysis agents to investigate how muscle stimulation drives functional transformations in late stages of tendon development. In Chapter 4, I will investigate how collagenous crosslinking contributes to the development of tendons multiscale mechanical behavior and its sensitivity to muscle activity. In chapter 5, I will discuss ongoing work to directly investigate changes within the collagenous ultrastructure utilizing advanced microscopy and deep learning tools. Finally, in Chapter 6, I will summarize the conclusion of my work and outline future directions.

Here, I aim to provide background on the field's current knowledge regarding the process of tenogenesis, with a particular focus on the known structural and mechanical changes that occur during development. However, an understanding of the fundamental structure-function relationships of mature tendons is first essential to gain a contextual understanding of the critical elements established during tenogenesis and their role in healthy tendons.

1.2 Mature Tendon Structure & Function

1.2.1 Tendon Structure & Composition

Tendon is composed of hierarchically organized collagen type I that is dominantly oriented along the longitudinal axis of the tissue (**Fig. 1.1**) [10, 26]. At the base of this structural hierarchy are individual collagen molecules (tropocollagen), composed of a ~300 nm long triple helix made of two α1 and one α1 peptide chains [26, 27]. At the ends of the helical tropocollagen are a loose assembly of amino-acid chains, called telopeptides, which contribute to local self-assembly behavior and the formation of intermolecular enzymatic/non-enzymatic crosslinks [28]. Tropocollagen molecules laterally self-assemble in a staggered quarter-overlap confirmation creating individual collagen fibrils [27, 29]. These fibrils then pack together into bundles to create fibers, which take on a crimp morphology preferentially oriented along the dominate axis of the tissue [30]. Fibers subsequently assemble into fascicles, containing dispersed populations of tendon fibroblasts (tenocytes) and tendon progenitor stem cells [17]. These tenocytes are organized in longitudinal columns with protruding cellular processes that surround fiber bundles and establish cell-cell contacts with adjacent columns of cells [10, 11]. Finally, fascicles bundle together to form the bulk tendon, where individual fascicles are separated by a connective tissue called the endotenon, which contains blood vessels to supply the necessary oxygen and nutrients [10, 31].

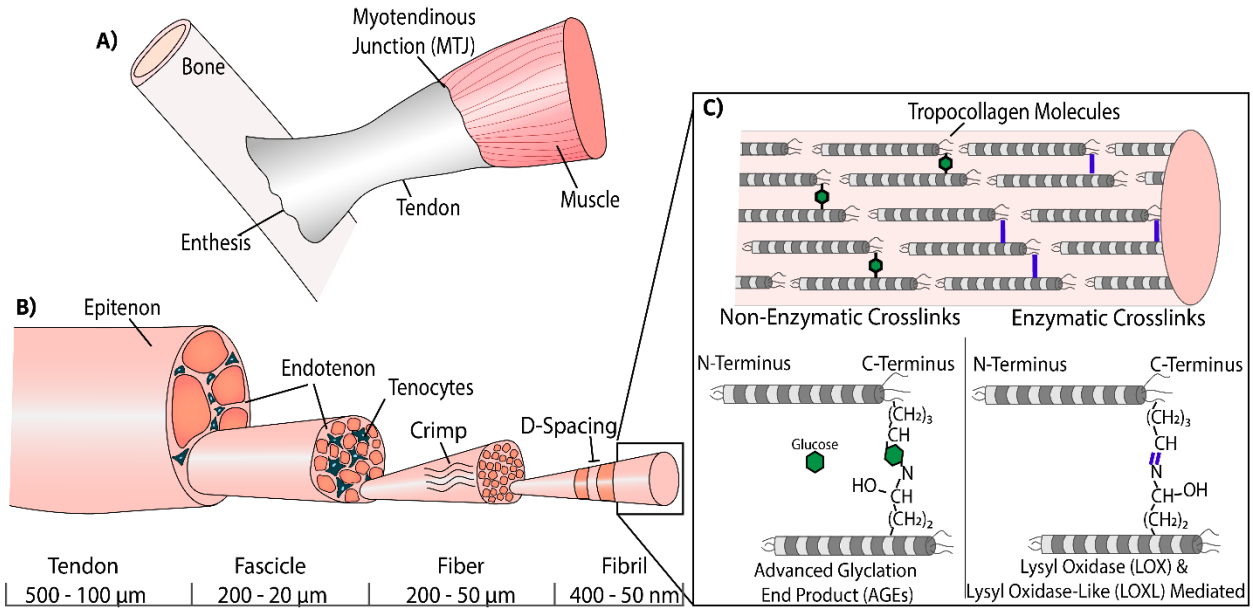

Figure 1.1: *Structural hierarcahy of tendon A) Schematic of the muscloskeletal unit. B) Hierarchical representation of tendon, in which the bulk tendon is composed of progressively smaller structural units of type I collagen. C) Intermolecular enzyamtic and non-enzymatic crosslinks within collagen fibrils. Non-enzyamtic crosslink formation via adanced glycation end-products (AGE). Enzyamtic crosslinks formation mediated via the Lysyl Oxidase (LOX) and LOX-like family of enzymes. [10,26]*

In comparison to other tissues, mature tendons have a limited population of cells interspersed within a highly organized extracellular matrix (ECM). The ECM is dominantly composed of type I collagen, accounting for up to 70 - 80% of the tendon dry weight [3, 32]. The remaining 20 - 30% of tendon dry weight is a mixture of minor collagens, elastin, and small leucine-rich proteoglycans (SLRPs) [3, 32–34]. In addition to type I collagen, several other fibrillar and non-fibrillar collagens (III, V, VI, and XI) exist within tendon and contribute to the development, maintenance, and failure of the tissue [3, 35, 36]. Understanding how these non-collagenous components facilitate matrix interactions is

essential to elucidating the mechanisms that govern development, homeostasis, and disease.

Minority Collagens

Of the minority collagens in tendon, type III collagen is the next abundant and accounts for roughly 8 – 9% of total collagen content [37, 38]. Collagen type III has been shown to play a critical role in modulating interactions between collagen type I molecules during development and normal homeostasis [5, 12, 33, 35]. More specifically, collagen type III is highly expressed within the interfibrillar matrix during early stages of tendon development and co-localizes with collagen type I, impeding the lateral fusion of adjacent collagen fibrils [36]. During later developmental stages, interfibrillar Collagen type III expression decreases rapidly and corresponds to an increase in collagen fibril diameters [36, 39]. Overall, the spatial and temporal patterning of collagen type III expression is critical to the structural arrangement of collagen fibrils and the corresponding mechanical capabilities of the tissues [29]. Within mature tendons, collagen type III expression is largely limited to the external endotenon sheath, suggesting its limited role in long-term maintenance of inter-fibrillar interactions [35]. Collagens V and XI have been shown to play a similar role as collagen III, aiding in collagen fibril nucleation and fibrillar assembly mechanisms [13]. However, their expression is largely confined to developmental periods, similarly suggesting their limited role in homeostatic remodeling in mature tendons.

Elastin

Elastin is a key protein within elastic fibers and contributes mechanical stability to tissue structures that undergo continuous repetitive loading [32, 40]. Within tendons, elastin is present in relatively low quantities and is predominantly localized to the interfascicles matrix [32]. Elastin content varies between tendons, with energy-storing tendons presenting a higher concentration of elastin than positional tendons [40–42]. Prior work has suggested that elastin augments the mechanical capabilities and fatigue resistance of energy-storing tendons, specializing them for their physiological function[35]. Elastin content and organization has been shown to be compromised with age and likely contributes to the increase in tissue failure within geriatric tendons [32, 41]. However, the exact mechanisms by which elastin modulates tendon structure-function behavior, and its variation within tendon groups, age, and disease aren't fully understood and requires further study.

Small-Leucine Rich Proteoglycans (SLRPs)

SLRPs expression is of particular interest as they are capable of directly altering cellular signaling activity and influencing tendon remodeling [33, 43–45]. SLRPs are ubiquitously expressed within tendons [38] and are composed of a core protein that is covalently bounded to glycosaminoglycans (GAG) chains. These GAG chains carry a highly negative charge group that attracts and binds to water, heavily contributing to the hydration state of the tissue (65 – 70% water by weight) [3]. SLRPs additionally have a high binding affinity with several collagenous components, including collagen types I, II, III, V, VI, and X, directly influencing the collagenous architecture in tendon [46]. More specifically, SLRP expression has been shown to be capable of stabilizing collagen type

I fibrils and impede collagenase degradation [44, 47]. SLRPs can additionally bind directly with growth factors, such as transforming growth factor β (TGF-β) [43, 45] and epidermal growth factor (EGF) [45, 48]. By binding these growth factors, SLRPs can directly modulate cellular proliferation, differentiation, and proteomic expression behavior. Numerous SLRPs exist within tendon tissue but decorin, biglycan, fibromodulin, and lumican are of particular importance [48].

Collagen Crosslinking

Covalent crosslinking of collagen directly contributes to the structural integrity and mechanical properties of adult tendon tissue. Recent reviews have provided a great summary of our current working knowledge of crosslinking within tendons [28, 49]. Briefly, crosslinking formation can be initiated via enzymatic or non-enzymatic pathways (**Fig. 1.1C**). Enzymatic covalent crosslinks are formed via the copper-dependent lysyl-oxidase (LOX) family of enzymes, comprised of LOX and LOX-like (LOXL) isoforms 1 – 4 [28]. Inactive proLOX is initially deposited within the EMC, requiring BMP-1 to proteolytically cleave the glycosylated N-terminal to produce the active LOX protein [50]. Following N-terminal cleavage, LOX interacts with lysine/hydroxylysine residues on the tropocollagen to produce reactive aldehyde species [28]. These telopeptide aldehydes then spontaneously react with adjacent lysine or hydroxylysine residues on adjacent molecules to create “immature” divalent crosslinks, linking two tropocollagen molecule units (**Fig. 1.2**) [28]. These immature crosslinks can be an aldimine or ketoimine variant depending on the hydroxylation state of the telopeptide lysine [40].

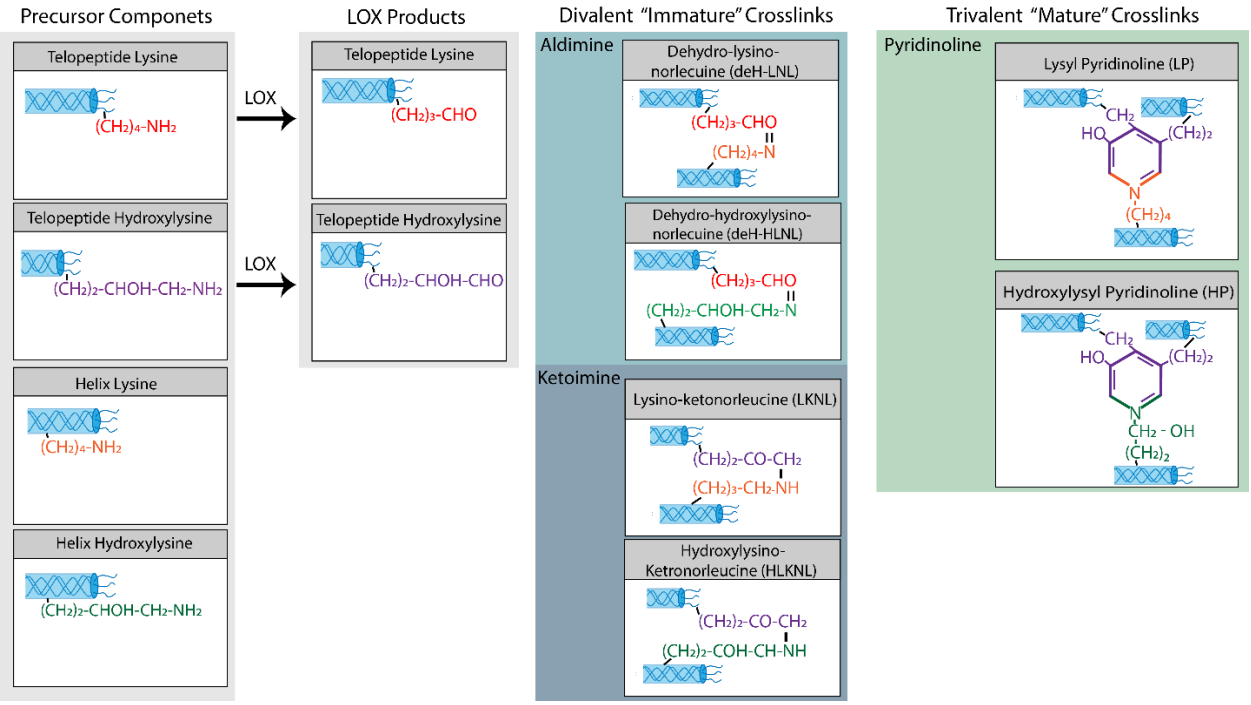

Figure 1.2: Molecular pathways of enzymatic collagen crosslinking in tendon tissue initiated by LOX and and LOX-L isoforms. Helical and telopeptide lysine/hydroxylysine residues are tracked by color. Immature divalent crosslinks are categorized as aldimine or ketoimine and mature trivalent crosslinks are categorized as pyridinolines. [36]

Aldimine variant crosslinks form when a reactive telopeptide lysine-aldehyde interacts with a helical lysine or hydroxylysine residue to produce a dehydro-hydroxylysine-norleucine (deH-HLNL) or dehydro-lysinonorleucine (deH-LNL) crosslink, respectively. Aldimine crosslinks are highly soluble in acid solutions and easily denatured at elevated temperatures [28, 51]. Ketoimine crosslinks form when the hydroxylated telopeptide lysine reacts with the ε-amino group of an adjacent helical lysine or hydroxylysine residue, producing a lysino-ketonorleucine (LKNL) or hydroxylysino-ketonorleucine (HLKNL) crosslink, respectively [28]. Unlike aldimine crosslinks, ketoimines are significantly more stable in elevated temperatures and acidic environments [28].

These ‘immature’ divalent crosslinks can further interact with telopeptide aldehyde residues on adjacent tropocollagen molecules to form ‘mature’ trivalent pyridinoline crosslinks, directly linking three molecular units. More specifically, two telopeptide hydroxylysyl-aldehyde resides and a helical hydroxylysine can produce a trivalent hydroxylysl-pyridinoline (LP-Pyr or HP) crosslink [51]. Alternatively, two telopeptide hydroxylysyl-aldehyde resides and a helical lysine can produce a trivalent lysyl-pyridinoline (L-Pyr or LP) crosslink. HP & LP crosslinks can additional be produced via the ketoimine crosslinks (LKNL & HLKNL). Where HLKNL or LKNL can interact with an adjacent hydroxylysine aldehyde to from an HP or LP crosslinks, respectively. Mature HP/LP crosslinks are resistant to elevated temperature and thermal denaturation [28, 51].

The variant of crosslink formed is highly dependent on the degree of hydroxylysine present and is known to vary greatly between collagen types and tissues [51, 52]. For example, rat tail tendons display limited hydroxylysine residues, resulting in ~ 70 times less mature HP/LP crosslinks in comparison to human patellar tendons [53]. The limited hydroxylysine within rat tail tendon forces aldimine crosslinks to dominate, creating a tissue that can be more easily denatured in elevated temperatures and acidic environments. The variability in lysine hydroxylation across tissues is suspected to contribute to the reduced biomechanical capabilities shown in positional tendons (i.e., rat tail tendons) in comparison to energy-storing tendon (i.e., human patellar). This is exemplified within genetic diseases such as Ehlers-Danlos syndrome (EDS), which compromises hydroxylation of lysine residues within collagens and increases tissue fragility [54, 55].

In contrast to LOX mediated crosslinking, non-enzymatic crosslinks are advanced glycation end-productions (AGEs) and formed via the reduction of sugars [28, 49]. Unlike LOX mediated crosslinking, AGE formation is largely nonspecific and produces both crosslinking and non-crosslinking compounds along the tropocollagen [56]. AGE crosslinks are facilitated via the glycation of protein residues, such as lysine, with sugars. AGEs are slow to form but accumulate with age due to limited collagen turnover within mature tendons [49, 53]. AGEs formation can be accelerated under specific disease states, such as diabetes, and is believed to contribute to impaired mechanical functionality [56]. However, AGEs crosslinks are relatively absent within developmental and neonatal periods.

1.2.2 Tendon Function

Tendons play an essential mechanical role within the body, enabling musculoskeletal movement and aiding in joint stability. Tendons are a compliant anisotropic biomaterial that presents high resistance to deformation under tension but easily buckles under compressive forces [57]. Upon tensile loading, tendons display a distinctive non-linear response, exhibited by a conventional stress-strain “j-curve” **(Fig. 1.3**). Under small strains, tendon presents a non-linear “toe” region, in which the tissue provides limited resistance to elongation (i.e., low stiffness). This is largely attributed to the periodic crimp morphology of the collagenous network, which presents a non-linear loading behavior as the crimp is pulled taut and collagen fibers are linearized [58]. With additional loading, the tissue enters the linear region, characterized by a heightened resistance to deformation but is still capable of elastic recovery. Finally, with further strains, the tissue processes into the “failure region” as the collagenous network is plastically deformed and local

microdamage accumulates, ultimately leading to catastrophic rupture and failure of the tissue [49, 50].

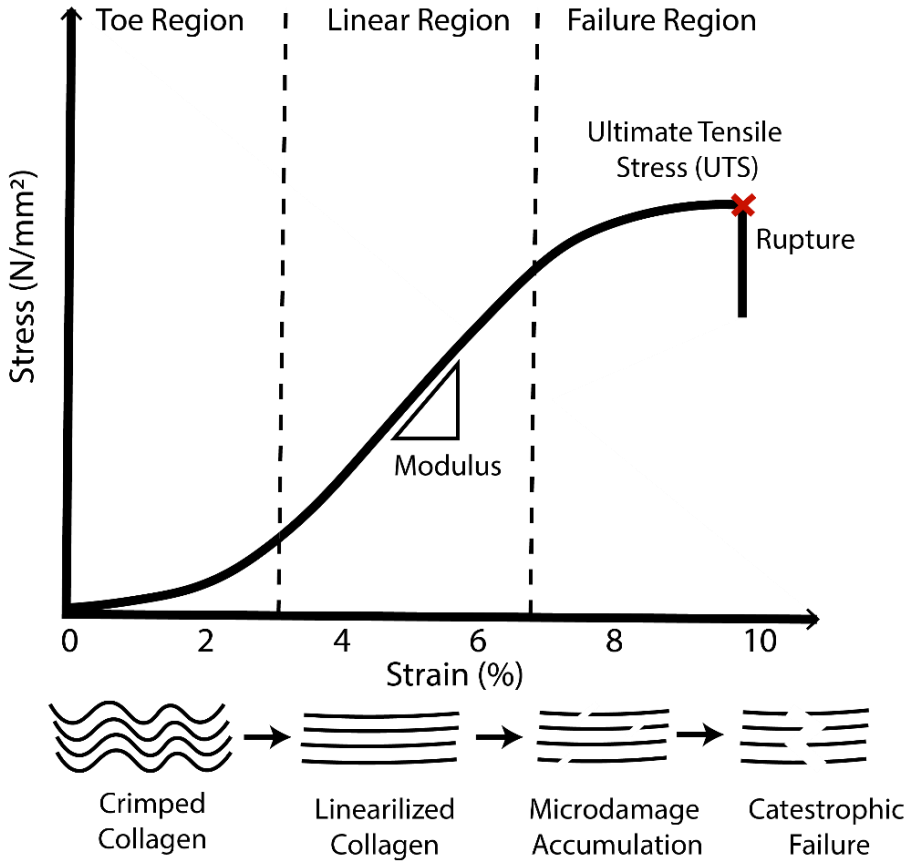

Figure 1.3: Characteristic uniaxial stress response of tendon. Defined regions and their general structure-function response indicated below the stress-strain curve.

While this general behavior is well conserved, there can be significant variations in the material properties across tendons depending on their physiological function [61]. For example, the composition and mechanical capabilities of rat tail tendons are typically much different than patellar tendons, largely tailored to their unique physiological requirements within the body [62]. This is typically reflected in their general classification as ‘positional’ or ‘energy storing’ tendons. Positional tendons (e.g., common digit extensor

or tail tendons) facilitate basic force transmission between the muscle and bone. However, energy storying tendons (e.g., Achilles & patellar tendons) experience higher strains *in vivo* and are capable of enhanced elastic recovery, optimized for energy use within the body [62, 63]. It's important to note that these classifications are generalizations that attempt to capture trends across tendons with similar functions. Indeed, even within the same tendon, mechanical properties can vary along the tissue length and width, particularly near the myotendinous junction and bone insertion [51, 63].

Multiscale Mechanics

The mechanical function of tendon is largely driven by the hierarchical arrangement of collagen and the deformation mechanisms that occur across multiple length scales[10, 64]. A proper understanding of how these distinctive collagenous elements deform and facilitate load transmission is critical to understanding structure-function relationships within mature and developing tendon tissues.

Mechanical capabilities at the fibrillar scale are mediated via the loading behavior of individual collagen molecules. Within fibrils, tropocollagen molecules are arranged in a quarter-stagger alignment, producing a semi-crystalline structure of laterally packed molecules [27]. This regular packing produces a characteristic D-period banding pattern along the length of the tissue, which can be directly measured under electron microcopy and small angle x-ray scattering techniques [59, 65, 66]. Upon fibrillar loading, approximately ~50 - 85% of the deformation is facilitated by stretching of the molecules, while the remainder is accommodated by sliding between molecules [66]. Shear forces are transmitted between fibrils largely via intermolecular hydrogen bonds and water-bridges. The formation of intermolecular crosslinks additionally contributed to load

transmission and inhibit excessing tropocollagen slippage [42]. Furthermore, crosslinking decreases the lateral spacing between molecular units, effectively increasing the packing density [67]. This has been shown to increase the stiffness of the fibril structure and thermodynamic stability of the semi-crystalline lattice [52, 53].

Despite a strong understanding of individual fibril structure-function relationships, there is still debate regarding how tensile loads are transmitted between fibril units. Specifically, it's unclear whether fibrils are structurally continuous along the tendon length and bear load independently, or if they are discontinuous and transfer load through interfibrillar shear forces. Most recently, Svensson et al. tracked more than 2,500 fibrils over 25 μm in human patellar and hamstring tendons and found only one that ended within the imaging window [68]. Using probabilistic analysis [68], they estimated that the fibrils were at least 14 mm long, which the authors suggested is long enough that, even if collagen fibrils in tendon are not structurally continuous, they functionally behave as such (i.e., tendon failure results from fibril rupture rather than excessive fibril sliding). These conclusions are supported by additional studies that found no fibril ends in mature rat ligaments or tail tendon fascicles and reported similar estimates of fibril lengths ranging from 0.86 mm to 12.7 mm depending on maturity [69, 70]. The interpretation that fibrils behave as functionally continuous structures is also consistent with mechanical data demonstrating that creep failure of bovine tail tendons under static load is the result of fibril denaturation and rupture rather than interfibrillar slippage [59]. Altogether, these findings suggest that collagen fibrils are structurally continuous and bear load independently.

On the other hand, there is a significant body of data suggesting that collagen fibrils in tendon are discontinuous and transfer load through viscous interfibrillar shear forces. Measurement of fibril strains using X-ray diffraction, confocal microscopy, and atomic force microscopy has shown that the fibril strains in rat tail fascicles and mouse Achilles tendons during uniaxial testing are significantly less than the bulk tissue strains [66, 71–73]. In these papers, the strain discrepancy between length scales is explained by relative sliding between discontinuous fibrils. Consistent with this hypothesis, additional studies using x-ray diffraction during tendon creep testing showed that the fibril strains remained constant while the tissue elongated [74]. Similarly, data from multiscale stress relaxation experiments demonstrate that fibril strains in tendon are time dependent and follow the viscoelastic response of the macroscale tissue stress but not the bulk tissue strain [71, 75, 76]. Furthermore, following short periods of creep loading, the fibrils fully recover their original length, suggesting that non-recoverable interfibrillar sliding is responsible for tendon creep [77, 78]. This is also consistent with work demonstrating that tendon multiscale mechanics can be uniquely explained by shear lag models incorporating plastic (i.e., non-recoverable) interfibrillar sliding and shear load transfer [64]. Similar sliding behavior is observed in tendon at smaller (i.e., collagen molecules) [79] and larger (e.g., fascicles) [80] length scales. Therefore, sliding between tendon subcomponents may be a hierarchically conserved phenomenon that sacrifices tissue stiffness for toughness [81, 82]. Together, these data suggest that fibrils in tendon are discontinuous, and this discontinuous structure has an important impact on tendon mechanics and function. Understanding how the structural arrangement contributes within the collagenous

network contributes to the loading behavior of tendon is critical to elucidate the mechanisms that drive functional tendon formation.

1.3 Embryonic Tendon Structure & Function

Tendon formation is a highly orchestrated process that describes the mechanisms by which tendon progenitor cells establish their cell fate, self-assemble, and undergo the coordinated deposition of collagen. The continuous deposition and modification of the fibril network occurs over embryonic and neonatal periods of development [12], corresponding to a substantial increase in the functional loading capabilities of the tissue[9]. Significant progress has been made over the last couple of decades outlining the hierarchical assembly of collagen *in vivo*, enabling this functional transformation. Despite this, its still unclear how the progressive maturation of the collagenous network is dynamically altering the mechanical microenvironment during development. To start addressing this gap in knowledge, we much first understand the fundamental structure-function relationships that are established during tenogenesis.

1.3.1 Cellular Organization & Collagen Synthesis

The early stages of tendon formation are driven by the initial expansion and self-organization of progenitor tendon cells [39, 83]. Early identification of tendon progenitor cells is indicated via the expression of the basic Helix-Loop-Helix (bHLH) transcription marker Scleraxis (Scx), which has been a robust developmental marker for tendon in zebrafish, chick, and mice models [84]. During early stages of development, tendon progenitor cells begin to preferentially orient themselves along the longitudinal axis of the tissue, presenting a rounded morphology and high packing density (**Fig. 1.4A - B**) [19,

85]. With time, cells form distinctive stacked columns, where extending cellular protrusions maintain cadherin-mediated contacts with neighboring columns of cells [11]. Importantly, this shift in cellular architecture results in the production of continuous extracellular channels that run parallel to the cell columns. Newly produced collagen is then deposited into these extracellular channels [8, 12], enabling the multiscale assembly of collagen structures along the longitudinal axis of the tissue.

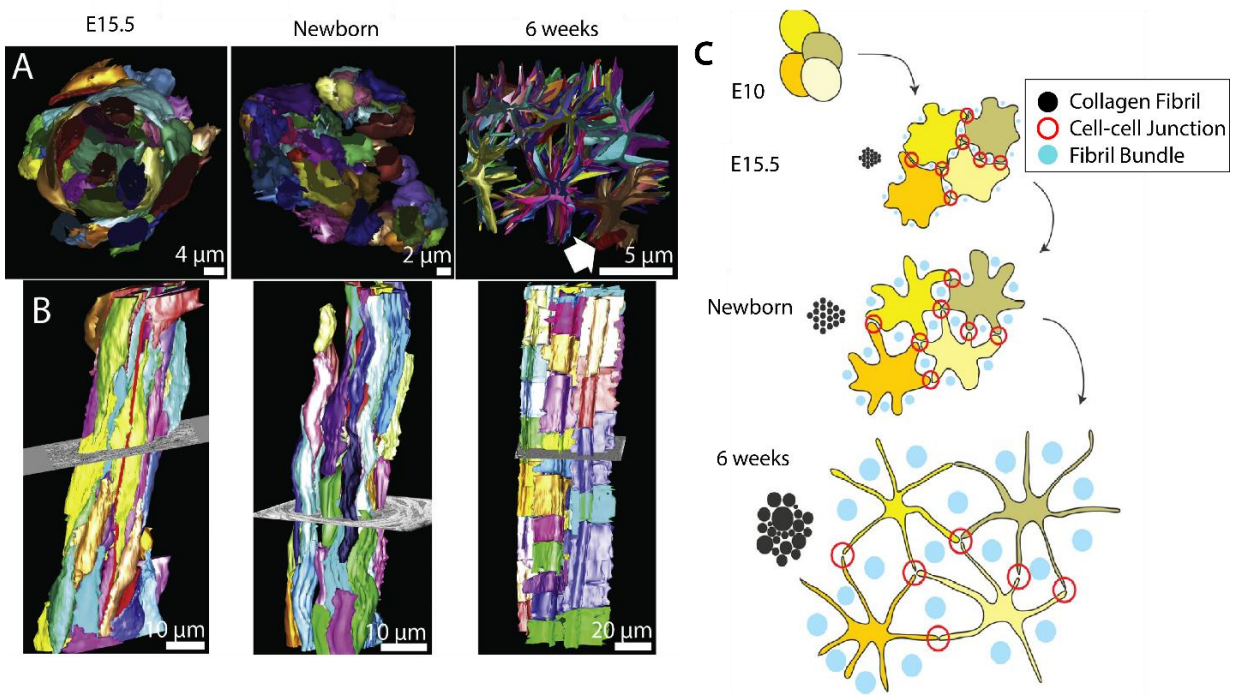

Figure 1.4: Three-dimensional reconstructions of tenocytes in mouse tail tendons during embryonic and postnatal stages of development. **A)** Transverse and **B)** longitudinal views of cells arrangement changes as a function of maturation. **C)** Schematic of tenocyte architecture changes during development. Figured adapted directly from Kalson et al., 2015 [85].

Type I Collagen is synthesized as a precursor molecule, procollagen, within the rough endoplasmic reticulum [86]. Procollagen is composed of two alpha (α1) and 1 alpha (α2) monomer chains, roughly ~1000 amino acids each [87, 88]. Following translation, pro-α chains undergo a series of modifications, namely the hydroxylation of proline and lysine residues [86]. The hydroxylation of lysine residues enables the formation of intermolecular crosslinks later in fibrillogenesis [28]. The residue site and quantity of hydroxylysine formation varies drastically between tissues and has critical implications on the final crosslinking fate of the tissue [28]. Alternatively, the hydroxylation of proline is highly conserved, accounting for ~13.3% of the final collagen dry mass and facilitates the formation of the triple helix structure [89]. More specifically, the hydrogen bonding generated via hydroxyproline residues on the α-chains stabilizes the procollagen helix structure and impedes further post-translational modification of the amino-acid residues [86, 89]. During synthesis, globular propeptides are additionally produced on the N- and C- terminal ends. These propeptides aid in the initial nucleation of the procollagen helix structure [37]. Furthermore, the propeptides increase the molecular solubility of the collagen precursor, discouraging premature collagen self-assembly [90].

1.3.2 Collagen Deposition, Growth, and Fusion

Following its initial synthesis, procollagen is transported from the ER to the Golgi apparatus, where it is packaged into secretory vacuoles for deposition into the ECM [8, 88]. These secretory vacuoles, termed Golgi-to-Plasma membrane carriers (GPCs), fuse with the plasma membrane to create long finger-like projections termed fibril-depositors or “fibrilopositiors”, which enable the deposition of the collagen into extracellular channels

[88, 91]. The deposition of these immature fibril intermediates marks the onset of tendon formation can be split into two primary phases.

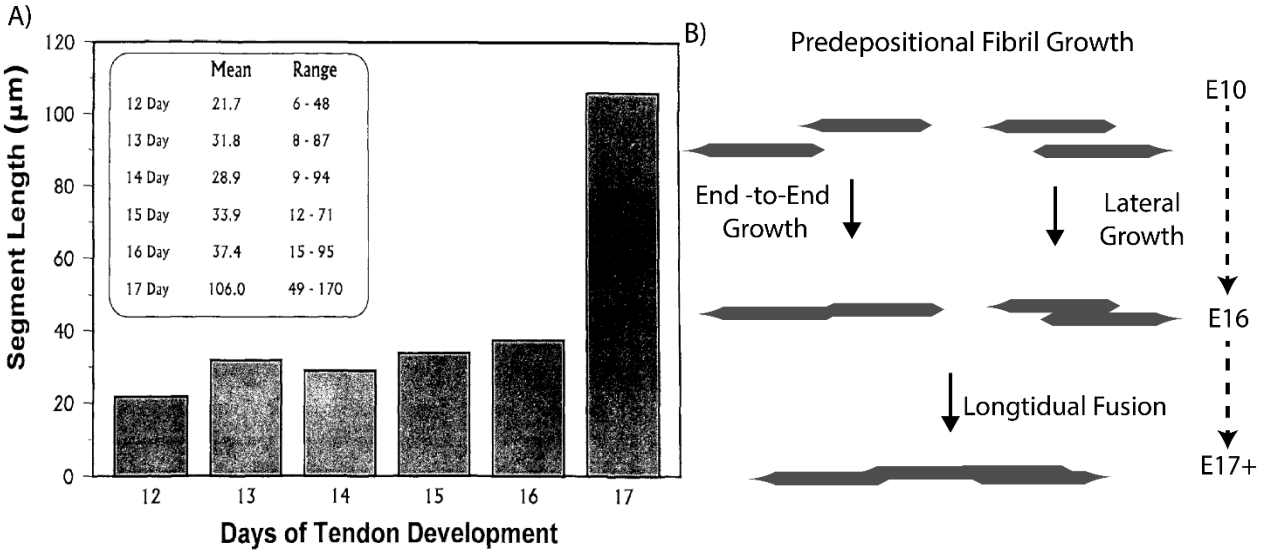

Figure 1.5: Fibril length changes during mid-to-late stages embryonic chick development. **A)** Fibril length changes a function of development. Abrupt increase in fibril lengths occur at E17, after which fibrils were unable to be isolated intact. **B)** Model of collagen fibril lengthening mechanisms during embryonic chick development. Figured adapted from Birk et al., 1989 [12].

During the initial phase, collagen molecules are secreted by the cell into fibrilopositors channels as soluble pro-collagen. The C- and N- terminal propeptides are cleaved via a family of metalloproteinases at the cell surface to create tropocollagen [88]. The cleavage of propeptides decreases molecular solubility by ~10,000 fold, enabling tropocollagen self-assembly [87]. However, this initial self-assembly process is tightly regulated via a family of collagens (Col. V/XI) [92] and other proteoglycans [13, 47, 93], to ensure proper orientation and size of the fibril. This process results in the production of short

intermediate collagen fibrils, roughly 10 μm in length and 20 nm in diameter [12]. During this same period, pro-LOX is proteolytically cleaved into LOX to enable crosslinking of early fibril intermediates [50].

Over time, these short intermediate collagen fibrils begin to accumulate within the extracellular matrix, marked by a substantial reduction in cellular volume fraction [85, 94]. This phase is highly conserved across animals, initiating at E14.5 in mice and E10 in chicks [65, 85]. During this period, fibrils may undergo small amounts of end-to-end and lateral growth to increase their length and diameter, respectively (**Fig. 1.5**). This preparatory phase has been shown to persist from E10 – E16 in chick embryos [65]. Mechanical tensile testing of tendons during this developmental period showed limited resistance to deformation, indicative that the collagenous network is not functionally load bearing [9, 95].

Phase two starts at later developmental stages, in which collagen fibrils abruptly undergo a highly coordinated series of fusion events, rapidly increasing both their diameter and length, respectively [9, 12]. This process coincides with a reduction in the interfibrillar matrix components decorin and type III collagen, enabling lateral fibril interactions [36, 47, 65]. This process occurs around ~E17 within chick embryos, and results in a ~3x increase in fibril length (30 μm to 120 μm) over a briefly 24 hour period [65]. Prior work has indicated that fibril fusion events persist with additional maturation, with fibril lengths in mature tissues having been estimated to be 0.86 – 12.7+ mm range [69, 70]. This transformation in the collagenous networks corresponds to a rapid increase in the tensile loading properties of tissue in chicks, with a ~10x increase in the tensile modulus between E12 and hatching (E20/E21) [9].

1.3.3 Regulators of Fibrillogenesis

Fibrillogenesis is regulated via a myriad of intercellular and extracellular mechanisms. A general understanding of how these components modulate the synthesis, deposition, modification, and assembly of collagen is essential to establishing the functional loading capabilities of tendon.

During the initial synthesis of collagen, the hydroxylation of lysine establishes the crosslinking potential of the tissue. More specifically, the formation of stable mature crosslinks is dependent on the presence of hydroxylysine residues on the telopeptide [28, 49]. Insufficient quantities of telopeptide hydroxylysines confines downstream crosslinking to amine crosslinks, which are more susceptible to denaturation and jeopardizes the mechanical capabilities of the tissue [53]. “Moderate” amounts of hydroxylysine will facilitate the formation of more stable divalent ketoimines but will be unable to form mature trivalent pyridinoline crosslinks without sufficient adjacent telopeptide hydroxylysine residues [28]. Specific lysyl hydroxylase isoforms (1 - 3) have been implicated in modulating site-specific lysine hydroxylation during post-translational modifications [96, 97]; suggesting that the crosslinking capacity of the collagen is established during synthesis and tendon-specific crosslinking differences is due to variable hydroxylation behavior. However, it is still largely unclear how lysyl hydroxylase is controlled during development and how it may vary between specific tendons.

Following synthesis, the packaging of pro-collagen additionally plays an important role in mediating fibril formation. Within the GPCs vacuoles, the proteinases required for pro-collagen processing (N-protinases: ADAMTS 2,3,14 | C-Proteinases: BMP1/mTolloid

family) are present but are neutral metalloproteinases, requiring a pH of 8.0 - 8.5 for optimum activity [88, 90]. Conversely, the pH in later stages of the secretory pathways is increasingly acidic and estimated to be ~ 6.0 [98]. At this relatively low pH, proteinase activity has been shown to be negligible [89, 90], suggesting that pro-collagen processing is largely confined to the extracellular matrix via environmental pH controls.

Following secretion into the ECM, pro-collagen is cleaved to enable the initial self-assembly of the tropocollagen into fibril structures. While pro-collagen cleavage alone is sufficient to initiate fibril formation [101], external regulation is required to control the direction and physical characteristics of the fibril structures. This regulation is mediated via interactions at the plasma membrane and within the interfibrillar matrix [38, 102, 103].

Interactions at the tenocyte plasma membrane have been heavily implicated in the control of fibril assembly during the early stages of collagen deposition. Indeed, recent work has shown fibronectin binding at the membrane operates as a critical intermediate for pro-collagen processing, fibril assembly, and crosslinking [102]. More specifically, surface integrins (α5β1) bind fibronectin to the membrane [104], which in turn sequesters BMP-1 to the cell surface. The presence of BMP-1 enables proteolytic cleavage of the C-propeptide, indicating that pro-collagen processing is laregly confined to the cell membrane [88]. Furthermore, BMP-1 aids in cleaving pro-LOX into LOX [28], enabling LOX-mediated crosslinking of the early fibril structure, stabilizing it. This is consistent with prior work that has indicated that LOX-mediated fibril crosslinking is confined to early stages of fibrillogenesis due to size restrictions in accessing hydroxylysine/lysine residues within the fibril bundle [49, 105].

Once initial self-assembly is conducted, the fibril intermediate is released into the fiber bundle where interfibrillar matrix components control lateral/longitudinal fibril interactions [38]. More specifically, type III collagen impairs lateral fibril interactions and is highly expressed within the interfascicle matrix during the early phases of fibril deposition [47]. Similarly, decorin expression is highly prevalent during early stages of fibrillogenesis and binds to collagen fibrils, impeding local interactions [13]. Other minority collagens (Col. V, XI, XII, XIV) and other SLRPs (biglycan, lumican, and fibromodulin) have shown similar patterns but are generally less expressed during development [38, 46]. Together, these interfibrillar matrix components allow a depository of short intermediate fibrils to accumulate within the fiber bundle in this premature state [65]. Once a critical threshold has been established, collagen III and decorin expression rapidly drops [9, 106], initiating the rapid fusion of adjacent fibril intermediates. The upstream biological mechanisms that trigger this change in interfibrillar matrix components are not well understood and represents a critical gap in knowledge.

Mechanical Stimulation

More recent work has investigated the role of mechanical stimulation in modulating these fibril interactions during development. Indeed, embryo motility has been shown to increase in the days preceding structural transformations within the fibril network [18], suggesting that mechanical stimulation is contributing to the regulation of the collagenous matrix. Furthermore, muscle activity is highly correlated with tendon size and can be impaired with paralysis agents [25, 107]. However, it is unclear how muscle contractions are eliciting mechanobiological activity within the developing tendon and how they contribute to fibrillogenesis.

Recent work has shown that paralysis agents impede LOX-mediated crosslinking within developing chick tendons, resulting in a reduction in their compressive modulus [108, 109]. While crosslinking has been shown to be essential within mature tendons, it's unclear if the crosslinking state of the developing tissue contributes to organization of the hierarchical fibril network.

Prior work has additionally suggested that mechanical stimulation during development may contribute to YAP/TAZ mechanobiological activity [110, 111 (BioRxiv)]. This is consistent with RT-qPCR studies tracking TAP/TAZ sensitive genes, which steadily increased during mid-to-late stages of tendon develop (E14 - E17) in chicks. Prior work has shown that YAP/TAZ activity plays a significant role in mediating skeletogenesis, particularly via interactions with canonical Wnt signaling [20]. However, the role of YAP/TAZ in tendon development has still not been elucidated. Interestingly, in vitro work has shown that YAP/TAZ expression is stimulated via cyclical strains and positively correlated with decorin expression [112]. These findings are inconsistent with developmental trends, in which decorin expression is decreasing in tandem with periods of high muscle activity during development [9]. Additional work is required to investigate how mechanobiological signaling is directly contributing to fibrillogenesis.

1.4. Research Objectives

The primary objective of this dissertation was to determine how structural changes with the collagenous matrix during development contribute to the functional capabilities of tendon. To do so, this work aimed to investigate the role of musculoskeletal stimulation in mediating the dynamic structure-function capabilities during tendon development.

To accomplish this, multiscale mechanical testing was conducted to investigate how fibril continuity dictate the loading behavior in mature tendons, establishing foundational structure-function relationships in tendon. Subsequent work applied these findings to investigate the multiscale mechanical behavior as a function of development to provide insight into how fibril length changes drive tendon formation. Paralysis agents and crosslinking inhibitors were then utilized to investigate how muscle stimulation and collagenous crosslinking contributes to the functional transformation during late stages of tendon development. Thermal characterization tools and serial-block face scanning-electron microscopy (SBF-SEM) were leveraged to directly quantify changes within the collagenous ultrastructure during development and under treatment conditions.

Collectively, these findings indicate that the functional transformation of tendons is established during development by an abrupt increase in collagen fibril lengths, and fibril lengthening mechanisms are dependent on muscle stimulation. Furthermore, while crosslinking is essential for the loading capabilities of the tissue, our findings suggest that they are largely insensitive to external stimuli. This work provides critical insights into the multiple processes which govern the formation of functional tendon tissues and will aid in advancing regenerative medicine and tissue engineering strategies.

1.5 References

1. Lantto I, Heikkinen J, Flinkkilä T, et al (2015) Epidemiology of Achilles tendon ruptures: Increasing incidence over a 33-year period: Clinical relevance level IV. Scand J Med Sci Sports 25:e133–e138. https://doi.org/10.1111/sms.12253

2. Lin TW, Cardenas L, Soslowsky LJ (2004) Biomechanics of tendon injury and repair. J Biomech 37:865–877. https://doi.org/10.1016/j.jbiomech.2003.11.005

3. Woo SL-Y, Debski RE, Zeminski J, et al (2000) Injury and Repair of Ligaments and Tendons. Annu Rev Biomed Eng 2:83–118. https://doi.org/10.1146/annurev.bioeng.2.1.83

4. Kedia M, Williams M, Jain L, et al (2014) The Effects of Conventional Physical Therapy and Eccentric Strengthening for Insertional Achillies Tendionopathy. Int J Sports Phys Ther 9:

5. Kadler KE, Hill A, Canty-Laird EG (2008) Collagen fibrillogenesis: fibronectin, integrins, and minor collagens as organizers and nucleators. Curr Opin Cell Biol 20:495–501. https://doi.org/10.1016/j.ceb.2008.06.008

6. Chang J, Garva R, Pickard A, et al (2020) Circadian control of the secretory pathway maintains collagen homeostasis. Nat Cell Biol 22:74–86. https://doi.org/10.1038/s41556-019-0441-z

7. Herchenhan A, Uhlenbrock F, Eliasson P, et al (2015) Lysyl Oxidase Activity Is Required for Ordered Collagen Fibrillogenesis by Tendon Cells. J Biol Chem 290:16440–16450. https://doi.org/10.1074/jbc.M115.641670

8. Holmes DF, Lu Y, Starborg T, Kadler KE (2018) Collagen Fibril Assembly and Function. In: Current Topics in Developmental Biology. Elsevier, pp 107–142

9. McBride DJ, Trelstad RL, Silver FH (1988) Structural and mechanical assessment of developing chick tendon. Int J Biol Macromol 10:194–200. https://doi.org/10.1016/0141-8130(88)90048-7

10. Rowe RWD (1995) The Structure of Rat Tail Tendon. Connect Tissue Res 14:9–20

11. Richardson SH, Starborg T, Lu Y, et al (2007) Tendon Development Requires Regulation of Cell Condensation and Cell Shape via Cadherin-11-Mediated Cell-Cell Junctions. Mol Cell Biol 27:6218–6228. https://doi.org/10.1128/MCB.00261-07

12. Birk DE, Nurminskaya MV, Zycband EI (1995) Collagen fibrillogenesis in situ: Fibril segments undergo post-depositional modifications resulting in linear and lateral growth during matrix development. Dev Dyn 202:229–243. https://doi.org/10.1002/aja.1002020303

13. Zhang G, Ezura Y, Chervoneva I, et al (2006) Decorin regulates assembly of collagen fibrils and acquisition of biomechanical properties during tendon development. J Cell Biochem 98:1436–1449. https://doi.org/10.1002/jcb.20776

14. Subramanian A, Kanzaki LF, Galloway JL, Schilling TF (2018) Mechanical force regulates tendon extracellular matrix organization and tenocyte morphogenesis through TGFbeta signaling. eLife 7:e38069. https://doi.org/10.7554/eLife.38069

15. Schiele NR, Marturano JE, Kuo CK (2013) Mechanical factors in embryonic tendon development: potential cues for stem cell tenogenesis. Curr Opin Biotechnol 24:834–840. https://doi.org/10.1016/j.copbio.2013.07.003

16. Patel D, Sharma S, Bryant SJ, Screen HRC (2017) Recapitulating the Micromechanical Behavior of Tension and Shear in a Biomimetic Hydrogel for Controlling Tenocyte Response. Adv Healthc Mater 6:1601095. https://doi.org/10.1002/adhm.201601095

17. McNEILLY CM, Banes AJ, Benjamin' M, Ralphs' JR (1996) Tendon cells in vivo form a three dimensional network of cell processes linked by gap junctions. J Anat 189:593–600

18. Wu K-C, Streicher J, Lee ML, et al (2001) Role of motility in embryonic development I: Embryo movements and amnion contractions in the chick and the influence of illumination: Embryonic Motility of the Chick. J Exp Zool 291:186–194. https://doi.org/10.1002/jez.1068

19. Kalson NS, Holmes DF, Herchenhan A, et al (2011) Slow stretching that mimics embryonic growth rate stimulates structural and mechanical development of tendon-like tissue in vitro. Dev Dyn 240:2520–2528. https://doi.org/10.1002/dvdy.22760

20. Teufel S, Hartmann C (2019) Chapter Nine - Wnt-signaling in skeletal development. In: Olsen BR (ed) Current Topics in Developmental Biology. Academic Press, pp 235–279

21. Rolfe RA, Scanlon O'Callaghan D, Murphy P (2021) Joint development recovery on resumption of embryonic movement following paralysis. Dis Model Mech 14:dmm048913. https://doi.org/10.1242/dmm.048913

22. Hosseini A, Hogg DA (1991) The effects of paralysis on skeletal development in the chick embryo. I. General effects. J Anat 177:159–168

23. Nowlan NC, Prendergast PJ, Murphy P (2008) Identification of Mechanosensitive Genes during Embryonic Bone Formation. PLoS Comput Biol 4:e1000250. https://doi.org/10.1371/journal.pcbi.1000250

24. Hall BK, Herring SW (1990) Paralysis and growth of the musculoskeletal system in the embryonic chick. J Morphol 206:45–56. https://doi.org/10.1002/jmor.1052060105

25. Schwartz AG, Lipner JH, Pasteris JD, et al (2013) Muscle loading is necessary for the formation of a functional tendon enthesis. Bone 55:44–51. https://doi.org/10.1016/j.bone.2013.03.010

26. Kastelic J, Galeski A, Baer E (1978) The Multicomposite Structure of Tendon. Connect Tissue Res 6:11–23. https://doi.org/10.3109/03008207809152283

27. Hodge AJ, Schmitt FO (1960) The Charge Profile of the Tropocollagen Macromolecule and the Packing Arrangment in Native-Type Collagen Fibrils. Proc Natl Acad Sci 46:186–197. https://doi.org/10.1073/pnas.46.2.186

28. Bailey AJ, Paul RG, Knott L (1998) Mechanisms of maturation and ageing of collagen. Mech Ageing Dev 106:1–56. https://doi.org/10.1016/S0047-6374(98)00119-5

29. Fratzl P, Misof K, Zizak I, et al (1998) Fibrillar Structure and Mechanical Properties of Collagen. J Struct Biol 122:119–122. https://doi.org/10.1006/jsbi.1998.3966

30. Connizzo BK, Yannascoli SM, Soslowsky LJ (2013) Structure–function relationships of postnatal tendon development: A parallel to healing. Matrix Biol 32:106–116. https://doi.org/10.1016/j.matbio.2013.01.007

31. Hudson DM, Archer M, King KB, Eyre DR (2018) Glycation of type I collagen selectively targets the same helical domain lysine sites as lysyl oxidase–mediated cross-linking. J Biol Chem 293:15620–15627. https://doi.org/10.1074/jbc.RA118.004829

32. Godinho MSC, Thorpe CT, Greenwald SE, Screen HRC (2017) Elastin is Localised to the Interfascicular Matrix of Energy Storing Tendons and Becomes Increasingly Disorganised With Ageing. Sci Rep 7:9713. https://doi.org/10.1038/s41598-017-09995-4

33. Scott JE, Orford CR, Hughes EW (1981) Proteoglycan-collagen arrangements in developing rat tail tendon. Biochem J 195:573–581

34. Iozzo RV, Murdoch AD (1996) Proteoglycans of the extracellular environment: clues from the gene and protein side offer novel perspectives in molecular diversity and function. FASEB J 10:598–614. https://doi.org/10.1096/fasebj.10.5.8621059

35. Buckley MR, Evans EB, Matuszewski PE, et al (2013) Distributions of types I, II and III collagen by region in the human supraspinatus tendon. Connect Tissue Res 54:374–379. https://doi.org/10.3109/03008207.2013.847096

36. Birk D, Mayne R (1997) Localization of collagen types I, III and V during tendon development. Changes in collagen types I and III are correlated with changes in fibril diameter. Eur J Cell Biol 72.4:352–261

37. Zhang G, Young BB, Ezura Y, et al (2005) Development of tendon structure and function: Regulation of collagen fibrillogenesis. J Musculoskelet Neuronal Interact 5:5–21

38. Taye N, Karoulias SZ, Hubmacher D (2020) The “other” 15–40%: The Role of Non-Collagenous Extracellular Matrix Proteins and Minor Collagens in Tendon. J Orthop Res 38:23–35. https://doi.org/10.1002/jor.24440

39. Tozer S, Duprez D (2005) Tendon and ligament: Development, repair and disease. Birth Defects Res Part C Embryo Today Rev 75:226–236. https://doi.org/10.1002/bdrc.20049

40. Eyre DR, Paz MA, Gallop PM (1984) CROSS-LINKING IN COLLAGEN AND ELASTIN. Annu Rev Biochem 53:717–48

41. Fang F, Lake SP (2016) Multiscale mechanical integrity of human supraspinatus tendon in shear after elastin depletion. J Mech Behav Biomed Mater 63:443–455. https://doi.org/10.1016/j.jmbbm.2016.06.032

42. Eekhoff JD, Fang F, Lake SP (2018) Multiscale mechanical effects of native collagen cross-linking in tendon. Connect Tissue Res 59:410–422. https://doi.org/10.1080/03008207.2018.1449837

43. Hosaka Y, Kirisawa R, Mafune N, Takehana K (2005) Downregulation of Decorin and Transforming Growth Factor-β1 by Decorin Gene Suppression in Tendinocytes. Connect Tissue Res 46:18–26. https://doi.org/10.1080/03008200590935510

44. Geng Y, McQuillan D, Roughley PJ (2006) SLRP interaction can protect collagen fibrils from cleavage by collagenases. Matrix Biol 25:484–491. https://doi.org/10.1016/j.matbio.2006.08.259

45. Chen S, Birk DE (2013) The regulatory roles of small leucine-rich proteoglycans in extracellular matrix assembly. FEBS J 280:2120–2137. https://doi.org/10.1111/febs.12136

46. Kalamajski S, Oldberg Å (2010) The role of small leucine-rich proteoglycans in collagen fibrillogenesis. Matrix Biol 29:248–253. https://doi.org/10.1016/j.matbio.2010.01.001

47. Douglas T, Heinemann S, Bierbaum S, et al (2006) Fibrillogenesis of Collagen Types I, II, and III with Small Leucine-Rich Proteoglycans Decorin and Biglycan. Biomacromolecules 7:2388–2393. https://doi.org/10.1021/bm0603746

48. Yoon JH, Halper J (2005) Tendon proteoglycans: biochemistry and function. J Musculoskelet Neuronal Interact 5:22–34

49. Ellingson A, Pancheri N, Schiele N (2022) Regulators of collagen crosslinking in developing and adult tendons. Eur Cell Mater 43:130–152. https://doi.org/10.22203/eCM.v043a11

50. Maruhashi T, Kii I, Saito M, Kudo A (2010) Interaction between Periostin and BMP-1 Promotes Proteolytic Activation of Lysyl Oxidase *. J Biol Chem 285:13294–13303. https://doi.org/10.1074/jbc.M109.088864

51. Horgan DJ, King NL, Kurth LB, Kuypers R (1990) Collagen crosslinks and their relationship to the thermal properties of calf tendons. Arch Biochem Biophys 281:21–26. https://doi.org/10.1016/0003-9861(90)90407-P

52. Herod TW, Chambers NC, Veres SP (2016) Collagen fibrils in functionally distinct tendons have differing structural responses to tendon rupture and fatigue loading. Acta Biomater 42:296–307. https://doi.org/10.1016/j.actbio.2016.06.017

53. Svensson RB, Mulder H, Kovanen V, Magnusson SP (2013) Fracture Mechanics of Collagen Fibrils: Influence of Natural Cross-Links. Biophys J 104:2476–2484. https://doi.org/10.1016/j.bpj.2013.04.033

54. Corsi A, Xu T, Chen X-D, et al (2002) Phenotypic Effects of Biglycan Deficiency Are Linked to Collagen Fibril Abnormalities, Are Synergized by Decorin Deficiency, and Mimic Ehlers-Danlos-Like Changes in Bone and Other Connective Tissues. J Bone Miner Res 17:1180–1189. https://doi.org/10.1359/jbmr.2002.17.7.1180

55. Yeowell HN, Walker LC (2000) Mutations in the Lysyl Hydroxylase 1 Gene That Result in Enzyme Deficiency and the Clinical Phenotype of Ehlers–Danlos Syndrome Type VI. Mol Genet Metab 71:212–224. https://doi.org/10.1006/mgme.2000.3076

56. Snedeker JG, Gautieri A (2014) The role of collagen crosslinks in ageing and diabetes - the good, the bad, and the ugly. Muscles Ligaments Tendons J 4:303–308

57. Elliott DH (1965) Structure and Function of Mammalian Tendon. Biol Rev 40:392–421. https://doi.org/10.1111/j.1469-185X.1965.tb00808.x

58. Hansen KA, Weiss JA, Barton JK (2002) Recruitment of Tendon Crimp With Applied Tensile Strain. J Biomech Eng 124:72–77. https://doi.org/10.1115/1.1427698

59. Hijazi KM, Singfield KL, Veres SP (2019) Ultrastructural response of tendon to excessive level or duration of tensile load supports that collagen fibrils are mechanically continuous. J Mech Behav Biomed Mater 97:30–40. https://doi.org/10.1016/j.jmbbm.2019.05.002

60. Zitnay JL, Jung GS, Lin AH, et al (2020) Accumulation of collagen molecular unfolding is the mechanism of cyclic fatigue damage and failure in collagenous tissues. Sci Adv 6:eaba2795. https://doi.org/10.1126/sciadv.aba2795

61. Thorpe CT, Stark RJF, Goodship AE, Birch HL (2010) Mechanical properties of the equine superficial digital flexor tendon relate to specific collagen cross-link levels: Tendon mechanical properties and collagen cross-links. Equine Vet J 42:538–543. https://doi.org/10.1111/j.2042-3306.2010.00175.x

62. Birch HL, Thorpe CT, Rumian AP (2013) Specialisation of extracellular matrix for function in tendons and ligaments. Muscles Ligaments Tendons J 3:12–22. https://doi.org/10.11138/mltj/2013.3.1.012

63. Thorpe CT, Godinho MSC, Riley GP, et al (2015) The interfascicular matrix enables fascicle sliding and recovery in tendon, and behaves more elastically in energy storing tendons. J Mech Behav Biomed Mater 52:85–94. https://doi.org/10.1016/j.jmbbm.2015.04.009

64. Szczesny SE, Elliott DM (2014) Incorporating plasticity of the interfibrillar matrix in shear lag models is necessary to replicate the multiscale mechanics of tendon fascicles. J Mech Behav Biomed Mater 40:325–338. https://doi.org/10.1016/j.jmbbm.2014.09.005

65. Birk DE, Zycband EI, Winkelmann DA, Trelstad RL (1989) Collagen fibrillogenesis in situ: fibril segments are intermediates in matrix assembly. Proc Natl Acad Sci 86:4549–4553. https://doi.org/10.1073/pnas.86.12.4549

66. Puxkandl R, Zizak I, Paris O, et al (2002) Viscoelastic properties of collagen: synchrotron radiation investigations and structural model. Philos Trans R Soc Lond B Biol Sci 357:191–197. https://doi.org/10.1098/rstb.2001.1033

67. Miles CA, Ghelashvili M (1999) Polymer-in-a-Box Mechanism for the Thermal Stabilization of Collagen Molecules in Fibers. Biophys J 76:3243–3252. https://doi.org/10.1016/S0006-3495(99)77476-X

68. Svensson RB, Herchenhan A, Starborg T, et al (2017) Evidence of structurally continuous collagen fibrils in tendons. Acta Biomater 50:293–301. https://doi.org/10.1016/j.actbio.2017.01.006

69. Craig AS, Birtles MJ, Conway JF, Parry DAD (1989) An Estimate of the Mean Length of Collagen Fibrils in Rat Tail-Tendon as a Function of age. Connect Tissue Res 19:51–62. https://doi.org/10.3109/03008208909016814

70. Provenzano PP, Vanderby R (2006) Collagen fibril morphology and organization: Implications for force transmission in ligament and tendon. Matrix Biol 25:71–84. https://doi.org/10.1016/j.matbio.2005.09.005

71. Szczesny SE, Elliott DM (2014) Interfibrillar shear stress is the loading mechanism of collagen fibrils in tendon. Acta Biomater 10:2582–2590. https://doi.org/10.1016/j.actbio.2014.01.032

72. Screen HRC, Lee DA, Bader DL, Shelton JC (2004) An investigation into the effects of the hierarchical structure of tendon fascicles on micromechanical properties. Proc Inst Mech Eng [H] 218:109–119. https://doi.org/10.1243/095441104322984004

73. Rigozzi S, Müller R, Stemmer A, Snedeker JG (2013) Tendon glycosaminoglycan proteoglycan sidechains promote collagen fibril sliding—AFM observations at the nanoscale. J Biomech 46:813–818. https://doi.org/10.1016/j.jbiomech.2012.11.017

74. Folkhard W, Mosler E, Geercken W, et al (1987) Quantitative analysis of the molecular sliding mechanisms in native tendon collagen — time-resolved dynamic studies using synchrotron radiation. Int J Biol Macromol 9:169–175. https://doi.org/10.1016/0141-8130(87)90047-X

75. Gupta HS, Seto J, Krauss S, et al (2010) In situ multi-level analysis of viscoelastic deformation mechanisms in tendon collagen. J Struct Biol 169:183–191. https://doi.org/10.1016/j.jsb.2009.10.002

76. Nemetschek Th, Jelinek K, Knörzer E, et al (1983) Transformation of the structure of collagen: A time-resolved analysis of mechanochemical processes using synchrotron radiation. J Mol Biol 167:461–479. https://doi.org/10.1016/S0022-2836(83)80345-3

77. Lee AH, Elliott DM (2019) Comparative multi-scale hierarchical structure of the tail, plantaris, and Achilles tendons in the rat. J Anat 234:252–262. https://doi.org/10.1111/joa.12913

78. Lee AH, Szczesny SE, Santare MH, Elliott DM (2017) Investigating mechanisms of tendon damage by measuring multi-scale recovery following tensile loading. Acta Biomater 57:363–372. https://doi.org/10.1016/j.actbio.2017.04.011

79. Gautieri A, Pate MI, Vesentini S, et al (2012) Hydration and distance dependence of intermolecular shearing between collagen molecules in a model microfibril. J Biomech 45:2079–2083. https://doi.org/10.1016/j.jbiomech.2012.05.047

80. Obuchowicz R, Ekiert M, Kohut P, et al (2019) Interfascicular matrix-mediated transverse deformation and sliding of discontinuous tendon subcomponents control the viscoelasticity and failure of tendons. J Mech Behav Biomed Mater 97:238–246. https://doi.org/10.1016/j.jmbbm.2019.05.027

81. Szczesny SE, Caplan JL, Pedersen P, Elliott DM (2015) Quantification of Interfibrillar Shear Stress in Aligned Soft Collagenous Tissues via Notch Tension Testing. Sci Rep 5:14649. https://doi.org/10.1038/srep14649

82. Karathanasopoulos N, Angelikopoulos P, Papadimitriou C, Koumoutsakos P (2017) Bayesian identification of the tendon fascicle's structural composition using finite element models for helical geometries. Comput Methods Appl Mech Eng 313:744–758. https://doi.org/10.1016/j.cma.2016.10.024

83. Gaut L, Duprez D (2016) Tendon development and diseases. WIREs Dev Biol 5:5–23. https://doi.org/10.1002/wdev.201

84. Huang AH, Lu HH, Schweitzer R (2015) Molecular regulation of tendon cell fate during development: MOLECULAR REGULATION OF TENDON FATE. J Orthop Res 33:800–812. https://doi.org/10.1002/jor.22834

85. Kalson NS, Lu Y, Taylor SH, et al (2015) A structure-based extracellular matrix expansion mechanism of fibrous tissue growth. eLife 4:e05958. https://doi.org/10.7554/eLife.05958

86. Silver FH, Freeman JW, Seehra GP (2003) Collagen self-assembly and the development of tendon mechanical properties. J Biomech 36:1529–1553. https://doi.org/10.1016/S0021-9290(03)00135-0

87. Humphries SM, Lu Y, Canty EG, Kadler KE (2008) Active Negative Control of Collagen Fibrillogenesis in Vivo: INTRACELLULAR CLEAVAGE OF THE TYPE I PROCOLLAGEN PROPEPTIDES IN TENDON FIBROBLASTS WITHOUT INTRACELLULAR FIBRILS . J Biol Chem 283:12129–12135. https://doi.org/10.1074/jbc.M708198200

88. Canty EG, Kadler KE (2005) Procollagen trafficking, processing and fibrillogenesis. J Cell Sci 118:1341–1353. https://doi.org/10.1242/jcs.01731

89. Jimenez S, Harsch M, Rosenbloom J (1973) Hydroxyproline stabilizes the triple helix of chick tendon collagen. Biochem Biophys Res Commun 52:106–114. https://doi.org/10.1016/0006-291X(73)90960-1

90. Kulonen E, Mathews MB, Dorfman A (1953) Studies in Procollagen. I. Solubility. Proc Soc Exp Biol Med 84:424–428. https://doi.org/10.3181/00379727-84-20668

91. Banos CC, Thomas AH, Kuo CK (2008) Collagen fibrillogenesis in tendon development: Current models and regulation of fibril assembly. Birth Defects Res Part C Embryo Today Rev 84:228–244. https://doi.org/10.1002/bdrc.20130

92. Parra ER, Teodoro WR, Velosa APP, et al (2006) Interstitial and Vascular Type V Collagen Morphologic Disorganization in Usual Interstitial Pneumonia. J Histochem Cytochem 54:1315–1325. https://doi.org/10.1369/jhc.6A6969.2006

93. Svensson L, Aszódi A, Reinholt FP, et al (1999) Fibromodulin-null Mice Have Abnormal Collagen Fibrils, Tissue Organization, and Altered Lumican Deposition in Tendon. J Biol Chem 274:9636–9647. https://doi.org/10.1074/jbc.274.14.9636

94. Goh KL, Holmes DF, Lu H-Y, et al (2008) Ageing Changes in the Tensile Properties of Tendons: Influence of Collagen Fibril Volume Fraction. J Biomech Eng 130:. https://doi.org/10.1115/1.2898732

95. Kalson NS, Holmes DF, Kapacee Z, et al (2010) An experimental model for studying the biomechanics of embryonic tendon: Evidence that the development of mechanical properties depends on the actinomyosin machinery. Matrix Biol 29:678–689. https://doi.org/10.1016/j.matbio.2010.08.009

96. Takaluoma K, Lantto J, Myllyharju J (2007) Lysyl hydroxylase 2 is a specific telopeptide hydroxylase, while all three isoenzymes hydroxylate collagenous sequences. Matrix Biol 26:396–403. https://doi.org/10.1016/j.matbio.2007.01.002

97. Myllylä R, Wang C, Heikkinen J, et al (2007) Expanding the lysyl hydroxylase toolbox: New insights into the localization and activities of lysyl hydroxylase 3 (LH3). J Cell Physiol 212:323–329. https://doi.org/10.1002/jcp.21036

98. Demaurex N, Furuya W, D'Souza S, et al (1998) Mechanism of Acidification of the trans-Golgi Network (TGN): IN SITU MEASUREMENTS OF pH USING RETRIEVAL OF TGN38 AND FURIN FROM THE CELL SURFACE. J Biol Chem 273:2044–2051. https://doi.org/10.1074/jbc.273.4.2044

99. Greenspan DS (2005) Biosynthetic Processing of Collagen Molecules. In: Brinckmann J, Notbohm H, Müller PK (eds) Collagen: Primer in Structure, Processing and Assembly. Springer, Berlin, Heidelberg, pp 149–183

100. Holden P, Meadows RS, Chapman KL, et al (2001) Cartilage Oligomeric Matrix Protein Interacts with Type IX Collagen, and Disruptions to These Interactions Identify a Pathogenetic Mechanism in a Bone Dysplasia Family *. J Biol Chem 276:6046–6055. https://doi.org/10.1074/jbc.M009507200

101. Godard P, Biebuyck JJ, Daumerie M, et al (1978) Crystallization and melting of aqueous gelatin. J Polym Sci Polym Phys Ed 16:1817–1828. https://doi.org/10.1002/pol.1978.180161009

102. Saunders JT, Schwarzbauer JE (2019) Fibronectin matrix as a scaffold for procollagen proteinase binding and collagen processing. Mol Biol Cell 30:2218–2226. https://doi.org/10.1091/mbc.E19-03-0140

103. Musiime M, Chang J, Hansen U, et al (2021) Collagen Assembly at the Cell Surface: Dogmas Revisited. Cells 10:662. https://doi.org/10.3390/cells10030662

104. Sechler JL, Corbett SA, Schwarzbauer JE (1997) Modulatory Roles for Integrin Activation and the Synergy Site of Fibronectin during Matrix Assembly. Mol Biol Cell 8:2563–2573. https://doi.org/10.1091/mbc.8.12.2563

105. Toroian D, Lim JE, Price PA (2007) The Size Exclusion Characteristics of Type I Collagen: IMPLICATIONS FOR THE ROLE OF NONCOLLAGENOUS BONE CONSTITUENTS IN MINERALIZATION*. J Biol Chem 282:22437–22447. https://doi.org/10.1074/jbc.M700591200

106. Kuo CK, Petersen BC, Tuan RS (2008) Spatiotemporal protein distribution of TGF-betas, their receptors, and extracellular matrix molecules during embryonic tendon development. Dev Dyn Off Publ Am Assoc Anat 237:1477–1489. https://doi.org/10.1002/dvdy.21547

107. Germiller JA, Lerner AL, Pacifico RJ, et al (1998) Muscle and Tendon Size Relationships in a Paralyzed Chick Embryo Model of Clubfoot. J Pediatr Orthop 18:314–318

108. Marturano JE, Xylas JF, Sridharan GV, et al (2014) Lysyl oxidase-mediated collagen crosslinks may be assessed as markers of functional properties of tendon tissue formation. Acta Biomater 10:1370–1379. https://doi.org/10.1016/j.actbio.2013.11.024

109. Pan XS, Li J, Brown EB, Kuo CK (2018) Embryo movements regulate tendon mechanical property development. Philos Trans R Soc B Biol Sci 373:20170325. https://doi.org/10.1098/rstb.2017.0325

110. Yeung C-YC, Zeef LAH, Lallyett C, et al (2015) Chick tendon fibroblast transcriptome and shape depend on whether the cell has made its own collagen matrix. Sci Rep 5:13555. https://doi.org/10.1038/srep13555

111. Jones DL, Daniels RN, Jiang X, et al (2022) Mechano-epigenetic regulation of extracellular matrix homeostasis via Yap and Taz. BioRxiv 2022.07.11.499650

112. Hayashi N, Sato T, Yumoto M, et al (2019) Cyclic stretch induces decorin expression via yes-associated protein in tenocytes: A possible mechanism for hyperplasia in masticatory muscle tendon-aponeurosis hyperplasia. J Oral Maxillofac Surg Med Pathol 31:175–179. https://doi.org/10.1016/j.ajoms.2018.12.012

Chapter 2: Tendon Multiscale Mechanics are Dependent on Collagen Fibril Continuity

Findings Published in:

Peterson, Benjamin E., and Spencer E. Szczesny. "Dependence of tendon multiscale mechanics on sample gauge length is consistent with discontinuous collagen fibrils." *Acta biomaterialia* 117 (2020): 302-309.

2.1 Introduction

The initial objective of this thesis work was to investigate changes in the multiscale mechanical properties of tendon during development. Prior work has suggested that the transformation in loading capabilities observed during late stages of tendon development is mediated by an increase in fibril lengths [1, 2]. Indeed, changes in fibril characteristics have been shown to impact the transmission of force through the ECM network [3–7]. However, there is still active debate concerning the continuity/connectivity of collagen fibrils within mature tendon system and their effects on the multiscale load transmission through the collagenous networks [8–10]. Determining how fibril continuity influences the multiscale mechanical response is a critical first step to understanding how changes in fibril length may contribute to changes in loading behavior in late stages of tendon development.

The objective of this study was to assess the functional length of collagen fibrils in mature tendon by investigating the dependence of tendon multiscale mechanics on sample gauge length. While the macroscale mechanical properties of tendon are known to be sensitive to sample gauge length [11], the microscale mechanisms mediating this

effect are unclear. We hypothesized that, as the grip-to-grip length approaches the average length of the collagen fibrils, the tendon multiscale mechanical response will shift from a discontinuous to continuous fibril loading behavior, which will provide an in direct estimate of the functional fibril length in tendon. Multiscale experimental testing was performed on rat tail tendon fascicles to examine differences in fibril strains compared to the bulk tissue strains at different gauge lengths.

This study provides critical knowledge regarding the structural benchmarks that need to be established during tendon development. Importantly, it also demonstrated that changes in fibril continuity can be directly measured via the multiscale strain response. These findings enable future studies to examine the multiscale strain behavior to indirectly evaluate changes in collagen fibril lengths.

2.2 Materials & Methods

2.2.1 Sample Preparation

Twenty-two tail tendon fascicles were harvested from six one-year old Long Evan rats received from a separate IACUC-approved study. Upon harvesting, each sample was dragged through wet filter paper with light pressure to remove the paratenon and then stained with dichlorotriazinylaminofluorescein (5-DTAF; Invitrogen, Waltham, MA). Specifically, samples were incubated on a rotating mixer at room temperature for twenty minutes in 1.5 ml of a 5 µg/ml solution of 5-DTAF and 0.1 M sodium bicarbonate buffer (pH 9.0) [12]. After incubation, samples were washed with phosphate-buffered saline (PBS) for ten minutes to remove unbound stain.

2.2.2 Mechanical Testing

After staining, the sample ends were potted with cyanoacrylate [Loctite 454] in custom machined grips that incorporated a sinusoidal gripping surface (**Fig. 2.1 A-B**). Tissue samples were mounted into grips and secured using a compression plate with the screws tightened to 5 in-lb of torque. Samples were randomly assigned to four different gauge lengths (GLs) of 30 mm (n = 6), 20 mm (n = 6), 10 mm (n = 5), and 5 mm (n = 5) while maintaining tissue hydration with PBS. All tests were conducted utilizing a 10 lb load cell (Model 31; Honeywell Inc., Charlotte, NC) with an accuracy and sampling frequency of ± 0.067 N and 100 Hz, respectively. In order to measure the fascicle dimensions, each sample was twisted and placed in a custom uniaxial tensile-testing device mounted atop an inverted confocal microscope (A1R HD, Nikon, Tokyo, Japan) (**Fig. 2.1C**) with a PBS bath to ensure adequate hydration during testing. The twisted samples were loaded to 1 mN, and a stitched z-stack image (2.175 µm z-step, 0.83 µm/px resolution) was captured spanning ~3.5 mm of the tissue centered at the sample's midpoint. From the helical profile of the twisted sample, measurements of the major and minor diameters were made and used to calculate the cross-sectional area assuming an elliptical cross-section. The samples were then untwisted and preloaded to 1 mN to establish their initial reference lengths 30.53 ± 0.07 mm, 20.13 ± 0.17 mm,10.64 ± 0.57 mm, 5.35 ± 0.06 mm). Finally, the samples were preconditioned at 1% grip-to-grip strain for 5 cycles at 0.03 Hz.

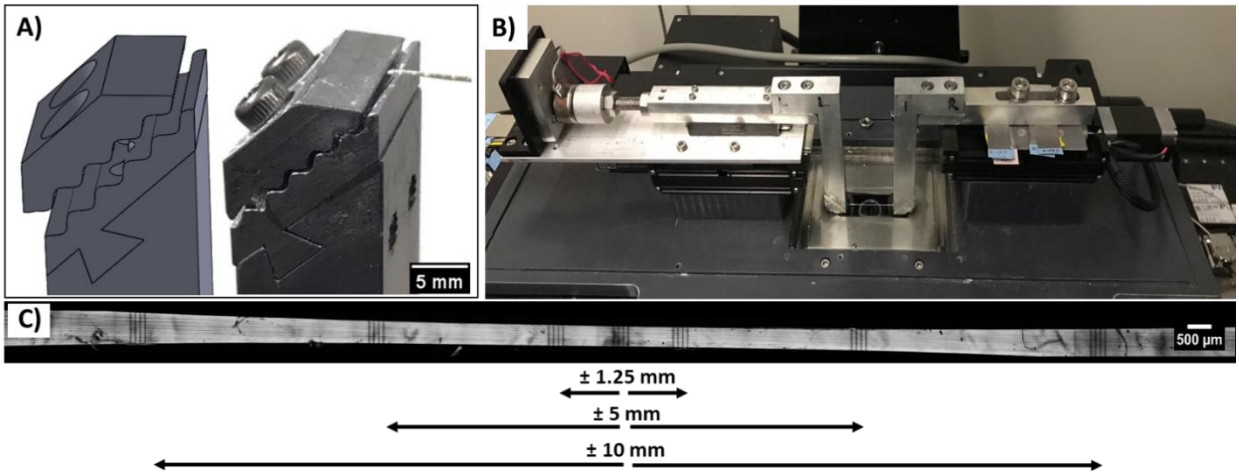

Figure 2.1: Experimental setup for multiscale mechanical testing. (A) Custom grips with a sinusoidal mounting face for compressing the tendon sample. B) Uniaxial tensile testing device mounted atop a confocal microscope. C) Representative image of a 30 mm gauge length sample with photobleached line (PBL) sets at the sample center and ± 1.25 mm, ± 5 mm, and ± 10 mm locations.

Following preconditioning, sets of photobleached lines (PBL) (4 lines, 100 µm apart, 5 µm wide) were bleached at the sample center and at ± 1.25 mm, ± 5 mm, and ± 10 mm from the center (as permitted by the sample gauge length) (Fig. 1D). Samples were then stretched in 2% grip-to-grip strain increments at 10%/min followed by a 15 min stress relaxation. At the end of each relaxation period, z-stack images (2.175 µm z-step, 0.83 µm/px resolution) were acquired at all PBL locations, and the microscope stage positions were recorded. Testing was stopped once there was a decrease in the equilibrium stress at the end of the relaxation period between strain increments. These incremental strain ramps and relaxation periods ensured that the applied stress values were stable while imaging the PBL sets, which were used to measure the fibril and macroscale tissue strains [13].

2.2.3 Image Processing and Data Analysis

Custom image processing code (MATLAB, MathWorks) was developed for determining the fibril strains from the PBL z-stack images as previously reported [13, 14]. In short, a two-dimensional projection of the curved tendon surface was generated using Sobel edge detection [14]. At every position across the tissue width, the pixel locations of each PBL were determined by the pixel with the lowest local intensity value. For each grip-to-grip strain increment, the microscale fibril strains were measured as the change in the distance between the photobleached lines within the PBL sites at the sample center and at the ± 1.25 mm locations. The fibril strains were then averaged across the three PBL sites to provide a single value for each grip-to-grip strain increment. The macroscale tissue strains were calculated optically as the change in distance between the centroid position of the ± 1.25 mm PBL sets as measured from the recorded microscope stage positions. To determine whether the collagen fibrils are functionally continuous, the fibril:tissue strain ratio was calculated at each grip-to-grip strain increment by dividing the fibril strain by the macroscale tissue strain. As previously shown [8], this ratio is equal to one in the case of continuous collagen fibrils and is below one for discontinuous fibrils.

The equilibrium modulus, ultimate tensile strength (UTS), and percent stress relaxation were calculated to determine the tendon macroscale response as a function of sample length. A moving average (step size = 30 data points) was used to smooth the values from the load cell. The equilibrium stress value for each grip-to-grip strain increment was calculated by averaging the last 30 seconds of data within the 15 min relaxation period and plotted versus the optically measured tissue strain. The equilibrium modulus for each sample was then calculated by fitting a line through the initial portion of

this stress-strain curve (i.e., data points between 0 and 1.5% strain). The UTS was defined as the peak stress value over the course of the test, and the percent stress relaxation was calculated as the relative decrease in stress during each relaxation period.

2.2.4 Grip Effects and Strain Heterogeneity

To ensure that the results for the smaller gauge length samples were not confounded by strain concentrations resulting from gripping, we evaluated the strain heterogeneity along the sample lengths at the highest grip-to-grip strain prior to the onset of failure (i.e., decrease in equilibrium stress). Specifically, the regional macroscale tissue strain was measured as the change in distance between each neighboring set of photobleached lines (i.e., strain between the grip interface and the 10 mm PBL set, 10 and 5 mm PBL sets, 5 and 1.25 mm PBL sets, 1.25 mm and center PBL sets). Given the symmetric placement of the PBL sets along the sample length, the regional strain values from each side of the sample were averaged together and plotted as a function of the distance between the grip and the sample center.

We also investigated whether potential strain heterogeneity across the sample length affected the measurement of the fibril:tissue strain ratio described above (section 2.3). To ensure consistency with previous work [13], the 30 mm gauge length samples were used for this evaluation. Specifically, the fibril strains were calculated by averaging the values at the ± 1.25 mm PBL locations, and the fibril:tissue strain ratio was calculated by dividing this value by the macroscale tissue strain measured between these two locations. This was repeated to calculate the fibril:tissue strain ratio using the ± 5 mm and ± 10 mm PBL sites. For each calculation of the fibril:tissue strain ratio, the change with increasing tissue strain was determined. By comparing the behavior of the fibril:tissue

strain ratios calculated using the different PBL sites, we can determine whether our measurements (and importantly our interpretation regarding fibril continuity) are influenced by the PBL locations.

2.2.5 Statistical Methods

Based on previous data [13], we expect that the fibril:tissue strain ratio will start at one and decrease with increasing applied tissue strains, which is consistent with discontinuous collagen fibrils and plastic interfibrillar shear load transfer [8]. Therefore, to evaluate whether the multiscale mechanical response at different gauge lengths is consistent with discontinuous fibrils, linear regressions were conducted to test whether the fibril:tissue strain ratio was negatively correlated with the applied tissue strain, and an ANCOVA was used to test for differences in the slope for each gauge length. Additionally, Student's t-tests were used to determine if the fibril:tissue strain ratio was different from one at the largest strain increment. However, given that the last strain increment exhibited a drop in the equilibrium stress, which may indicate fibril rupture, we also analyzed the data excluding the last strain increment and any data points where there was a reduction in sample number due to sample rupture. A one-way ANOVA was conducted to test whether the UTS and macroscale equilibrium modulus were affected by the sample gauge length. Post-hoc Dunnett's tests corrected for multiple comparisons were then conducted to evaluate the UTS and modulus differences compared to the 30 mm gauge length samples. An ANCOVA was utilized to test whether the percent stress relaxation (controlling for the applied tissue strain) was dependent on the sample gauge length with Bonferroni post-hoc tests. Finally, an ANCOVA was conducted to test whether the slope between the fibril:tissue strain ratio and the applied tissue strain was dependent on the

location of the PBL sets for the 30 mm samples. All data sets were confirmed to be normally distributed with a Kolmogorov-Smirnov test prior to statistical assessment. Statistical tests were conducted utilizing GraphPad Prism (Version 8.3.0) and R (Version 3.6.6), statistical significance was set to $p < 0.05$, and all data are presented as the mean ± the standard deviation.

2.3 Results

2.3.1 Accounting for Strain Heterogeneity Along Sample Length

Using the multiple sets of lines photobleached onto each sample, the macroscale tissue strains were calculated at various points along the sample length to assess the strain heterogeneity and possible grip effects for each gauge length. At 6% grip-to-grip strain, a clear strain gradient was observed with large strains near the grip interface and low strains near the center of the sample (**Fig. 2.2**). Importantly, we did not find large macroscale tissue strains at the sample center for the short gauge length samples. This suggests that, even for the 5 mm gauge length samples, the macroscale strain measurements calculated using the ± 1.25 mm PBL sites did not include the strain concentrations at the grips. Additionally, we confirmed that this strain heterogeneity was also observed with different types of sample grips to ensure that it is not an artifact unique to our setup (**Fig. 2.3**).

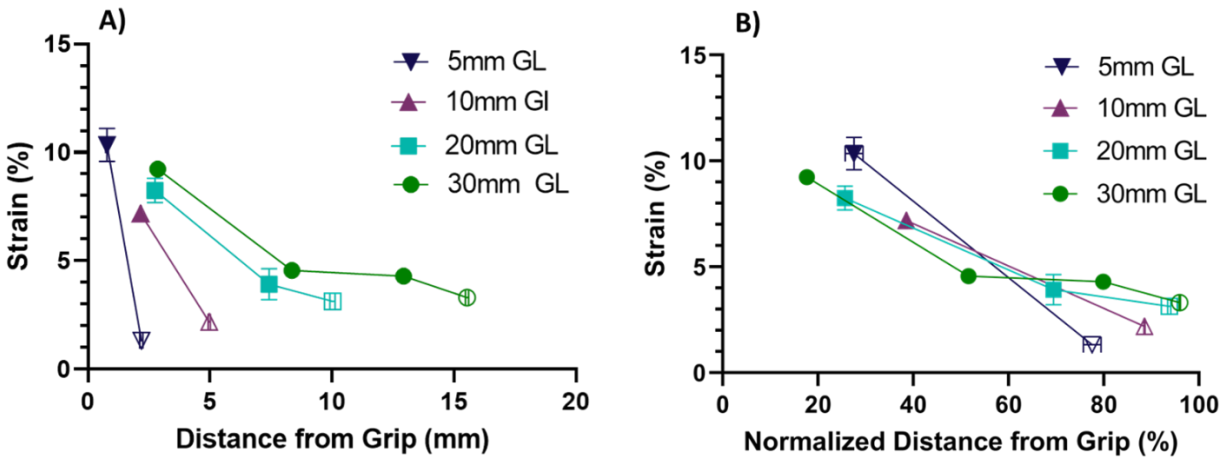

Figure 2.2: *Strain heterogeneity along tissue length at 6% grip-to-grip strain for each sample gauge length.* ***A)*** *All sample lengths exhibited significant strain gradients, which increased with decreasing sample length.* ***B)*** *Normalizing the distance from the grip by the length between the grip and the sample center shows that the macroscale tissue strains nearest the sample center calculated using the ± 1.25 mm PBL sets (unfilled data points) are comparable for all groups.*

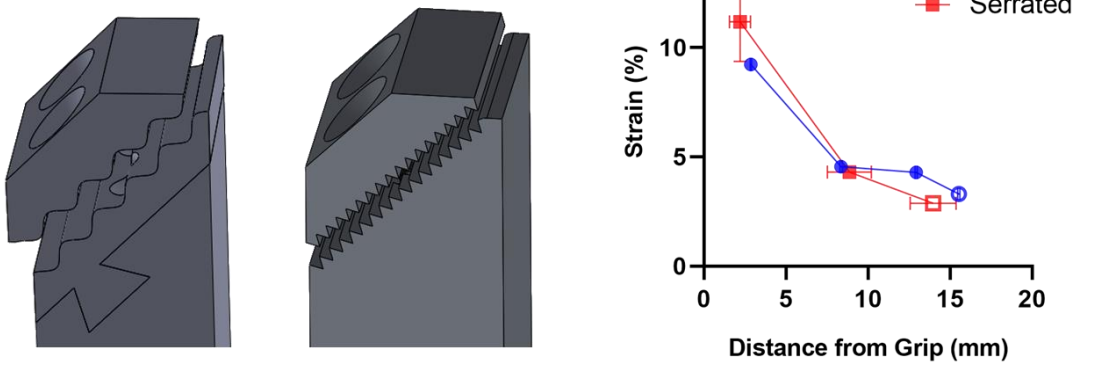

Figure 2.3: Strain heterogeneity along tissue length at 6% grip-to-grip strain for a 30 mm gauge length (GL) sample utilizing different grip types (sinusoidal and serrated). Both samples, regardless of the grip type used, exhibited a similar strain gradient from the grip interface towards the sample center. Macroscale tissue strains calculated using the ± 1.25 mm PBL sets (unfilled data points) are comparable and not unique to the gripping technique utilized in our setup.

The large macroscale tissue strain gradients observed in Fig. 2 suggest that the measurement of the fibril:tissue strain ratio may be dependent on the location of the photobleached lines. In addition, as the distance separating the PBL sets is reduced, the strain between the PBL sets (i.e., macroscale tissue strain) will approach the strain between the individual photobleached lines (i.e., fibril strain). Therefore, we investigated whether the negative correlation between the fibril:tissue strain ratio and the applied tissue strain observed previously using PBL sites at ± 5 mm [13] is still measurable when using the ± 1.25 mm PBL sites. Tests conducted on 30 mm gauge length samples indicate that, while the absolute value of the fibril:tissue strain ratio depends on the location of the PBL sites used to calculate the macroscale strains, the dependence on the applied tissue strain remains consistent (**Fig. 2.4**). Specifically, the fibril:tissue strain ratio at the last strain increment was significantly less than one ($p < 0.001$) for all PBL site locations. Additionally, linear regressions showed a significant negative slope ($p < 0.001$) with increasing applied tissue strain regardless of which PBL sites were utilized. Furthermore, the slopes themselves were not statistically different from one another ($p = 0.72$). Altogether, these findings demonstrate that the data obtained using the ± 1.25 mm PBL sites is consistent with previous studies showing discontinuous collagen fibril behavior for 30 mm tendon fascicles and can be used to compare results from samples with smaller gauge lengths without influence from gripping artifacts.

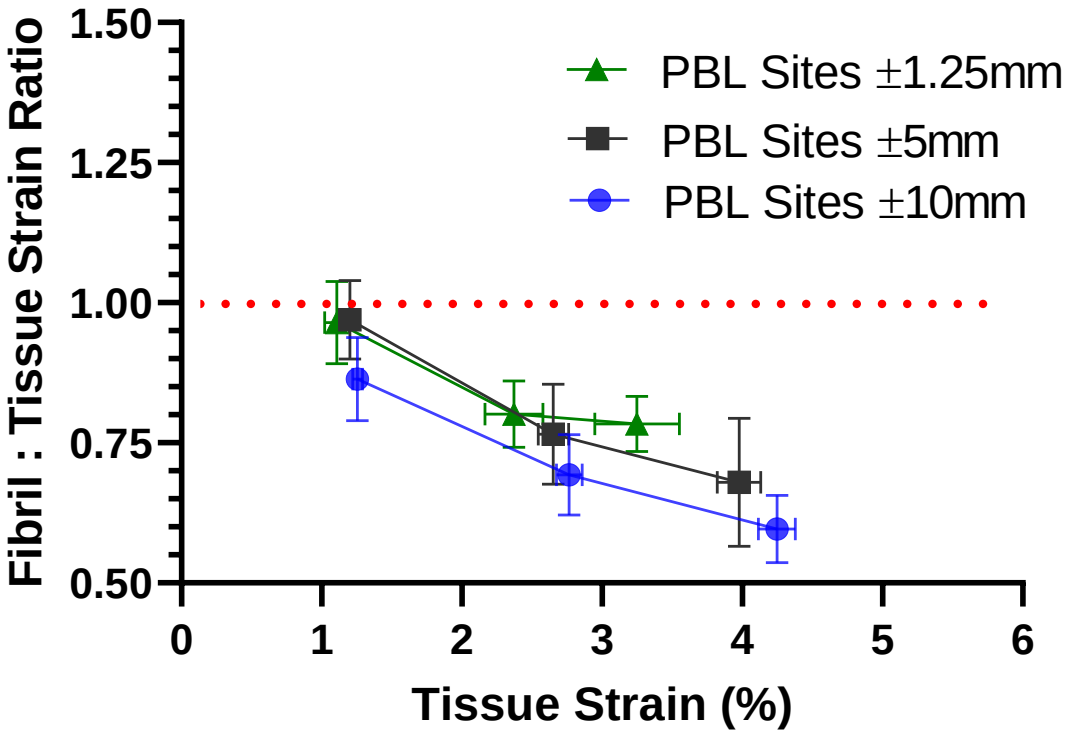

Figure 2.4: Fibril:tissue strain ratio in 30 mm long samples calculated using PBL sets at different positions along sample length. Regardless of the PBL sets used to measure the multiscale tendon strains, the fibril:tissue strain ratio showed the same negative correlation with the applied tissue strain ($p = 0.72$). This demonstrates that the ±1.25 mm PBL sets can be used to measure a valid fibril:tissue strain ratio.

2.3.2 Dependence of Tendon Multiscale Mechanics on Sample Gauge Length

After validating that the ± 1.25 mm PBL sets can be used to provide accurate measurements of the fibril:tissue strain ratio and macroscale tissue strains, we used these PBL sets to investigate whether tendon multiscale mechanics is affected by the sample length. At the macroscale level, we found a clear difference between the shorter (≤ 10 mm) and longer (≥ 20 mm) samples (**Fig. 2.5**). Specifically, the 5 mm and 10 mm samples had a significantly greater equilibrium modulus compared to the 30 mm samples ($p < 0.001$). Note that only the data points between 0 and 1.5% tissue strain were used to calculate the equilibrium modulus. The stress relaxation following each strain increment increased with the applied tissue strain ($p < 0.001$) and was dependent on the sample gauge length ($p < 0.001$) (**Fig. 2.5C**). Post-hoc comparisons with the 30 mm samples demonstrated that the stress relaxation was not different for the 20 mm samples ($p = 0.8$) but was increased for the 5 and 10 mm samples ($p < 0.01$ and $p < 0.05$, respectively). Finally, no difference was observed with sample length for the UTS ($p = 0.41$) (Fig. 4D).

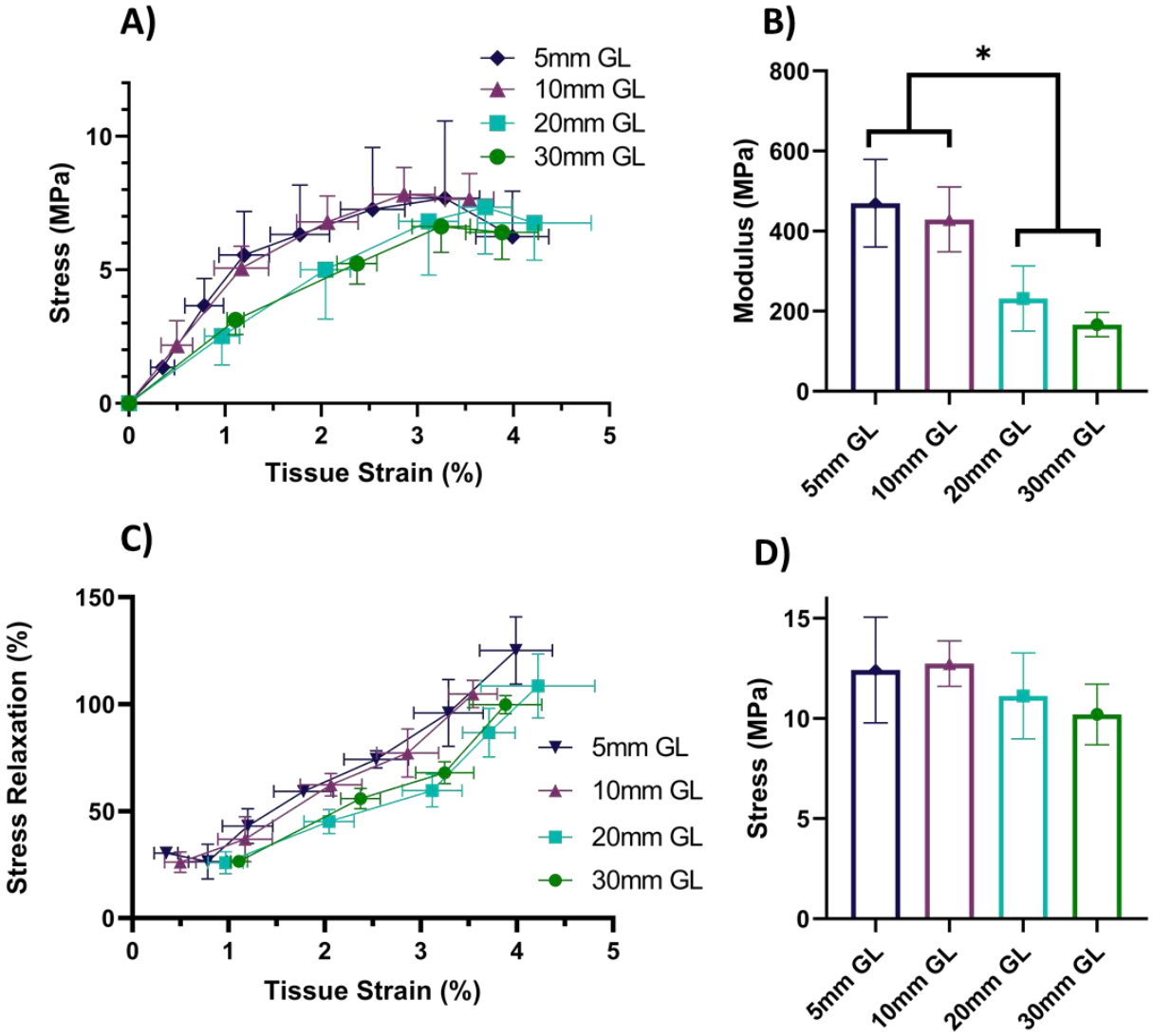

Figure 2.5: Tendon macroscale mechanical response at various gauge lengths. **A)** Equilibrium stress vs strain response for 30 mm (n=6), 20 mm (n=6), 10 mm (n =5) and 5 mm (n =5) gauge lengths. Note that, while one-sided error bars were used for clarity, the error is still symmetric about the mean. **B)** The macroscale tissue equilibrium modulus of the 5 mm and 10 mm samples was significantly greater than the 30 mm gauge length samples (* $p < 0.001$). **C)** The stress relaxation was also significantly greater in the 5 mm and 10 mm samples compared to the 30 mm samples ($p < 0.001$). **D)** While the ultimate tensile stress exhibited an increasing trend with decreasing gauge length, the difference was not statistically significant ($p = 0.41$).

Using the entire dataset for the analysis of the fibril strains, we found that the fibril:tissue strain ratio ultimately dropped below one for all sample lengths (30 mm: $p < 0.0001$, 20 mm: $p < 0.05$, 10 mm: $p < 0.005$, 5 mm: $p < 0.05$) (**Fig. 2.6A**). Additionally, there was a negative correlation between the fibril:tissue strain ratio and the applied tissue strain for all samples (30mm: $p < 0.0001$, 20mm: $p < 0.05$, 10 mm: $p < 0.01$, 5mm: $p < 0.001$) and the slopes were not significantly different between groups ($p = 0.50$). Given that sample failure may be due to fibril rupture [15, 16], which would decrease the fibril lengths and reduce the fibril:tissue strain ratio, we also analyzed the results excluding the data points suggestive of sample failure (i.e., the final strain increment that exhibited a drop in the equilibrium stress and any data points where there was a reduction in sample number due to sample rupture). With these adjustments, we found that the fibril:tissue strain ratio still dropped below one for the 30 mm and 20 mm gauge lengths ($p < 0.0001$ and $p < 0.05$, respectively) (**Fig. 2.6A**). However, prior to the onset of sample failure, the fibril:tissue strain ratio for the 5 mm and 10 mm samples was not statistically different from one ($p = 0.77$ and $p = 0.15$, respectively). Additionally, linear regressions of the fibril:tissue strain ratio with the applied tissue strain through only the pre-failure increments (filled data points) demonstrated a negative correlation for the 30 mm and 10 mm samples ($p < 0.0001$ and $p < 0.05$, respectively), while the 20 mm and 5 mm samples did not ($p = 0.09$ and $p = 0.27$, respectively). Therefore, the 5 mm gauge length samples were the only group that exhibited both a fibril:tissue strain ratio that was equivalent to one and was independent of the applied tissue strain prior to the onset of sample failure.

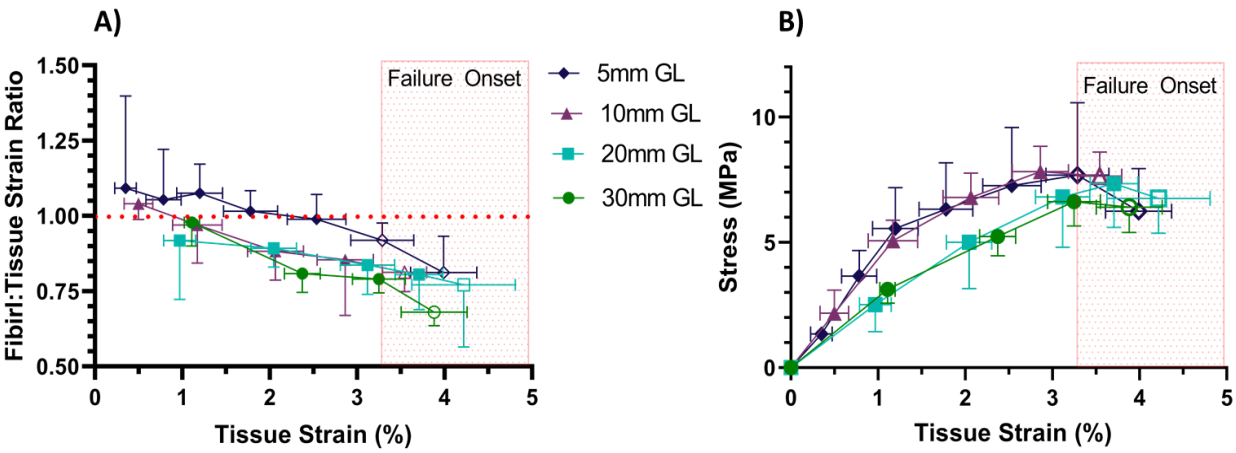

Figure 2.6: Multiscale mechanical response as a function of applied tissue strain for all sample gauge lengths (GL). **A)** Analysis of the full dataset demonstrated that ultimately the fibril:tissue strain ratio dropped below one for all samples (30 mm: $p < 0.0001$, 20 mm: $p < 0.05$, 10 mm: $p < 0.005$, 5 mm: $p < 0.05$) and was negatively correlated with applied tissue strain (30 mm: $p < 0.0001$, 20 mm: $p < 0.05$, 10 mm: $p < 0.01$, 5 mm: $p < 0.001$). Exclusion of data points suggestive of sample failure (unfilled markers) shows that the fibril:tissue strain ratio prior to failure still dropped below one for the 30 and 20 mm GL samples ($p < 0.0001$ and $p < .05$, respectively) and was negatively correlated with tissue strain for the 30 mm and 10 mm GL samples ($p < 0.001$ and $p < 0.05$ respectively). However, prior to failure, the fibril:tissue strain ratio for the 5 mm samples did not drop below one and was independent of applied tissue strain. **B)** Equilibrium stress vs. tissue strain for all samples, modified from Figure 2.5A. Unfilled data points indicate the strain increments where there was a drop in the equilibrium stress or there was a reduction in sample size due to sample rupture. The light red box is intended to highlight that the onset of sample failure (i.e., unfilled markers) is generally consistent for all sample lengths. While one-sided error bars were used for clarity, the error is symmetric about the mean.

2.4 Discussion

This study demonstrated that sample gauge length has a significant effect on the multiscale mechanical properties of tendon fascicles. More specifically, prior to the onset of failure, rat tail tendon fascicles with gauge lengths greater or equal to 20 mm exhibited a fibril:tissue strain ratio that is less than one and that decreases with increasing applied

tissue strain. Previous studies have suggested that this behavior is indicative of discontinuous fibrils that transfer loads via plastic interfibrillar sliding [8, 13]. In contrast, rat tail tendon fascicles with a 5 mm gauge length exhibited a pre-failure fibril:tissue strain ratio equivalent to one that is independent of the bulk macroscale tissue strain, suggesting that, prior to the onset of failure, the collagen fibrils were continuous between the grips at this gauge length [8]. This interpretation is further supported by an increase in the macroscale equilibrium tissue modulus in the 5 mm gauge length samples. Interestingly, the 10 mm gauge length samples exhibited a mixture of discontinuous and continuous fibril behavior. That is, while the 10 mm samples had a macroscale equilibrium modulus that was identical to the 5 mm samples, they exhibited a decrease in the fibril:tissue strain ratio with increasing applied tissue strain prior to the onset of failure, which is similar to the 30 mm samples and consistent with plastic sliding between discontinuous fibrils [8, 13]. We hypothesize that the 10 mm gauge length represents a transition between discontinuous and continuous fibril behavior in which a mixed population of continuous/discontinuous fibrils exists between the grips. This interpretation is consistent with previous estimates of fibril lengths of 0.86 - 12.7 mm in mature rat tail tendons [17, 18]. Furthermore, for a fibril length of 5-10 mm, shear lag modeling suggests that an interfibrillar shear stress of approximately 1 kPa is necessary to produce the multiscale mechanical behavior of tendon fascicles [13], which is within the 32 ± 33 kPa estimate obtained from previous experiments [14]. Together, these data support the hypothesis that collagen fibrils in rat tail tendon fascicles are discontinuous and have a length on the order of 5 to 10 mm.

After the onset of failure (i.e., a drop in the equilibrium stress), all samples, regardless of gauge length, exhibited a mechanical behavior consistent with discontinuous fibrils (i.e., a fibril:tissue strain ratio that was less than one and negatively correlated with the applied tissue strain) (**Fig. 2.6**). It is possible that the rapid reduction in the fibril:tissue strain ratio after the onset of failure for the 5 mm samples is due to rupture of a substantial proportion of the collagen fibrils. Further inspection of the multiscale mechanics of the 5 mm samples suggests that some fibril rupture may occur even in the pre-failure region of the stress-strain curve. Specifically, at approximately 1% tissue strain, there is a clear decrease in the slope of the stress-strain curve for the 5 mm samples (**Fig. 2.6B**). Interestingly, there also appears to be a decrease in slope for the fibril:tissue strain ratio (**Fig. 2.6A**) and an increase in the stress relaxation (**Fig. 2.5C**) for the 5 mm samples at this same data point. While speculative, we hypothesize that, prior to 1% applied tissue strain, the 5 mm samples have structurally continuous fibrils between the grips, agreeing with the constant fibril:tissue strain ratio of one, increased macroscale equilibrium modulus, and stable stress relaxation. Beyond 1% tissue strain, some of the fibrils rupture, initiating a partially discontinuous fibril response with a reduced macroscale tissue modulus and a decrease in the fibril:tissue strain ratio with increasing applied tissue strain. Additionally, the stress relaxation begins to increase with tissue strains above 1%. At the onset of macroscale sample failure (**red region in Fig. 2.6**), the fibril:tissue strain ratio drops more rapidly due to pervasive fibril rupture, which then leads to rupture of the whole sample.

This interpretation that the 5 mm samples undergo progressive fibril rupture during testing is consistent with studies suggesting that collagen fibrils are at least functionally

(if not structurally) continuous and that the primary failure mechanism within tendon is fibril rupture rather than excessive interfibrillar sliding [15, 16]. That is, even if the fibrils are discontinuous, they are long enough such that the axial stress that accumulates in the fibrils due to interfibrillar load transfer exceeds the fibril ultimate tensile strength [8]. This would suggest that regardless of fibril continuity, tendon failure is due to fibril failure. This is supported by a recent study by Hijazi et al. showing that tendon creep failure under static loading is the result of fibril denaturation and rupture rather than uncontrolled interfibrillar sliding [15]. Our current data also support this idea; even though the 5 mm samples initially behave as though the fibrils are continuous between the grips, they have a similar ultimate tensile strength as the 30 mm samples (Fig. 4D), which exhibit a discontinuous fibril behavior throughout testing. Furthermore, the greater stress relaxation in the 5 mm and 10 mm samples above 1% tissue strain (Fig. 4C) suggests that interfibrillar sliding [19–21] and fibril failure/denaturation [15, 22, 23] contribute additively to tendon viscoelastic behavior. This is further supported by the rapid increase in stress relaxation after the onset of failure (> 3.25% tissue strain) for all sample gauge lengths.

Based on current findings and existing literature, we propose that collagen fibrils are discontinuous with a length of 5-10 mm and that tendon damage is a combination of non-recoverable interfibrillar sliding and fibril rupture. With initial loading, there is little damage to the collagen fibrils, which is supported by creep testing showing that, prior to tertiary creep, the collagen fibrils are undamaged and exhibit full elastic recovery with unloading [15, 24]. At this point, permanent tendon elongation is due to non-recoverable interfibrillar sliding potentially resulting from damage to sacrificial small diameter fibrils

that transmit load between the larger diameter axial load-bearing collagen fibrils [5, 9, 25]. Nevertheless, the shear stress generated via interfibrillar sliding is sufficient to rupture these large diameter fibrils leading to macroscale tissue failure [15]. This is consistent with plastic shear lag modeling, which suggests that the interfibrillar shear stress would be about 1 kPa for collagen fibrils that, based on our current data, are approximately 10 mm long [13]. Assuming that the interfibrillar overlap between fibrils is on average half of the fibril length, the maximum axial stress within the fibrils can be calculated as $\tau L/r$ [10], where τ is the interfibrillar stress, L is the average fibril length, and r is the average fibril radius (i.e., 70 nm [17, 26]). This would produce a maximum fibril stress of about 140 MPa, which is within the range of the UTS estimated from mechanical testing of individual collagen fibrils [27, 28].

A significant issue with comparing mechanical data for soft tissue samples with varying gauge lengths is accounting for gripping artifacts. Indeed, using optical strain measurements, we found that there were large strain gradients along the sample lengths. Because these gradients were greatest for the samples with the smallest gauge lengths, the strains near the center of the samples (i.e., within the ± 1.25 mm PBL sites) were similar across groups and not affected by the large strain concentrations at the grips (**Fig. 2.4**). Therefore, the optical measurements of the macroscale tissue strain in this central region enabled accurate evaluation of the effects of sample gauge length on the multiscale mechanics of tendon fascicles. Highlighting this point, a previous study that used grip-to-grip measurement of the tissue strains found that the modulus of tendon fascicles decreases with smaller sample gauge lengths [11], which is the exact opposite

of our data. Since their calculations includes the strain concentrations at the grips, it is likely that the difference in methodology accounts for these incongruent findings.

A limitation to this study is that confocal microscopy does not have sufficient resolution to image collagen fibrils directly. Indeed, the resolution of our images was 0.83 μm/pixel, which is approximately 6 times the average fibril diameter [26]. However, this is significantly less than the 10–50 μm diameter of fibril bundles (i.e., fibers) [24]. Given that the photobleached lines remained continuous throughout testing down to the individual pixel, this suggests that our microscale measurements represent a local average of the individual fibril strains rather than the strains of fibril bundles. This is further supported by the fact that studies using X-ray diffraction to directly measure fibril strains in tendon also found that the fibril strains are substantially less than the applied tissue strains [19, 29]. An additional limitation is that rat tail tendon fascicles may not be representative of clinically relevant human tendons. While they share the same general hierarchical collagenous structure as other tendons [24], rat tail tendon fascicles also have certain unique structural features (e.g., acid-labile crosslinks) [16]. Nevertheless, previous studies estimated comparable fibril lengths in human patellar and hamstring tendons (> 14 mm) and rat tail tendon fascicles (~ 13 mm), suggesting that our findings may indeed apply to human tissue. Finally, it is possible that fibril lengths vary with age. Indeed, fibril lengths are known to change rapidly during embryonic and neonatal stages of development [1, 17, 30]. Future work will investigate whether these structural changes are responsible for the functional changes in tendon mechanics observed during the same time period [31].

2.5 Conclusions

This study demonstrates that sample gauge length has a significant effect on the multiscale mechanical properties of tendon fascicles. Specifically, as the gauge length is reduced, the fibril strains become equal to the macroscale tissue strains and the tissue equilibrium modulus increases. Together, this supports our hypothesis that collagen fibrils in tendon are discontinuous and suggests that they are approximately 5-10 mm long in rat tail tendon fascicles. While not structurally continuous, the significant length of the fibrils suggest that they may operate functionally continuous under physiological conditions, such that ultimate tendon failure is due to fibril rupture rather than excessive interfibrillar sliding. Nevertheless, establishing that the load-bearing fibrils are discontinuous highlights the importance of the intervening structures that transmit interfibrillar loads (e.g., small diameter sacrificial collagen fibrils) [9, 25].

This information provides critical information regarding how structural elements contribute to the loading capabilities of tendon and establish clear benchmarks required for functional tendon formation. Furthermore, these findings demonstrate that changes in fibril continuity can be measured by the multiscale loading behavior of the tendon. Suggesting that changes in fibril length during development may be measure via the multiscale mechanical response of the maturing tissue. Additionally, these experiments set clear testing protocols for future testing of embryonic tendons. Where a testing gauge length of 10+ mm is required to avoid potential artifacts in embryonic tendon testing.

2.6 References

1. Birk DE, Nurminskaya MV, Zycband EI (1995) Collagen fibrillogenesis in situ: Fibril segments undergo post-depositional modifications resulting in linear and lateral growth during matrix development. Dev Dyn 202:229–243. https://doi.org/10.1002/aja.1002020303

2. Birk DE, Zycband EI, Winkelmann DA, Trelstad RL (1989) Collagen fibrillogenesis in situ: fibril segments are intermediates in matrix assembly. Proceedings of the National Academy of Sciences 86:4549–4553. https://doi.org/10.1073/pnas.86.12.4549

3. Kalson NS, Holmes DF, Herchenhan A, et al (2011) Slow stretching that mimics embryonic growth rate stimulates structural and mechanical development of tendon-like tissue in vitro. Dev Dyn 240:2520–2528. https://doi.org/10.1002/dvdy.22760

4. Chen S, Birk DE (2013) The regulatory roles of small leucine-rich proteoglycans in extracellular matrix assembly. FEBS J 280:2120–2137. https://doi.org/10.1111/febs.12136

5. Fessel G, Snedeker JG (2009) Evidence against proteoglycan mediated collagen fibril load transmission and dynamic viscoelasticity in tendon. Matrix Biology 28:503–510. https://doi.org/10.1016/j.matbio.2009.08.002

6. Kalamajski S, Oldberg Å (2010) The role of small leucine-rich proteoglycans in collagen fibrillogenesis. Matrix Biology 29:248–253. https://doi.org/10.1016/j.matbio.2010.01.001

7. Banos CC, Thomas AH, Kuo CK (2008) Collagen fibrillogenesis in tendon development: Current models and regulation of fibril assembly. Birth Defects Research Part C: Embryo Today: Reviews 84:228–244. https://doi.org/10.1002/bdrc.20130

8. Szczesny SE, Elliott DM (2014) Incorporating plasticity of the interfibrillar matrix in shear lag models is necessary to replicate the multiscale mechanics of tendon fascicles. Journal of the Mechanical Behavior of Biomedical Materials 40:325–338. https://doi.org/10.1016/j.jmbbm.2014.09.005

9. Szczesny SE, Fetchko KL, Dodge GR, Elliott DM (2017) Evidence that interfibrillar load transfer in tendon is supported by small diameter fibrils and not extrafibrillar tissue components: INTERFIBRILLAR LOAD TRANSFER IN TENDON. J Orthop Res 35:2127–2134. https://doi.org/10.1002/jor.23517

10. Svensson RB, Herchenhan A, Starborg T, et al (2017) Evidence of structurally continuous collagen fibrils in tendons. Acta Biomaterialia 50:293–301. https://doi.org/10.1016/j.actbio.2017.01.006

11. Legerlotz K, Riley GP, Screen HRC (2010) Specimen dimensions influence the measurement of material properties in tendon fascicles. Journal of Biomechanics 43:2274–2280. https://doi.org/10.1016/j.jbiomech.2010.04.040

12. Szczesny SE, Edelstein RS, Elliott DM (2014) DTAF Dye Concentrations Commonly Used to Measure Microscale Deformations in Biological Tissues Alter Tissue Mechanics. PLoS ONE 9:e99588. https://doi.org/10.1371/journal.pone.0099588

13. Szczesny SE, Elliott DM (2014) Interfibrillar shear stress is the loading mechanism of collagen fibrils in tendon. Acta Biomaterialia 10:2582–2590. https://doi.org/10.1016/j.actbio.2014.01.032

14. Szczesny SE, Caplan JL, Pedersen P, Elliott DM (2015) Quantification of Interfibrillar Shear Stress in Aligned Soft Collagenous Tissues via Notch Tension Testing. Sci Rep 5:14649. https://doi.org/10.1038/srep14649

15. Hijazi KM, Singfield KL, Veres SP (2019) Ultrastructural response of tendon to excessive level or duration of tensile load supports that collagen fibrils are mechanically continuous. Journal of the Mechanical Behavior of Biomedical Materials 97:30–40. https://doi.org/10.1016/j.jmbbm.2019.05.002

16. Svensson RB, Mulder H, Kovanen V, Magnusson SP (2013) Fracture Mechanics of Collagen Fibrils: Influence of Natural Cross-Links. Biophysical Journal 104:2476–2484. https://doi.org/10.1016/j.bpj.2013.04.033

17. Craig AS, Birtles MJ, Conway JF, Parry DAD (1989) An Estimate of the Mean Length of Collagen Fibrils in Rat Tail-Tendon as a Function of age. Connective Tissue Research 19:51–62. https://doi.org/10.3109/03008208909016814

18. Provenzano PP, Vanderby R (2006) Collagen fibril morphology and organization: Implications for force transmission in ligament and tendon. Matrix Biology 25:71–84. https://doi.org/10.1016/j.matbio.2005.09.005

19. Puxkandl R, Zizak I, Paris O, et al (2002) Viscoelastic properties of collagen: synchrotron radiation investigations and structural model. Phil Trans R Soc Lond B 357:191–197. https://doi.org/10.1098/rstb.2001.1033

20. Gupta HS, Seto J, Krauss S, et al (2010) In situ multi-level analysis of viscoelastic deformation mechanisms in tendon collagen. Journal of Structural Biology 169:183–191. https://doi.org/10.1016/j.jsb.2009.10.002

21. Karathanasopoulos N, Angelikopoulos P, Papadimitriou C, Koumoutsakos P (2017) Bayesian identification of the tendon fascicle's structural composition using finite element models for helical geometries. Computer Methods in Applied Mechanics and Engineering 313:744–758. https://doi.org/10.1016/j.cma.2016.10.024

22. Zitnay JL, Jung GS, Lin AH, et al (2020) Accumulation of collagen molecular unfolding is the mechanism of cyclic fatigue damage and failure in collagenous tissues. Sci Adv 6:2795-2804. https://doi.org/10.1126/sciadv.aba2795

23. Lin AH, Allan AN, Zitnay JL, et al (2020) Collagen denaturation is initiated upon tissue yield in both positional and energy-storing tendons. Acta Biomaterialia 118:153–160. https://doi.org/10.1016/j.actbio.2020.09.056

24. Lee AH, Elliott DM (2019) Comparative multi-scale hierarchical structure of the tail, plantaris, and Achilles tendons in the rat. J Anat 234:252–262. https://doi.org/10.1111/joa.12913

25. Chang J, Garva R, Pickard A, et al (2020) Circadian control of the secretory pathway maintains collagen homeostasis. Nat Cell Biol 22:74–86. https://doi.org/10.1038/s41556-019-0441-z

26. Flint MH, Craig AS, Reilly HC, et al (1984) Collagen Fibril Diameters and Glycosaminoglycan Content of Skins— Indices of Tissue Maturity and Function. Connective Tissue Research 13:69–81. https://doi.org/10.3109/03008208409152144

27. Svensson RB, Hansen P, Hassenkam T, et al (2012) Mechanical properties of human patellar tendon at the hierarchical levels of tendon and fibril. Journal of Applied Physiology 112:419–426. https://doi.org/10.1152/japplphysiol.01172.2011

28. Yang L, van der Werf KO, Dijkstra PJ, et al (2012) Micromechanical analysis of native and cross-linked collagen type I fibrils supports the existence of microfibrils. Journal of the Mechanical Behavior of Biomedical Materials 6:148–158. https://doi.org/10.1016/j.jmbbm.2011.11.008

29. Folkhard W, Mosler E, Geercken W, et al (1987) Quantitative analysis of the molecular sliding mechanisms in native tendon collagen — time-resolved dynamic studies using synchrotron radiation. International Journal of Biological Macromolecules 9:169–175. https://doi.org/10.1016/0141-8130(87)90047

30. Richardson SH, Starborg T, Lu Y, et al (2007) Tendon Development Requires Regulation of Cell Condensation and Cell Shape via Cadherin-11-Mediated Cell-Cell Junctions. Mol Cell Biol 27:6218–6228. https://doi.org/10.1128/MCB.00261-07

31. McBride DJ, Trelstad RL, Silver FH (1988) Structural and mechanical assessment of developing chick tendon. International Journal of Biological Macromolecules 10:194–200. https://doi.org/10.1016/0141-8130(88)90048-7

Chapter 3: Mechanical Stimulation via Muscle Activity is Necessary for the Maturation of Tendon Multiscale Mechanics during Embryonic Development

Work Published in:

Peterson, B. E., Rolfe, R. A., Kunselman, A., Murphy, P., & Szczesny, S. E. (2021). Mechanical Stimulation via Muscle Activity is Necessary for the Maturation of Tendon Multiscale Mechanics during Embryonic Development. *Frontiers in cell and developmental biology*, 2471.

Findings from this chapter were the product of a collaborative study with Dr. Rebecca Rolfe and Dr. Paula Murphy from Trinity College, Dublin. More specifically, Dr. Rolfe carried out the reported histological characterization and, together with Dr. Murphy, contributed to the immobilization paradigm utilized in this study. The multiscale mechanical testing presented within this chapter varies from the original publication, in which a more thorough immobilization scheme was utilized to better investigate the role the muscle a paralysis in tendon development.

3.1 Introduction

The testing in the previous chapter demonstrated that the multiscale mechanical response in tendon is dependent on the continuity of the collagen fibril network and can be utilized for testing small tissue systems. More specifically, we demonstrated that fibril engagement can be artificially induced by a reduction in testing gauge length, increasing fibril loading and the ultimate macroscale tissue mechanics. These finding illustrate the distinctive importance of fibril lengths on the transmission of force throughout the collagenous ECM. Based on these findings, we hypothesized that an increase in collagen fibril lengths during development can be detected by a relative increase in the multiscale mechanical response.

Therefore, the primary objective of this study was to evaluate the multiscale mechanics of embryonic tendons to evaluate the structure-function relationships during late stages of chick development. Subsequent work then aimed to identify the role of muscle activity in driving tendon maturation by treating embryos with muscle paralysis agents. Specifically, we simultaneously measured the macroscale tensile mechanics and the deformations of the collagen fibrils (i.e., tensile strains) in tendons from chick embryos at different developmental stages. We hypothesized that the increase in tendon macroscale mechanical properties observed during development would coincide with an increase in the fibril strains and a reduction in interfibrillar sliding, which is consistent with increasing fibril lengths [1]. Additionally, we hypothesized that skeletal muscle paralysis would retard the changes in both the fibrillar deformations (i.e., strains) and the macroscale tensile properties observed during late embryogenesis. These findings will provide valuable insight into the structural mechanisms that drive tendon development and the role of mechanical stimulation in producing a robust tensile load-bearing tissue.

3.2 Materials and Methods

3.2.1 Chick Embryo Incubation and Manipulations

Chick embryos were used for this study since their relatively large size and accessibility simplifies mechanical testing procedures and experimental perturbations of muscle activity. Fertilized eggs (White Leghorn or Ross 308) were obtained from their respective suppliers (Poultry Education and Research Center, Pennsylvania State University or Allenwood Broiler Breeders, Kildare, Ireland) and incubated at 37.7^{o}C. All work at the Pennsylvania State University was approved by the Institutional Animal Care and Use Committee. Work on chick embryos does not require a license from the Irish

Ministry of Health under European Legislation (Directive 2010/63/EU); however, all work was approved by the Trinity College Dublin Ethics committee.

For embryo immobilization, the eggs were windowed at E3 and staged using Hamburger-Hamilton (HH) criteria. Briefly, 3 – 5 ml of albumin was removed from each egg using a wide gauge needle (16 ½). Scissors were then used to make a ~2 cm diameter window in the upper surface of the egg, which was covered with transparent tape to make an airtight seal. Eggs were checked daily to remove any unviable embryos. Immobilization was induced by dripping a treatment solution on the chorioallantoic membrane through the eggshell window (**Fig. 3.1**). Rigid paralysis of the skeletal muscles was induced by treatment with the neuromuscular blocking agent decamethonium bromide (DMB; Sigma Aldrich, St. Louis, MO) [2, 3] Flaccid paralysis was induced by treatment of the acetylcholine binding agent pancuronium bromide (PB; MP Biomedicals, Santa Ana, CA) [2–4]. As described in **Fig. 3.1**, immobilization was induced at E13 (HH39) with either 100ul of 0.2% DMB or 0.2% PB. Subsequent 50ul doses of the same 0.2% drug solution was administered daily from E14 - E19 to maintain immobilization. All solutions were prepared in sterile Hank's Balanced Salt Solution (HBSS, Gibco, Waltham, MA) with 1% antibiotic/antimycotic (penicillin, streptomycin, amphotericin B; Sigma Aldrich, St. Louis, MO). Control embryos were treated with HBSS and antibiotic/antimycotic alone.

Visual inspection of embryonic motility was used to assess musculoskeletal activity during development to determine the effectiveness of the treatments [5]. Control, rigid paralysis, and flaccid paralysis treated embryos (n = 5 - 6) were randomly selected for motility assessments from E15 (HH41) – E19 (HH45). Briefly, embryos were visually examined in the incubator daily through the transparent window over a 2-minute interval in real-time and any discernable individual movement (i.e., kicking or twisting) was counted. Motility counts (events / 2 mins) were averaged within each group to get a representative value for each treatment condition per day. Embryos were sacrificed either by sustained exposure to -20^{o}C followed by cervical dislocation or by decapitation and immediate placement in ice-cold phosphate buffered saline (PBS). All embryos were staged using Hamburger and Hamilton criteria [6] to ensure proper developmental comparisons as represented in **Fig. 3.1.**

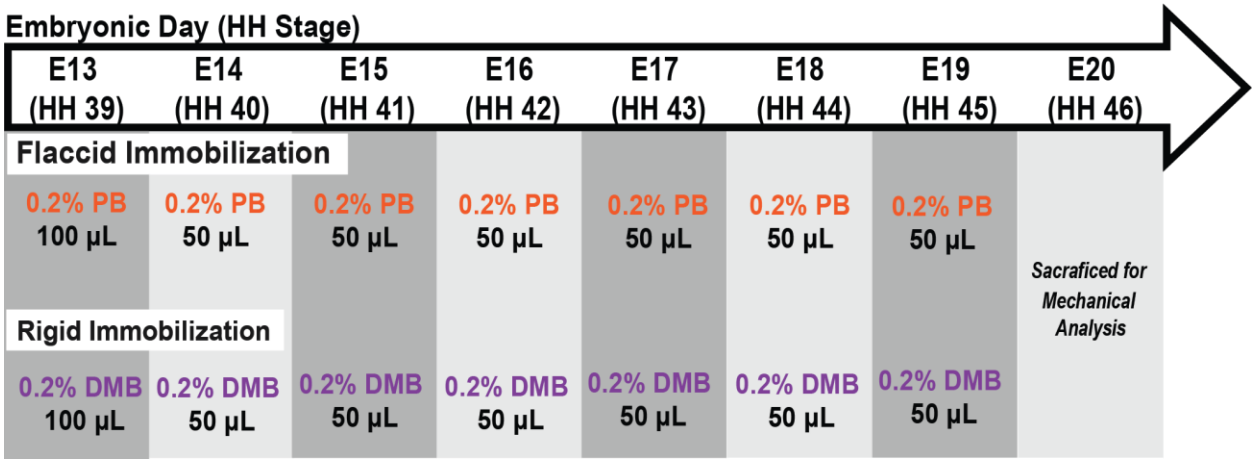

Figure 3.1: Schematic of immobilization treatment regimens via flaccid (PB) or rigid (DMB) paralysis agents. Embryos sacrificed for mechanical testing at E20. Abbreviations: HH, Hamburger and Hamilton stage; DMB, Decamethonium Bromide; and PB, Pancuronium Bromide.

3.2.2 Multiscale Mechanical Testing

Sample Preparation

Flexor digitorum brevis (FDB) digit II tendons from control embryos sacrificed at E16 (HH42) (n = 6), E18 (HH44) (n = 7), and E20 (HH46) (n = 7) were used to assess the multiscale mechanical changes during late embryonic development. Tendons (n = 7) from intermediate DMB and PB immobilized embryos were sacrificed at E20 (HH46), along with vehicle controls, to investigate the effect of immobilization during the same timeframe (**Fig. 3.1**). Hindlimbs were dissected and the FDB digit II tendon was isolated under a stereomicroscope (SMZ455T, Nikon, Tokyo, Japan). Upon harvesting, each sample was dragged through wet lens paper with light pressure to remove the paratenon sheath and then stained with dichlorotriazinylaminofluorescein (5-DTAF, Invitrogen, Waltham, MA) by incubating in a 5 µg/ml solution of 5-DTAF and 0.1 M sodium bicarbonate buffer (pH 9.0) for 10 minutes at room temperature. After incubation, samples were washed with PBS for ten minutes to remove unbound stain.

Mechanical Testing

A 10 mm spacer was placed between two custom grips [7] and a small amount of cyanoacrylate glue (Loctite 454) was placed on each grip face. Each stained sample was carefully lowered onto the grips such that the tarsometatarsal region of the tendon spanned the 10 mm gauge length with at least 5 mm of tissue within each grip face. Additional cyanoacrylate was added to each grip face and a drop of adhesive accelerator (Loctite 713; 3M, Charlotte, NC) was used to “pot” the tissue ends. Finally, a compression plate was added to each grip and tightened to ~ 5 inch-pounds of torque while maintaining tissue hydration with PBS.

The gripped samples were transferred to a custom uniaxial tensile-testing device mounted atop an inverted confocal microscope (Nikon A1R HD) with a PBS bath to ensure adequate hydration during testing. A preload of 0.1 g was applied, and the grip-to-grip distance was measured to establish the initial reference length. Sets of photobleached lines (PBL) (4 lines, 80 µm apart, 3 µm wide) were bleached at the sample center and ± 1.5 mm from the center (**Fig. 3.2**). Reference z-stack images were captured (2.5 µm z-step, 0.66 µm/px resolution) at each of the three PBL sites. The sample profile in the volumetric images was used to calculate the sample cross-sectional area (CSA) at all three PBL locations assuming an elliptical cross-section, which were averaged to determine a single CSA value. Samples were then stretched in 2% grip-to-grip strain increments at 10%/min followed by a 20-minute stress relaxation period. A prolonged relaxation period was applied to ensure that the applied stress values were stable prior to imaging [7]. At the end of each relaxation period, z-stack images were acquired at all PBL locations, and the confocal stage positions were recorded. Samples were then incrementally loaded, following the same procedure, until failure.

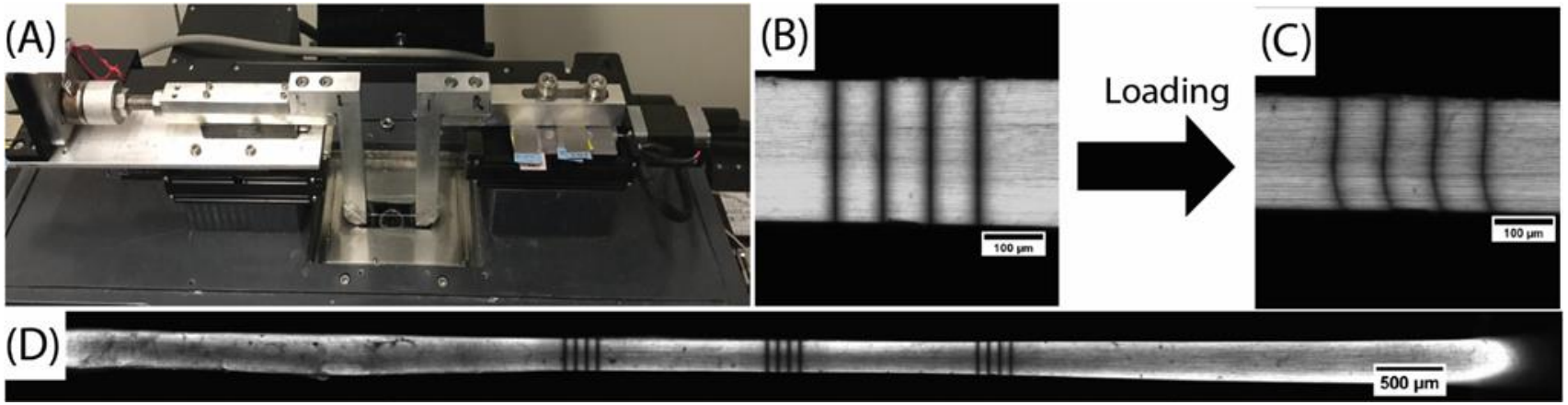

Figure 3.2. Experimental setup for multiscale mechanical testing. **(A)** Custom uniaxial tensile testing device mounted atop a confocal microscope. **(B & C)** Representative images of a photobleached line (PBL) site at prior to and after loading, respectively. **(D)** Tendon sample held at a 10 mm gauge length with PBL sets at the sample center and ± 1.5 mm.

Image Processing & Data Analysis

Custom image processing code (MATLAB, Mathworks) was used to determine the bulk macroscale tissue strains and the microscale fibril strains from the PBL z-stack images as previously reported [7]. Briefly, a Sobel edge detection strategy was utilized to create a two-dimensional projection of the curved tendon surface. At every position along the tissue width, the locations of the PBLs were identified as the pixel with the lowest local intensity value. For each strain increment and at each of the three PBL locations (sample center and ±1.5 mm), the microscale fibril strains were measured as the change in distance between the photobleached lines at every pixel location across the tissue width. Note that these measurements are representative local averages of the actual fibril strains since our imaging resolution was 0.66 μm/px while the average diameter of collagen fibrils in embryonic chick tendons ranges from 45 nm to 60 nm [8]. The measured fibril strains were then averaged across all pixels within a given set of PBLs, as well as between all three PBL locations, to generate a single representative value for fibril strains after each loading increment. To account for potential gripping artifacts, the macroscale bulk tissue strains were optically calculated utilizing the displacement of the peripheral (±1.5 mm) PBL sets. The fibril:tissue strain ratio was calculated at each applied strain increment by dividing the average fibril strain over the bulk tissue strain. Previous work from our lab has demonstrated that a fibril:tissue strain ratio less than one is expected for discontinuous fibrils and that the strain ratio will approach a value of one as the fibril lengths increase [1]. The level of interfibrillar sliding was quantified by the tortuosity (i.e., waviness) of the PBLs. Briefly, the angle of each

PBL (relative to the transverse axis of the tendon) was calculated at each pixel location along the tissue width and the standard deviation of these angles was calculated to characterize the representative amount of interfibrillar sliding [7]. Interfibrillar sliding was calculated after each strain increment at all PBL sites and averaged to obtain a single value.

The equilibrium modulus and ultimate tensile strength (UTS) were calculated to determine the macroscale mechanical properties of the samples. A moving average (window size = 30 data points) was used to smooth the output from the load cell. The equilibrium stress value for each strain increment was calculated by averaging the last 30 seconds of data within the 20-minute stress relaxation period and was plotted versus the optically tracked bulk tissue strains. The equilibrium modulus was calculated individually for each sample by fitting a line through the second loading increment and the increment preceding the UTS in an effort to minimize the contributions of the toe and failure regions, respectively. Individual sample moduli were then averaged to get a representative modulus for the group. The UTS was defined as the peak equilibrium stress value over the course of the test.

3.2.3 Morphological Analysis

Sectioning and Staining

All morphological processing and analysis were conducted by Dr. Rebecca Rolfe, Trinity College, Dublin. Embryos were sacrificed daily from E15 (HH41) to E20 (HH46) to assess the structural changes that occur during late tendon development. Briefly, the hindlimbs (distal to the knee joint) from each specimen were processed for paraffin wax

sectioning. A full series of longitudinal sections (8 µm) or cross sections (8 µm) through the midpoint of the tarsometatarsal region of interest (ROI) were prepared for each specimen (**Fig. 3.3**). Sections were dewaxed, rehydrated, and stained to highlight connective tissue using Masson Trichrome (HT15; Sigma-Aldrich, St. Louis, MO) or a fluorescently tagged natural pan-collagen binding protein (CNA35-eGF) [9]. Plasmid DNA encoding enhanced green fluorescent protein (eGFP) fused to the collagen binding protein (CNA35-eGFP) was kindly provided by the laboratory of Maarten Merkx, processed and purified as previously described [10]. Antigen retrieval was performed on histological sections using 0.01 M sodium citrate (pH 8) for 20 mins at 90°C prior to blocking of non-specific binding using 1% bovine serum albumin (BSA) in PBS for 1 h at room temperature. Slides were incubated overnight at 4°C with CNA35-eGFP (1 - 2 mg/ml) at a dilution of 1:20 - 1:50 in blocking solution. Post-antibody washes were performed in PBS and counterstained with DAPI. Histological specimens were photographed using an Olympus DP72 camera and CellSens software (v1.6). Confocal microscopy was carried out on a Leica SP8 scanning confocal using a 20X magnification objective. The confocal stack was processed and analyzed using ImageJ (v2.1.0/1.53c) software.

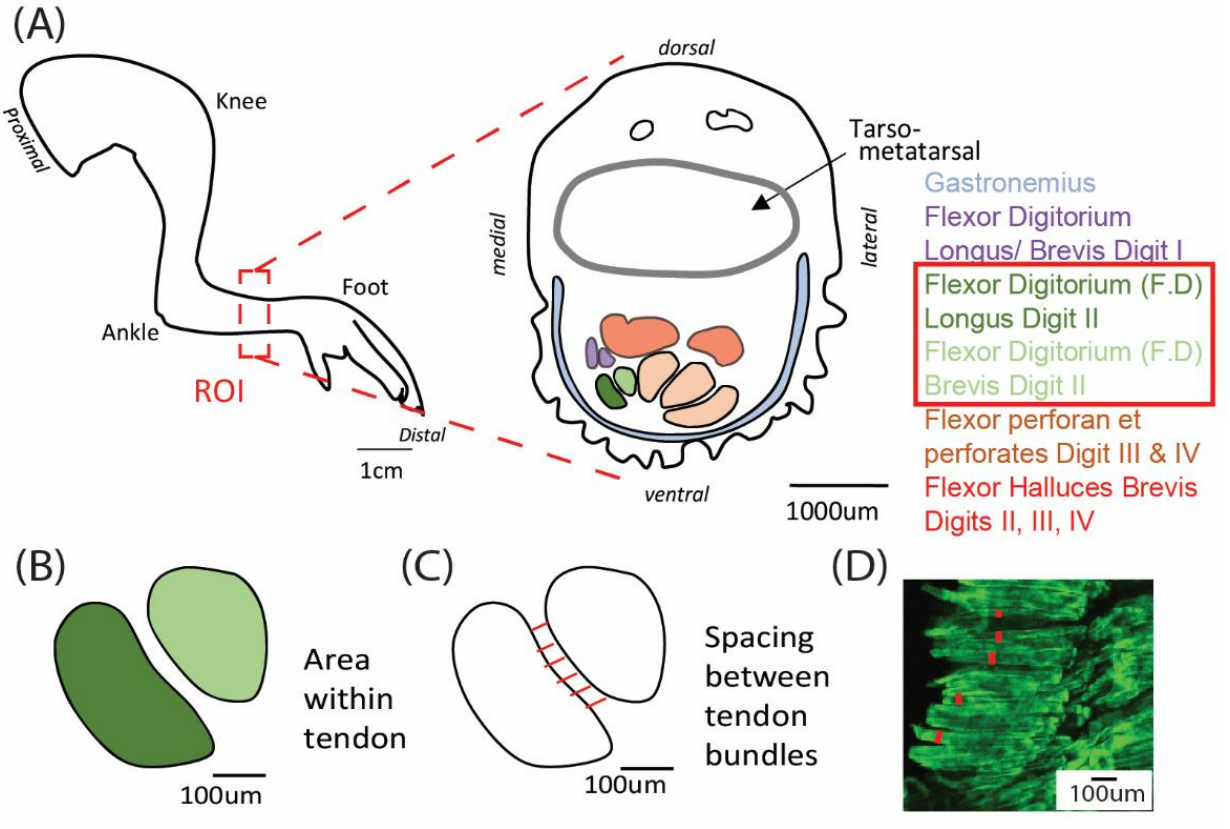

Figure 3.3: (A) Schematic of a chick embryonic hindlimb showing a region of interest (ROI) through the tarsometatarsal region, and detailed morphology of cross-sections through this ROI with individual tendons labelled and color matched. **(B)** Schematic of the flexor digitorium longus and brevis digit II tendons to quantify the cross-sectional area within a tendon, **(C)** and the spacing between tendons, shown by red lines. **(D)** Confocal data of collagen binding protein (CNA35-eGFP) stained fibers were used to measure fiber diameter, indicated with individual red lines. All scale bars indicated. – Figure generated by Dr. Rebecca Rolfe, Trinity College Dublin.

Measurement of Morphological Parameters

The cross-sectional areas of the flexor digitorum longus (FDL) and the flexor digitorum brevis (FDB) digit II tendons were measured from embryos across embryonic days E15 (HH41) - E19 (HH45) (n=2 for each, except E17 (HH43), n=5) using measurements from 7-14 adjacent Masson Trichrome stained cross-sections through a 700-1300 µm portion of the medial tarsometatarsal region of interest (ROI; **Fig. 3.3**). The boundary of collagen positive (blue) staining at the bundle edge was defined as the boundary of the tendon for quantification. The cross-sectional area of the FDL and FDB tendons were quantified independently using ImageJ (v2.1.0/1.53c).

The same medial ROI was used to assess the spacing between the FDL and FDB tendons over time (**Fig. 3.3**). For each section from each sample, 6-10 measurements were taken across the extent of the interface (where approximately parallel) between the tendons, and averaged, to represent the spacing between the tendons (**Fig. 3.3C)**; red lines indicate typical regions for measurement).

The collagen fiber diameters were estimated from confocal fluorescence volumetric images of the CNA35-eGFP stain across developmental stages. Two to three image planes from 5-9 ROIs (100 μm^2) per specimen were analyzed, which provided a measurement of 79-117 individual fibers per specimen (**Fig. 3.3**). Individual fibers in the 100 μm^2 ROI were measured using ImageJ software from edge to edge (**Fig. 3.3C)** as determined by a higher intensity of CNA35-eGFP fluorescence.

3.2.4 Statistical Analysis

Significance was set at $p \leq 0.05$ for all tests. For mechanical characterization, statistical analysis was conducted using SAS (9.4) and GraphPad Prism (8.3.0). A one-way ANOVA was conducted to evaluate the UTS and equilibrium modulus with respect to development or paralysis treatment. Post-hoc Tukey's tests corrected for multiple comparisons were conducted to evaluate the UTS and modulus with increased maturation. A post-hoc Dunnett's test corrected for multiple comparisons evaluated the effect of immobilization treatments compared to the vehicle control. An ANCOVA with Bonferroni post-hoc tests was used to determine if the embryonic motility was affected by development or immobilization treatment. Differences in the fibril:tissue strain ratio and interfibrillar sliding were evaluated using a linear mixed model that takes into consideration the correlated strain increments per specimen as a covariate [11]. A linear-regression was conducted to test whether the fibril:tissue strain ratio was negatively correlated with applied tissue strain and a one-sample t-test was conducted to determine if the group mean was significantly less than 1. For morphological analysis, differences in tendon area, distances between tendons, and fiber diameter were assessed by univariate ANOVA followed by Tukey post-hoc tests using SPSS (SPSS Statistics v26, IBM). Fiber bundle anisotropy was evaluated by a one-way ANOVA with a Dunnet's post-hoc test corrected for multiple comparisons.

3.3 Results

3.3.1 Changes in Tendon Multiscale Mechanics and Structure with Development

There was a significant increase in the macroscale modulus with development (**Fig. 3.4B**) ($p < 0.0001$) with significant differences observed between E16 (HH42) and

both E18 (HH44) ($p < 0.0001$) and E20 (HH46) ($p < 0.0001$) as well as between the E18 (HH44) and E20 (HH46) timepoints ($p < 0.05$). The ultimate tensile stress (UTS) was also significantly increased at later developmental timepoints (**Fig. 3.4C**) ($p < 0.0001$) with similar individual differences between the E16 (HH42) and both E18 (HH44) ($p < 0.001$) and E20 (HH46) timepoints ($p < 0.0001$) as well as between the E18 (HH44) and E20 (HH46) timepoints ($p < 0.001$). Finally, there was a significant increase in the tendon cross-sectional area as measured by confocal microscopy with development (**Fig. 3.4D**) ($p < 0.01$). Post-hoc comparisons found a significant difference between E16 (HH42) and E20 (HH46) ($p < 0.01$) as well as between E18 (HH44) and E20 (HH46) ($p < 0.05$) but no difference the E16 (HH42) and E18 (HH44) samples. These large changes in macroscale mechanics are consistent with prior data showing increases in mechanical properties during late tendon development [8].

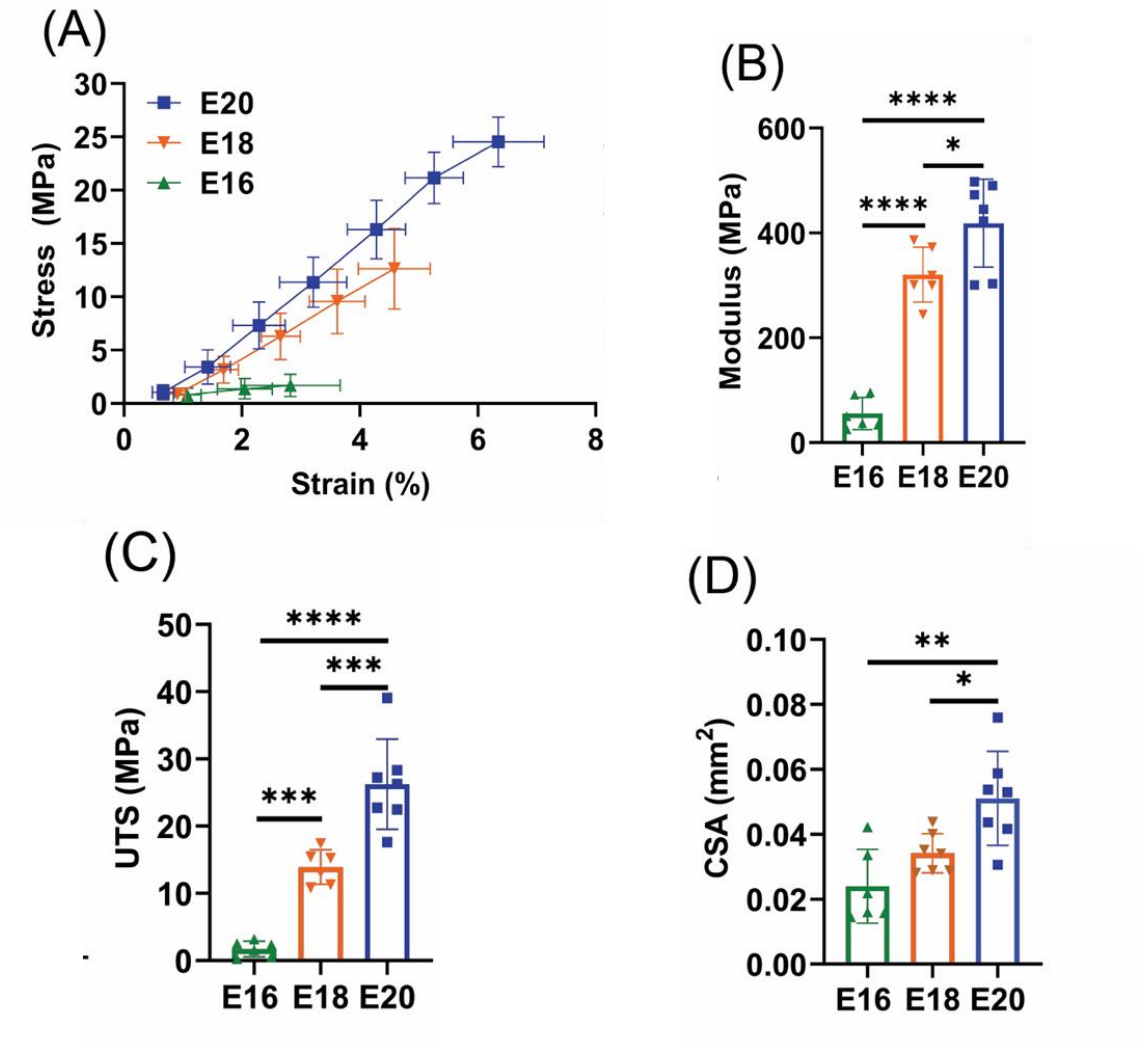

Figure 3.4. Flexor digitorum brevis (FDB) digit II tendon macroscale mechanical response with maturation. **(A)** Equilibrium stress vs. strain response for E16 (HH42, n = 6), E18 (HH43, n = 7), and E20 (HH46, n = 7) timepoints. **(B)** Significant increase in equilibrium modulus response with embryonic maturation. **(C)** Significant increase in ultimate tensile stress (UTS) with development. **(D)** A significant increase in the cross sectional (CSA) of the tendon was observed with maturation when measured under confocal microscopy. Significance was tested with a one-way ANOVA with post hoc Tukey's test corrected for multiple comparisons. Data represented as mean ± standard deviation. *p < 0.05, **p < 0.01,***p < 0.001, and ****p < 0.0001.

To assess the mechanisms underlying these macroscale mechanical changes during development, we measured the fibril:tissue strain ratio and interfibrillar sliding as a function of applied tissue strain. Previous work has demonstrated that a fibril:tissue strain ratio less than one is expected for discontinuous fibrils and that the fibril:tissue strain ratio will increase (while the interfibrillar sliding will decrease) as the collagen fibrils elongate [1, 12]. All embryonic samples, regardless of their developmental timepoint, displayed a mean fibril:tissue strain ratio that was less than one and negatively correlated with the applied tissue strain (**Fig. 3.5A**) (Control: $p < 0.05$, PB: $p < 0.0001$, DMB, $p < 0.001$). A linear mixed model found a significant increase in the fibril:tissue strain ratio between E16 and both the E18 (HH44) ($p < 0.05$) and E20 (HH46) ($p < 0.001$) timepoints.

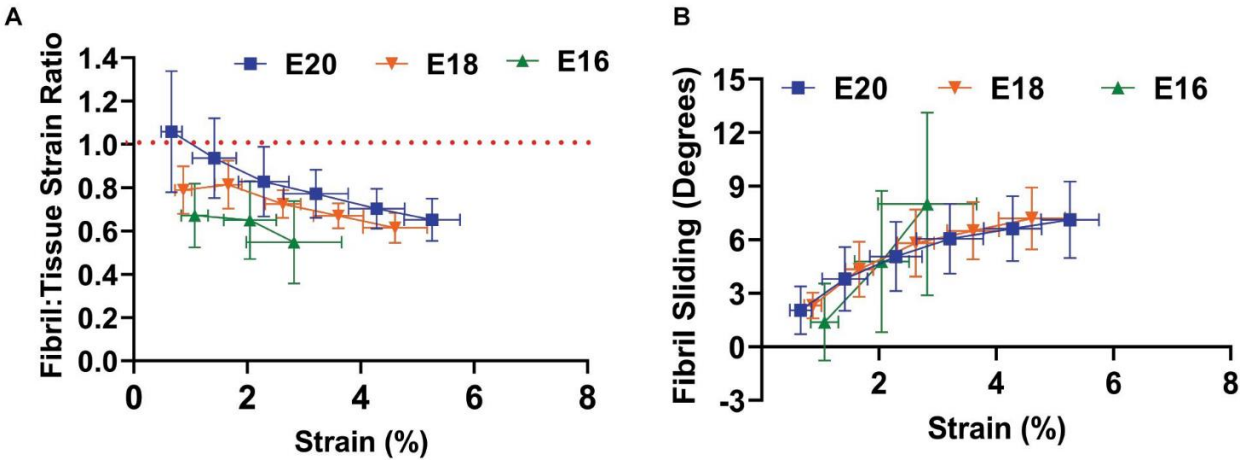

Figure 3.5: Multiscale mechanical response of the flexor digitorum brevis (FDB) digit II tendon as a function of applied tissue strain with increasing development. A significant increase in the fibril: tissue strain ratio was observed between E16 (HH42) vs. E18 (HH43; $p < 0.05$) and E16 (HH42) vs. E20 (HH46; $p < 0.001$). Data represented as mean ± standard deviation.

To profile the morphological changes in the FDL and FDB tendons over the developmental time window, transverse histological sections through the tendon midpoint were analyzed (**Fig. 3.2; Fig. 3.6A**). An increase in tendon size was observed through measurements of the cross-sectional area (**Fig. 3.6B**); in both tendons there was a steady increase in the mean value during development with a larger step increase at E17 (HH43), particularly for the FDL. The distance (spacing) between the tendons did not change significantly over time, but there was a visible increase between E15 (HH41) and E16 (HH46) (**Fig. 3.6A**), reflected in the mean distance measurement (**Fig. 3.6C**). Longitudinal sections, stained with the fluorescently tagged pan-collagen binding protein CNA35-eGFP, allowed visualization of the underlying collagen network across time **(Fig. 3.6D**). The fibril bundles (fibers) visibly enlarged, reflected in an incremental increase in the average fibril bundle diameter over time (**Fig. 3.6E**). There was no obvious change in the alignment of the fibril bundles over time, at least at this level of resolution.

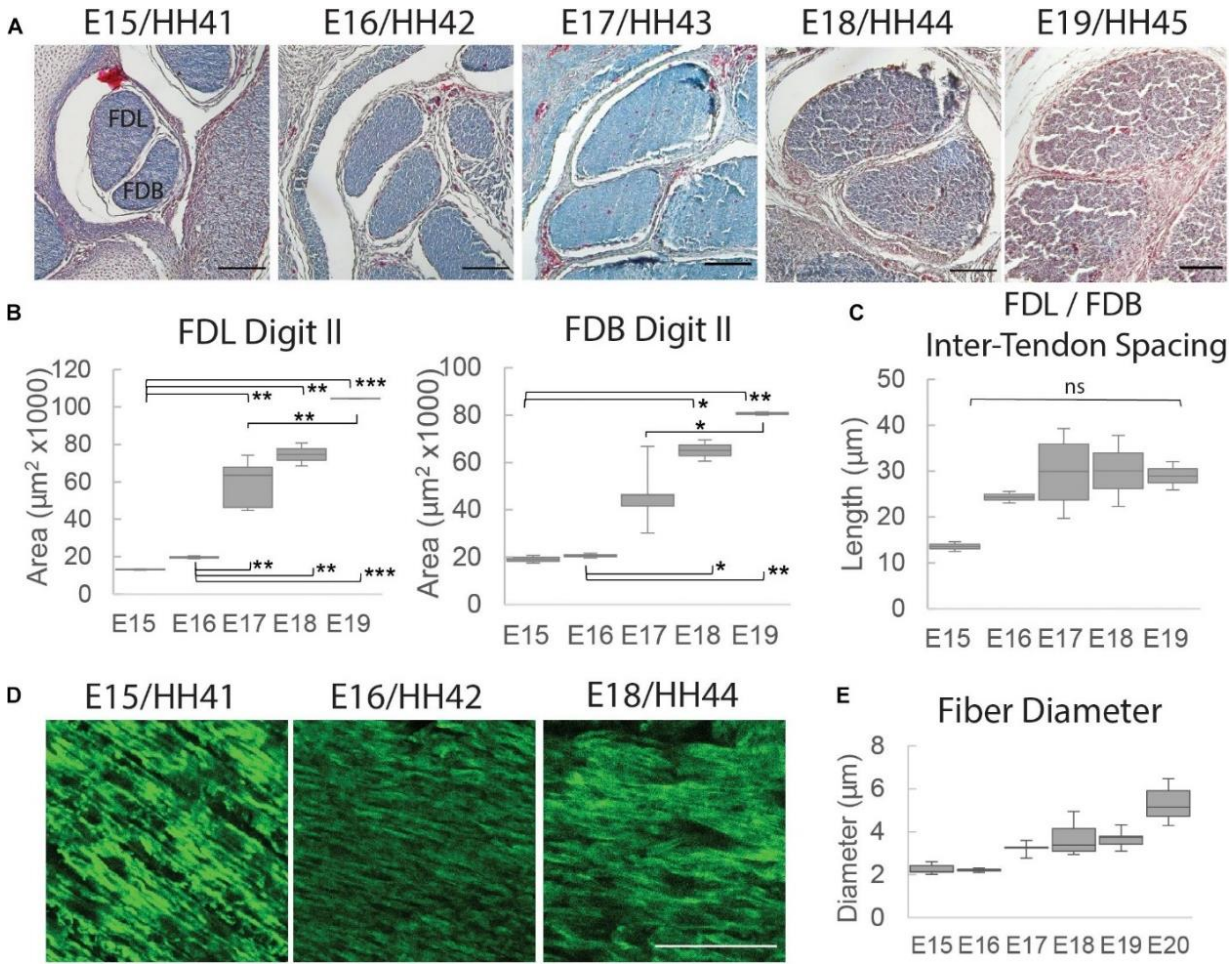

Figure 3.6. Structural analysis of tendons between E15 (HH41) and E19 (HH45). **(A)** Cross-sectional profile of the flexor digitorum longus (FDL) and brevis (FDB) digit II tendons stained with Masson Trichrome in the tarsometatarsal region of the developing chick hindlimb over embryonic days, as indicated. Scale bar 100 µm. **(B)** Box plots of cross-sectional area of the FDL and FDB digit II tendon over developmental time (plot whiskers indicate min and max data values). **(C)** Box plot of spacing measurements between the FDL and FDB digit II tendons over developmental time (measurements taken through a 700 – 1,330 µm portion of the medial tarsometatarsal region, see Supplementary Figure 1). **(D)** Images of longitudinal tendon fibers in the tarsometatarsal region stained with collagen binding protein over developmental time. Scale bar 50 µm. **(E)** Box plot of tendon fiber diameter measurements over time. Statistical analysis was carried by univariate ANOVA followed by Tukey post hoc tests. For (B) n = 2 per day except E17 (HH43) n = 5; For **(E)** n = 1 (multiple sections from 1 specimen/stage measured). *p ≤ 0.05, **p ≤ 0.01, and ***p ≤ 0.001. – Data Collected & Analyzed by Dr. Rebecca Rolfe, Trinity College Dublin

3.3.2 Effect of Muscle Paralysis on Tendon Development

Rigid and flaccid paralysis treatments significantly reduced embryonic motility through the target period (DMB: $p < 0.05$, PB $p < 0.05$) (**Fig. 3.7A**). No significant difference in motility was observed between the rigid DMB or flaccid PB paralysis treatments ($p = 0.76$). After validating the immobilization treatments, we investigated their effect on the mechanical and structural changes that occur during late embryonic development (**Fig. 3.7B-D**). At the macroscale level, both rigid (DMB) and flaccid paralysis (PB) significantly reduced the equilibrium modulus compared to vehicle control samples (**Fig. 3.7C**) ($p< 0.01$ and $p < 0.05$, respectively).

To investigate how the multiscale mechanics were perturbed under paralysis conditions, we measured the fibril:tissue strain ratio and interfibrillar sliding as a function of applied tissue strain for each treatment group. All samples (control, PB, and DMB) displayed a mean fibril:tissue strain ratio that was less than one ($p < 0.05$) and was negatively correlated with applied tissue strain (**Fig. 3.7D**) ($p < 0.001$). A linear mixed model found a significant decrease in the fibril:tissue strain ratio for the both immobilization treatments compared to control tissues ($p < 0.05$).

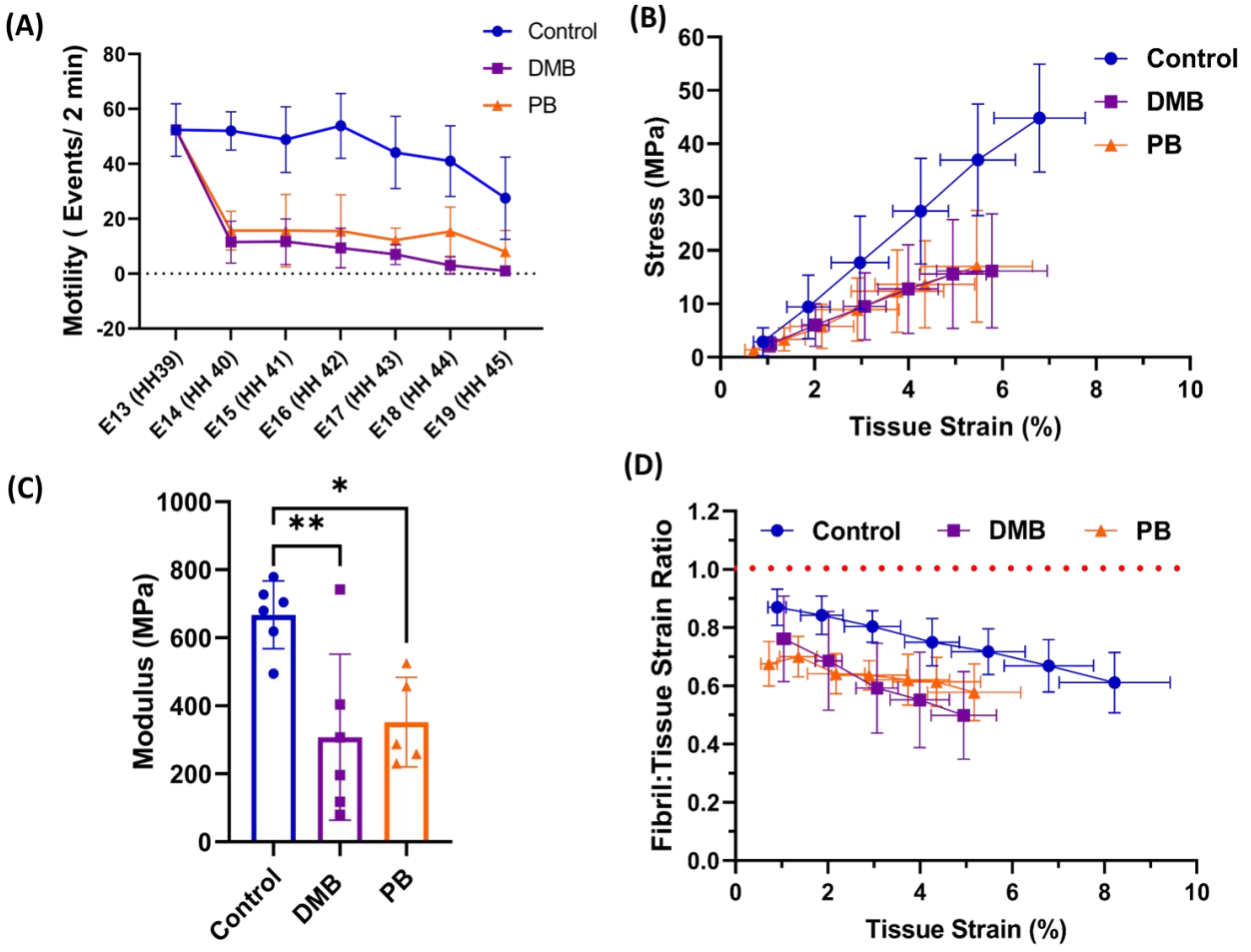

Figure 3.7: Muscle paralysis and its effect on the multiscale mechanical properties of the flexor digitorum brevis (FDB) digit II tendon during development **(A)** Paralysis treatments and saline control were conducted from E13 (HH39) – E19 (HH45). Significant decrease in motility was observed under rigid (DMB, $p < 0.01$) and flaccid (PB, $p < 0.01$). No significant difference in motility behavior was observed between the two immobilization methods. **(B)** Equilibrium stress vs. applied strain for E20 (HH46) samples following saline (n=6), DMB (n = 6), or PB (n= 5) treatments. **(C)** Equilibrium modulus is significantly reduced with both rigid paralysis (DMB, $p < 0.01$) and flaccid (PB, $p < 0.05$) treatments. **(D)** Multiscale mechanical response at E20 (HH46) as a function of applied tissue strain after immobilization treatments. The fibril:tissue strain ratio was significantly lowered following both rigid (DMB, $p < 0.05$) and flaccid paralysis (PB, $p < 0.05$) in comparison to saline controls. Data represented as mean ± standard deviation. $*p < 0.05$, $**p < 0.01$.

3.4 Discussion

This study demonstrated that there is a pivotal shift within tendon structure-function relationships during late stages of embryonic development that facilitates the functional load-bearing capabilities of tendons. Specifically, there is an increase in the fibril:tissue strain ratio after E16 (HH42) in chick embryos (**Fig. 3.4**), which is consistent with an increase in the length of the collagen fibrils [12, 13] and the increase in macroscale tensile mechanics (**Fig. 3.4**) [8]. Similar maturation at the microscale level has also been observed via measurement of the compressive mechanical properties of developing chick calcaneal tendons via atomic force microscopy [14]. It is also important to note that the E20 (HH46) tissue still displayed a negatively correlated fibril:tissue strain ratio at larger applied strains, which is consistent with discontinuous fibrils and not progressive breakage of continuous fibrils [7]. However, the observed upward shift in the fibril:tissue strain ratio with maturation indicates a transition in the collagenous loading behavior, in which strains are being transferred to the collagen fibrils more directly. While shorter fibrils should exhibit more relative sliding with tissue stretch [1, 12], no significant difference in interfibrillar sliding was observed between E16 and the later developmental timepoints. We have previously observed similar discrepancies between the change in the fibril:tissue strain ratio (or lack thereof) and the measurement of interfibrillar sliding, which we believe is due to heterogenous tissue loading possibly caused by gripping artifacts [15]. Additionally, the rapid changes in tissue ultrastructure observed at E16 [13] is likely responsible for the large variance in the interfibrillar sliding for this developmental timepoint, which may have masked a possible difference in the interfibrillar sliding. Rapid

development at this timepoint is further supported by morphological analysis of the FDB and FDL tendons, which showed a significant increase in the CSA (**Fig. 3.6B**) and an incremental increase in the average fiber diameter with development in the samples assayed (**Fig. 3.6E**). Together, this study supports our hypothesis that there is a reorganization of the collagenous network during late stages of tenogenesis that increases the strain transmitted to the collagen fibrils and generates a rapid increase in tendon mechanical properties.

Our findings also demonstrate that the observed changes in fibril loading and macroscale tensile mechanics are impeded by musculoskeletal paralysis, suggesting that mechanical stimulation during late stages of tenogenesis is critical to mediating developmental changes in the collagen fibril network. Specifically, both rigid and flaccid muscle paralysis reduced the macroscale modulus and UTS of the tissue. Similarly, both immobilization methods reduced the fibril:tissue strain ratio (**Fig. 3.7D**), suggestive of an impaired fibril loading behavior following the loss of muscle activity.

Interestingly, no differences in effect were observed between the two modes of immobilization despite their different mechanism of inducing paralysis. More specifically, PB competitively blocks the acetylcholine receptor at the motor endplate to inhibit muscle contraction, causing flaccid or limp paralysis [3]. In contrast, DMB irreversibly binds to acetylcholine receptors in the motor endplate to induce permanent contraction of muscle, generating a prolonged static load across the tissue [3]. These findings indicate that the static tension generated via the prolonged muscle contractions under DMB treatment was insufficient to elicit the mechanobiological activity required to initiate this collagenous

transformation in the tendon. This suggests that cyclical muscle stimulation plays an essential role in the formation of tendon tissue.

While our data suggest that mechanical stimulation plays an important role in driving the structural and mechanical changes observed during late tendon development, the biological mechanisms mediating this are unclear. Prior work has shown that the loss of mechanical stimulation during late stages of tendon development reduces LOX expression, inhibiting cross-linking activity within the collagenous network and reducing the tissue compressive modulus [16, 17]. Furthermore, a recent study has identified that increases in collagenous crosslinking and tissue stiffness is directly regulated by Piezo1 activation by shear deformation resulting from fiber/fibril sliding [18]. This suggests that the effects of mechanical stimulation on tendon development may be mediated by increased collagen crosslinks driven by activation of mechanosensitive ion channels. Still, numerous other ECM components are known to regulate collagen fibril interconnections, and it is not clear how they are affected by mechanical stimulation. For example, decorin and biglycan bind to the surface of collagen fibrils and inhibit collagen fibril fusion [19–22], which may explain the rapid change in collagen fibril structure during late tendon development [20, 23]. Furthermore, their relative expression decreases during development precisely when fibril lengths/diameters grow rapidly. However, previous work indicates that decorin expression is positively correlated to mechanical stimulation [24]. This suggests that the reduction in the fibril:tissue strain ratio (potentially due to a retardation in collagen fibril elongation) seen with immobilized animals (**Fig. 3.7D**) may not be due to a change in decorin or biglycan expression. Another important note is that there were still significant increases in tendon macroscale mechanics with immobilized

animals when compared to normally developing E16 tissue, suggesting that some load-bearing elements may develop independently of mechanosensitive mechanisms. Further investigations are required to characterize the changes in tendon structure-function relationships during late tendon development, its sensitivity to musculoskeletal stimulation, and other regulatory mechanisms that link these two. Overall, this study supports our hypothesis that mechanical stimulation during late tendon development plays a critical role in mediating the gross structural and mechanical changes across multiple length scales.

A limitation to this study is that confocal microscopy does not have the optical resolution required to directly visualize collagen fibrils. That is, our imaging resolution is 0.66 μm/px, while the average diameter of collagen fibrils during these developmental timepoints range from 45 nm to 60 nm [8]. However, fibril bundles (i.e., fibers) during this same developmental window are approximately 2 - 5 μm in diameter [25], suggesting that we are capturing a localized average fibril response. Finally, changes in fibril structure (e.g., fibril length, diameter, and interfibrillar spacing) and their dependence on musculoskeletal activity during late tendon development were not directly measured. Nevertheless, this study provides valuable insight into the multiscale structure-function relationships of developing tendons and the importance of mechanical stimulation in producing a robust tensile load-bearing soft tissue. While there is limited knowledge translating our findings within chick embryos to humans, we believe that this study provides foundational knowledge into the structure-function mechanisms that dictate critical periods of tendon development.

3.5 References:

1. Szczesny SE, Elliott DM (2014) Interfibrillar shear stress is the loading mechanism of collagen fibrils in tendon. Acta Biomaterialia 10:2582–2590. https://doi.org/10.1016/j.actbio.2014.01.032

2. Pitsillides AA (2006) Early effects of embryonic movement: “a shot out of the dark.” J Anatomy 208:417–431. https://doi.org/10.1111/j.1469-7580.2006.00556.x

3. Osborne AC, Lamb KJ, Lewthwaite JC, et al Short-term rigid and flaccid paralyses diminish growth of embryonic chick limbs and abrogate joint cavity formation but differentially preserve pre-cavitated joints. 9

4. Reiser PJ, Stokes BT, Walters PJ (1988) Effects of immobilization on the isometric contractile properties of embryonic avian skeletal muscle. Experimental Neurology 99:59–72. https://doi.org/10.1016/0014-4886(88)90127-6

5. Wu K-C, Streicher J, Lee ML, et al (2001) Role of motility in embryonic development I: Embryo movements and amnion contractions in the chick and the influence of illumination: Embryonic Motility of the Chick. J Exp Zool 291:186–194. https://doi.org/10.1002/jez.1068

6. Hamburger V, Hamilton HL (1951) A series of normal stages in the development of the chick embryo. J Morphol 88:49–92. https://doi.org/10.1002/jmor.1050880104

7. Peterson BE, Szczesny SE (2020) Dependence of tendon multiscale mechanics on sample gauge length is consistent with discontinuous collagen fibrils. Acta Biomaterialia 117:302–309. https://doi.org/10.1016/j.actbio.2020.09.046

8. McBride DJ, Trelstad RL, Silver FH (1988) Structural and mechanical assessment of developing chick tendon. International Journal of Biological Macromolecules 10:194–200. https://doi.org/10.1016/0141-8130(88)90048-7

9. Aper SJA, van Spreeuwel ACC, van Turnhout MC, et al (2014) Colorful Protein-Based Fluorescent Probes for Collagen Imaging. PLoS ONE 9:e114983. https://doi.org/10.1371/journal.pone.0114983

10. Mohammadkhah M, Simms CK, Murphy P (2017) Visualisation of Collagen in fixed skeletal muscle tissue using fluorescently tagged Collagen binding protein CNA35. Journal of the Mechanical Behavior of Biomedical Materials 66:37–44. https://doi.org/10.1016/j.jmbbm.2016.10.022

11. Diggle P, Diggle D of M and SPJ, Diggle PJ, et al (2002) Analysis of Longitudinal Data, Second Edition. OUP Oxford

12. Szczesny SE, Elliott DM (2014) Incorporating plasticity of the interfibrillar matrix in shear lag models is necessary to replicate the multiscale mechanics of tendon fascicles. Journal of the Mechanical Behavior of Biomedical Materials 40:325–338. https://doi.org/10.1016/j.jmbbm.2014.09.005

13. Birk DE, Nurminskaya MV, Zycband EI (1995) Collagen fibrillogenesis in situ: Fibril segments undergo post-depositional modifications resulting in linear and lateral growth during matrix development. Dev Dyn 202:229–243. https://doi.org/10.1002/aja.1002020303

14. Marturano JE, Arena JD, Schiller ZA, et al (2013) Characterization of mechanical and biochemical properties of developing embryonic tendon. Proc Natl Acad Sci USA 110:6370–6375. https://doi.org/10.1073/pnas.1300135110

15. Szczesny SE, Fetchko KL, Dodge GR, Elliott DM (2017) Evidence that interfibrillar load transfer in tendon is supported by small diameter fibrils and not extrafibrillar tissue components: INTERFIBRILLAR LOAD TRANSFER IN TENDON. J Orthop Res 35:2127–2134. https://doi.org/10.1002/jor.23517

16. Makris EA, Responte DJ, Paschos NK, et al (2014) Developing functional musculoskeletal tissues through hypoxia and lysyl oxidase-induced collagen cross-linking. Proc Natl Acad Sci USA 111:. https://doi.org/10.1073/pnas.1414271111

17. Pan XS, Li J, Brown EB, Kuo CK (2018) Embryo movements regulate tendon mechanical property development. Phil Trans R Soc B 373:20170325. https://doi.org/10.1098/rstb.2017.0325

18. Passini FS, Jaeger PK, Saab AS, et al (2021) Shear-stress sensing by PIEZO1 regulates tendon stiffness in rodents and influences jumping performance in humans. Nat Biomed Eng 5:1457–1471. https://doi.org/10.1038/s41551-021-00716-x

19. Graham HK, Holmes DF, Watson RB, Kadler KE (2000) Identification of collagen fibril fusion during vertebrate tendon morphogenesis. The process relies on unipolar fibrils and is regulated by collagen-proteoglycan interaction. Journal of Molecular Biology 295:891–902. https://doi.org/10.1006/jmbi.1999.3384

20. Zhang G, Ezura Y, Chervoneva I, et al (2006) Decorin regulates assembly of collagen fibrils and acquisition of biomechanical properties during tendon development. J Cell Biochem 98:1436–1449. https://doi.org/10.1002/jcb.20776

21. Douglas T, Heinemann S, Bierbaum S, et al (2006) Fibrillogenesis of Collagen Types I, II, and III with Small Leucine-Rich Proteoglycans Decorin and Biglycan. Biomacromolecules 7:2388–2393. https://doi.org/10.1021/bm0603746

22. Dunkman AA, Buckley MR, Mienaltowski MJ, et al (2013) Decorin expression is important for age-related changes in tendon structure and mechanical properties. Matrix Biology 32:3–13. https://doi.org/10.1016/j.matbio.2012.11.005

23. Robinson PS, Huang T-F, Kazam E, et al (2005) Influence of Decorin and Biglycan on Mechanical Properties of Multiple Tendons in Knockout Mice. Journal of Biomechanical Engineering 127:181–185. https://doi.org/10.1115/1.1835363

24. Hayashi N, Sato T, Yumoto M, et al (2019) Cyclic stretch induces decorin expression via yes-associated protein in tenocytes: A possible mechanism for hyperplasia in masticatory muscle tendon-aponeurosis hyperplasia. Journal of Oral and Maxillofacial Surgery, Medicine, and Pathology 31:175–179. https://doi.org/10.1016/j.ajoms.2018.12.012

25. Silver FH, Freeman JW, Seehra GP (2003) Collagen self-assembly and the development of tendon mechanical properties. Journal of Biomechanics 36:1529–1553. https://doi.org/10.1016/S0021-9290(03)00135-0

Chapter 4: Intermolecular Crosslinks are Required for Functional Tendon Formation but are Not Reliant on Muscle Stimulation

4.1 Introduction:

In the previous chapter, our data showed that embryonic chick tendons undergo a reorganization of the collagenous network during late stages of development that increases fibril load transmission and generates a rapid increase in tendon mechanical properties. These findings are consistent with a progressive increase in collagen fibril lengths during development, which reduces interfibrillar sliding and amplifies fibril loading [1, 2]. Our data further demonstrated that muscle immobilization impedes this mechanical transformation within the developing tissue, suggesting that muscle activity regulates fibril lengthening *in vivo*. Despite these findings, it is still unclear if the structure-functional transformation is mediated solely by fibril lengthening events or if other modifications to the extracellular matrix (i.e., intermolecular crosslinks) are contributing to the response.

During development, collagen is enzymatically crosslinked via lysyl oxidase (LOX) and a LOX-like family (LOXL 1-4) to form divalent and trivalent crosslinks, interconnecting adjacent tropocollagen molecules [3, 4]. The accumulation of intermolecular crosslinks is known to directly modulate the mechanical capabilities of tendon across multiple length scales [5–8]. At the macroscale, increased crosslinks have been shown to positively correlated with the macroscale modulus and ultimate tensile stress (UTS) of tendons in humans , horse, and bovine tendons [6, 8, 9]. Work in rat tail tendons has further shown that an injection of a LOX inhibitor, β-aminopropionitrile (BAPN), can directly impair the modulus and UTS of the tissue [10, 11]. Crosslinking has been further shown to vary

between specialized tendons (i.e., energy storing vs. positional), contributing to their distinctive failure mechanisms upon overloading [6, 8].

At a fibril scale, intermolecular crosslinks has shown to increase fibril stiffness via the stabilization of the tropocollagen network [12]. Following BAPN treatment, rat tail tendon fibrils readily deform under loads, likely contributing to increase in compliance observed at the tissue-scale [11]. Recent work in *in vitro* tendon constructs has further shown that BAPN treatments result in abnormal collagen fibril morphologies [13], suggesting that LOX-mediated crosslinking is required during fibrillogenesis. This is consistent with prior studies in chick embryos which displayed a reduction in trivalent pyridinoline crosslinks in calcaneal tendons following LOX inhibition [14], resulting in a reduction in the compressive modulus. Despite these findings, it's still unclear if crosslinking is directly mediating the rapid structural transformation observed during late stages of tendon development and the exponential increase in tensile mechanical capabilities.

Prior work has shown that thermodynamic characterization can be utilized to functionally quantify the crosslinking within tendon tissues [6, 15]. More specifically, crosslinking alters the thermodynamic transition from a highly ordered helix to a denatured arrangement of randomly ordered α-chain coils [16]. This can be measured using Differential Scanning Calorimetry (DSC) to measure the denaturation enthalpy and denaturation temperature of the tendon. Denaturation enthalpy describes the thermal energy required to break the intra-helical hydrogen bonds between amide and carboxyl residues of adjacent α-chains, and the extra-helical hydrogen bonds between the helix and surrounding water molecules [16]. Conversely, the denaturation temperature represents the average kinetic energy of the α-chains at the point of maximum energy

absorption during the denaturation process. This phenomenon is highly regulated by the structural arrangement of tropocollagen in the fibril structure [17]. Where crosslinks decrease the lateral spacing between adjacent molecules [16], reducing the conformational freedom of the denatured α-chains, effectively increasing the kinetic energy barrier (i.e., temperature) required to break their confinement.

In this chapter, we aimed to investigate how collagenous crosslinking contributes to the development of tendon multiscale mechanics and its sensitivity to musculoskeletal activity. To accomplish this, we leveraged BAPN treatments to inhibit LOX mediated crosslink formation during late stages of tendon development [18]. A combination of multiscale mechanical testing, differential scanning calorimetry, and acid solubility assays were to evaluate changes in crosslinking during development and immobilization. We hypothesize that while crosslinking is essential to the functional loading capabilities of tendon, they will be largely unaffected by musculoskeletal paralysis and fibril length changes are the primary mechanism driving the functional capabilities of tendon during late stages of tenogenesis. These finding will provide valuable insight into the structure-function elements that drive the mechanical transformation observed during late stages of tendon development and their dependence on musculoskeletal stimulation.

4.2 Materials & Methods:

4.2.1 Animal Methodology

Embryos were prepped and windowed according to protocols outlined in Chapter 3, Section 3.2. Similarly, immobilization treatments were conducted following the procedures outlined in Chapter 3, Section 3.2.1.

Lysyl oxidase (LOX) mediated crosslink formation was inhibited via the treatment of β-aminopropionitrile (BAPN; Thermo Scientific, Waltham, MA) to the chorioallantoic membrane. BAPN irreversibly blocks LOX and LOXL-4 activity, impairing aldehyde formation at telopeptide lysine or hydroxylysine residues, impeding downstream crosslink formation [18, 19]. Embryos were treated with at E15 with 400 uL of a 5 mg ml^{-1} solution of BAPN, rocking eggs to evenly distribute the drug across the CAM. Solutions were prepared with a sterile HBSS with 1% antibiotic/antimycotic. Controls were treated with HBSS and antibiotic/antimycotic alone.

Visual inspection of embryonic motility was conducted to assess the effects of immobilization and crosslink inhibition treatments on musculoskeletal activity, utilizing methodologies outlined in Chapter 3, Section 3.2.

Embryos for all treatment conditions were sacrificed at E20 via 15-minute exposure to -20oC followed by decapitation. All embryos were staged using Hamburger and Hamilton criteria [20] to ensure proper developmental comparisons. Embryo hindlimbs were isolated, wrapped in gauze, hydrated in PBS, and stored at -20^{o}C until testing.

4.2.2 Multiscale Mechanical Testing

Sample preparation and multiscale mechanical testing was conducted as outlined in Chapter 3, Section 3.2.2.

4.2.3 Differential Scanning Calorimetry

Samples were assessed using differential scanning calorimetry (DSC) to provide a quantitative assessment of functional collagen crosslinking in tendons during physiological development and under paralysis/BAPN treatments. To increase tissue mass, both the flexor digitorium brevis & longus digit II tendons were isolated from each avian hindlimb and pooled. Samples were blotted on lens paper to remove excess moisture and weighted. Samples were placed within an aluminum DSC pan (TA Instruments, T210707) and gently pressed into the bottom of the pan to maximize the tissue contact area. The lid (TA Instruments, T210416) was added and the pan was hermetically sealed. Calorimetry was performed using a DSC Q2000 (TA Instruments, New Castle, DE), accurate to 0.1^{o}C. Samples were allowed to equilibrate at 30^{o}C and the ramped to 70-75^{o}C at a rate of 3^{o}C/min [21]. All tests were conducted using a sealed empty pan as an internal reference.

DSC endotherms were analyzed using TA Universal Analysis software (Version 4.5A, TA Instruments) to collect the peak denaturation temperature (T_{peak}) and specific enthalpy of denaturation (Δh) for each distinctive endotherm present (**Fig. 4.1**). Utilizing the analysis software, a flat line was drawn across each endotherm peak. The T_{peak} was calculated as the minima of the endotherm curve, describing the peak change in heat flow and the point at which ~50% of the protein has denatured. The specific enthalpy of denaturation for each distinctive peak was calculated by the TA Universal Analysis

software, where a tangent line was draw across the endotherm and the area under the curve was calculated (**Fig. 4.1**). The percentage of enthalpy absorbed at a lower peak temperature (Peak 1 ΔH / Total ΔH) was calculated to assess the relative amount of

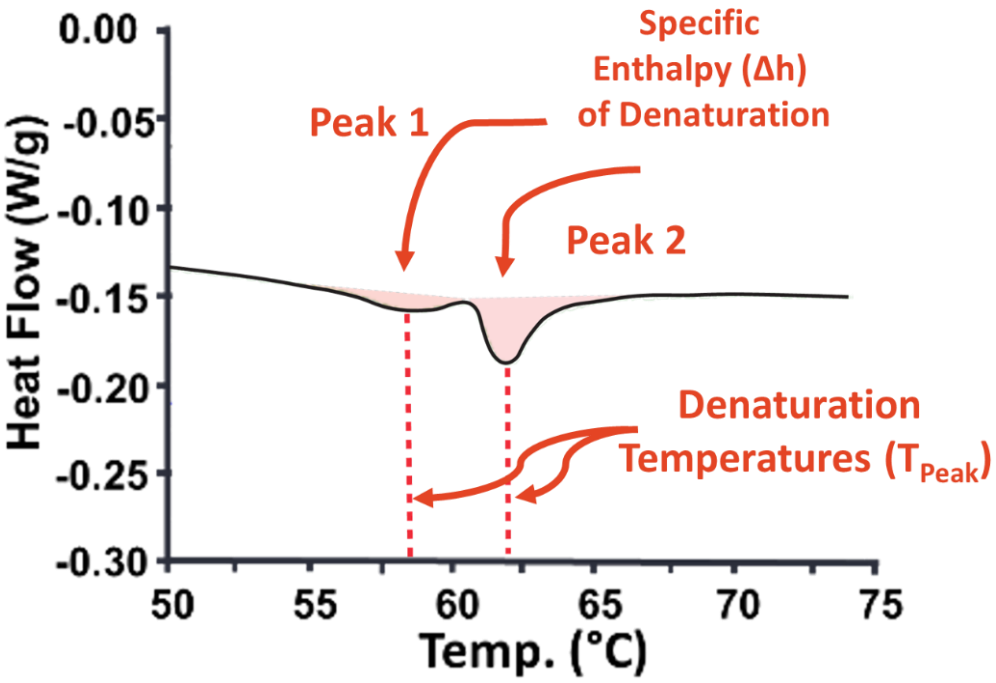

Figure 4.1: Representative differential scanning calorimetry endotherm. Multiple peaks represent unique populations of protein with distinctive denaturation behavior. T_{peak} described the temperature at which collagen denaturation is maximal. Area under the curve represents the specific enthalpy of denaturation (Δh).

collagen with diminished crosslinking.

4.2.4 Acid Solubility

An acid solubility assay was conducted to evaluate freely soluble collagen within the tissue to indirectly measure the degree of crosslinking as a function of development and paralysis/BAPN treatments. Solubility assays were performed following $NaBH_4$ reduction, to quantify soluble un-crosslinked collagen and crosslink stabilized collagen.

More specifically, following $NaBH_4$ reduction, all immature (aldimine & ketoimine) and mature crosslinks (HP/LP) are acid-stable and solubilized collagen fractions are representative of immature un-crosslinked collagen [3, 4, 22].

Samples were reduced in $NaBH_4$ following protocols previously outlined by Svennsson et al. [22]. Briefly, a $NaBH_4$ (MP Biomedicals, Santa Ana, CA) solution was freshly prepared at a concentration of 5 mg/mL in 0.15 NaOH. On a shaker plate, tissue samples were placed in 8 ml of 0.15 mM PBS (pH = 7.4) and 0.5 mL of the $NaBH_4$ solution was added in 15-minute increments for one hour. After reduction, tendons were washed twice in 0.15mM PBS for 5 minutes. Tissue samples were dabbed with Kimwhip to remove excessive surface moisture and then proceeded for acid solubility assay.

Samples subsequently were dissolved in 1mL of 0.05M acetic acid for 18h at ~4^{o}C on a shaker plate. Solutions were ultracentrifuged at 100,000 x g for 1 hour at 4^{o}C to separate the solubilized collagen within the supernatant and insolubilized collagen within a pellet. Half of the supernatant (0.5 ml) was removed, leaving 0.5 mL of the solute with the pellet. Collagen content of the two fractions was determined using a commercial colorimetric hydroxyproline assay (QuickZyme, BioVendor LLC) and FlexStation3R plate reader. All samples were tested in biological & technical duplicates and averaged to get a representative value collagen content for each condition. Solubility was expressed as a percent of the collagen within the supernatant over the total collagen between the two fractions. To account for the residual supernatant left within the pellet fraction, its contribution was calculated and subtracted from the hydroxyproline mass of the pellet fraction and added to the total supernatant content.

4.2.5 Statistical Methods

Statistical differences in fibril:tissue strain ratio were evaluated using a linear mixed model with strain as a covariate as outlined in Chapter 3, Section 3.2.4. A one-way ANOVA with a Dunnett's post-hoc test was used to evaluate differences in modulus, thermal properties, and acid solubility with respect to paralysis or BAPN treatments. A one-way ANOVA with a Tukey's post-hoc test was used to evaluate differences in thermal properties and solubility behavior as a function of development. Significance was set at $p < 0.05$.

4.3 Results

4.3.1 BAPN Effects on Multiscale Mechanics

In comparison to saline controls, no significant reduction in embryonic motility was observed following BAPN treatment at E15 (**Fig. 4.2A**). BAPN treatments resulted in a significant reduction in the macroscale modulus of the tissue in comparison to saline controls ($p < 0.001$; **Fig. 4.2 B&C**). To investigate how the multiscale mechanics were affected following a reduction of LOX mediated crosslinks, we measured the fibril:tissue strain ratio as a function of applied tissue strain for each group. Both the control and BAPN treated tissue showed an average fibril:tissue strain ratio that was significantly less than one ($p < 0.05$) and negatively correlated with applied tissue strain (**Fig. 4.2D**). A linear mixed model found a significant reduction in the fibril:tissue strain ratio following BAPN treatments ($p < 0.001$) in comparison to saline control.

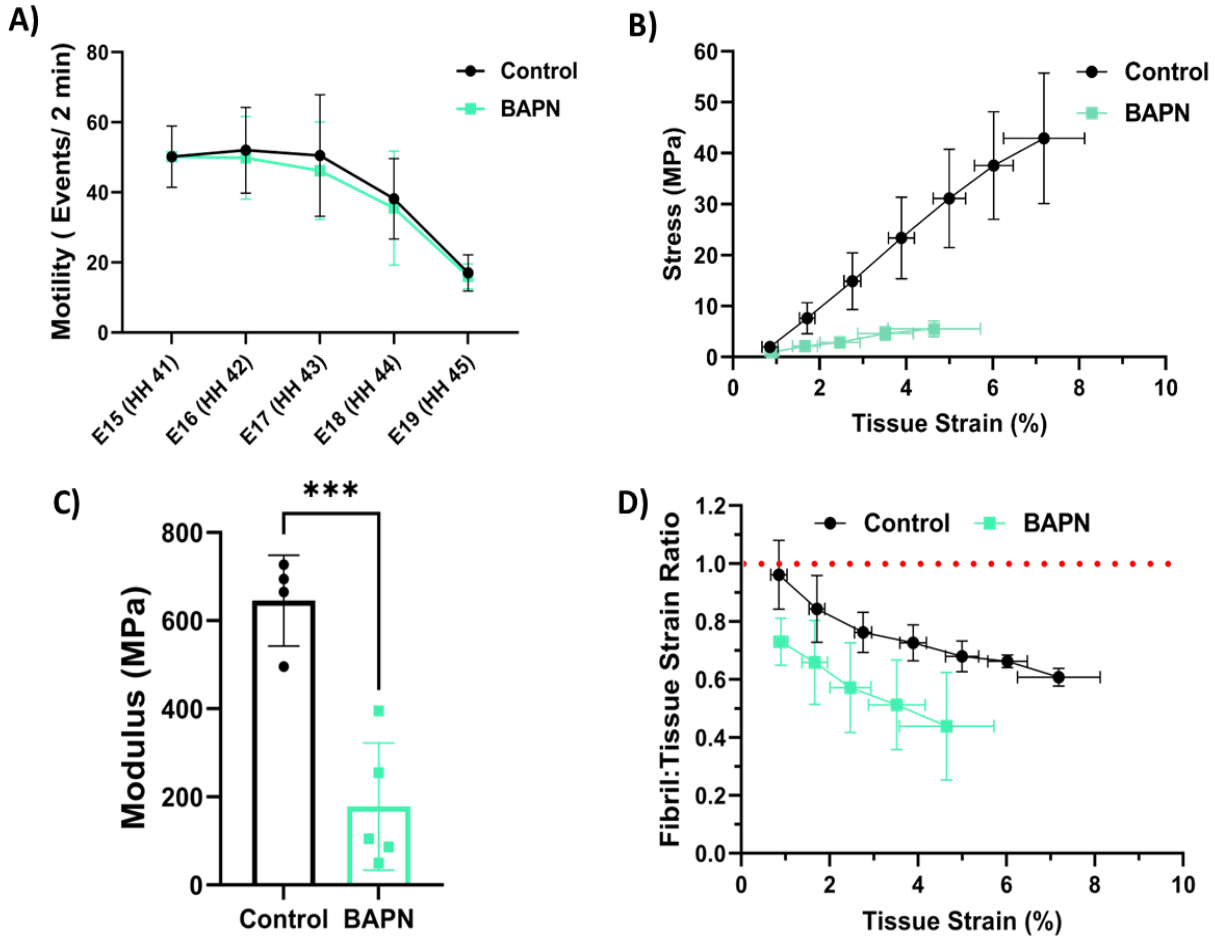

Figure 4.2*:* LOX mediated crosslink inhibition and its effect on the multiscale mechanical properties of the flexor digitorum brevis (FDB) digit II tendon during development (A) BAPN and saline control solutions were administered from E15 (HH41) – E19 (HH45). No significant difference in motility behavior was observed following BAPN treatments. (B) Equilibrium stress vs. applied strain for E20 (HH46) samples follow saline (n = 4) or BAPN (n = 5) treatments. (C) Equilibrium modulus is significantly reduced following BAPN treatments ($p < 0.001$). (D) Multiscale mechanical response at E20 (HH46) as a function of applied tissue strain after BAPN treatments. The fibril:tissue strain ratio was significantly reduced ($p < 0.001$) following BAPN treatments in comparison to saline controls. Data represented at mean ± standard deviation.

*p< 0.05, ∗∗p < 0.01, p*** < 0.001.

4.3.2 Thermodynamic and Solubility Behavior

Differential scanning calorimetry was leveraged to assess changes within the thermal stability of the collagenous network as a function of development. Two distinctive endotherm peaks were observed across all developmental timepoints, as indicated in representative endotherm plots (**Fig. 4.3**). With development, there was an increase in total specific enthalpy of denaturation and peak denaturation temperatures in comparison to the E20 timepoints (**Table 4.1**). The Peak 1 enthalpy / total enthalpy plot was used to capture the amount of protein in the more easily denatured state and be proportional to the entire system. A significant reduction in Peak 1/ Total enthalpy was observed between the E18 and E20 timepoints ($p < 0.05$).

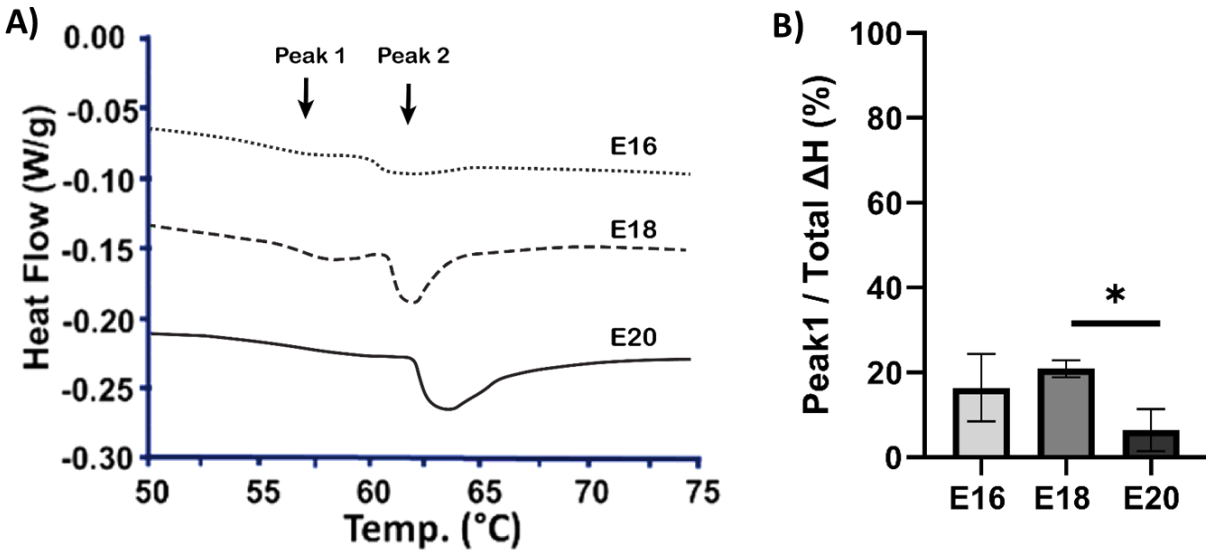

Figure 4.3: Thermodynamic denaturation behavior as a function of development. **A)** Representative endotherms at embryonic day 16, 18, and 20. Arrows mark the two peaks of enthalpy absorption. B) Peak 1 enthalpy/ Total enthalpy plot. Data represented as mean ± standard deviation. * $p< 0.05$.

Table 4.1: Thermal properties of embryonic tendons as a function of development or paralysis/crosslink inhibition. Statistical comparisons for development are done with respect to E20 timepoint and treatments are compared to respective controls. * p< 0.05, ** p<0.01, *** p<0.001

	ΔH(J/g)		T_{peak}(°C)	
	Total ΔH	**Peak 1 / Total ΔH (%)**	**Peak 1**	**Peak 2**
E20 (n=4)	2.56 ± 0.46	6.39% ± 4.95%	59.67 ± 0.33	63.05 ± 0.57
E18 (n=4)	1.97 ± 0.22	20.86% ± 2.0%	58.47 ± 0.23	62.29 ± 0.30
E16 (n=4)	0.88 ± 0.18	16.4% ± 7.97%	57.02 ± 0.15	61.46 ± 0.22
Control (n=4)	2.06 ± 0.48	7.28% ± 5.99%	59.46 ± 0.38	63.18 ± 0.46
PB (n=3)	1.67 ± 0.06	24.87% ± 9.76%	57.77 ± 0.17	62.04 ± 0.25
DMB (n=3)	2.53 ± 0.43	4.25% ± 2.18%	57.61 ± 0.47	61.74 ± 0.36
Control (n=3)	2.53 ± 0.43	3.11% ± 1.03%	57.93 ± 0.95	63.60 ± 0.25
BAPN (n=3)	2.88 ± 0.43	88.04% ± 5.99%	57.28 ± 0.64	62.85 ± 0.04
	p < 0.05	p < 0.01	p < 0.001	

Differential scanning calorimetry was subsequently conducted to evaluate the effects of crosslink inhibition and musculoskeletal immobilization (DMB and PB treatment) on the thermodynamic characteristics of the collagenous network (**Fig. 4.4, Table 4.1**). Following crosslink inhibition two distinctive endotherm peaks were still apparent across all treatment conditions; however, the Peak 2 population was notably smaller in the BAPN treated samples (**Fig. 4.4A**). The BAPN treated embryos showed no significant difference in the total enthalpy in comparison to their saline controls (**Table 4.1**). However, there was a significant increase in the enthalpy absorbed in the peak 1 ($p < 0.001$) population relative to the total enthalpy in the system. Following immobilization treatments, neither flaccid (PB) or rigid (DMB) paralysis resulted in a significant reduction in the total enthalpy of the system (**Table 4.1**). However, both forms of paralysis resulted in a significant reduction in the denaturation enthalpy of the Peak 1 and Peak 2 population ($p < 0.05$).

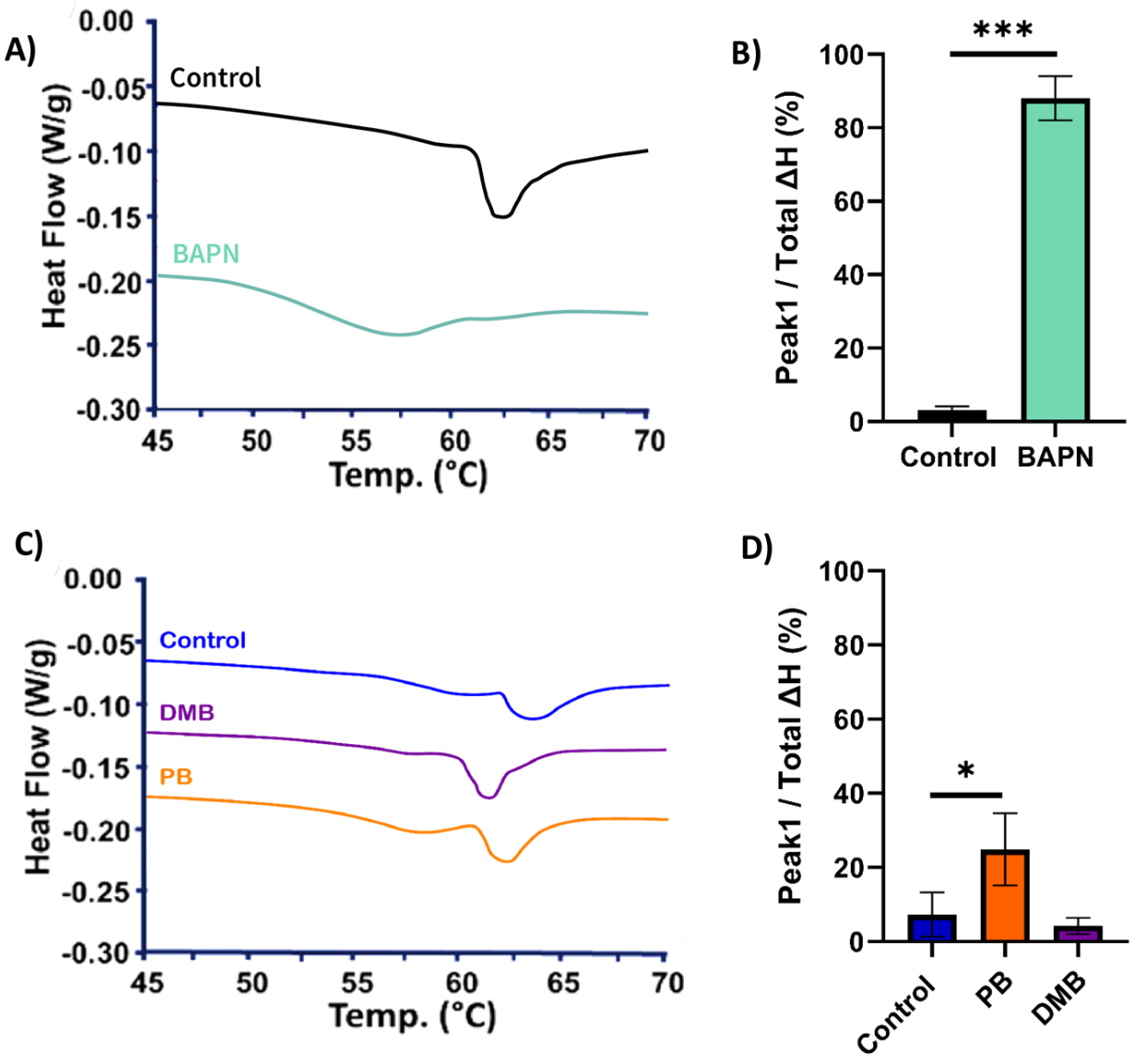

Figure 4.4: Thermodynamic denaturation behavior as a function of crosslink inhibition and paralysis treatments. A) Representative endotherms of E20 tissue following crosslink inhibition with BAPN treatment and saline controls. B) Peak 1 enthalpy / Total enthalpy plot following BAPN treatment. C) Representative endotherms of E20 tissue following rigid paralysis (DMB) or flaccid paralysis (PB) in comparison to saline controls. D) Peak 1 enthalpy/ Total enthalpy plot following immobilization. Data represented as mean ± standard deviation. * $p< 0.05$, ** $p< 0.01$, *** $p < 0.001$

Only the flaccid paralysis treatment resulted in a significant increase in the relative enthalpy in the Peak1 population relative to the total enthalpy of the system (**Fig. 4.4D**).

An acid solubility assay was subsequently conducted to evaluate the amount of liable, un-crosslinked collagen that was present during development and following treatment conditions. During developing, no significant change in acid liability was observed. A significant increase in soluble collagen was observed following rigid paralysis (DMB) ($p < 0.05$), however no change was observed following flaccid (PB) paralysis. Following BAPN treatment an increasing trend was observed, however statistical significance could not be calculated due to small sample size (Cnt; n=1). It's important to note that aside from the BAPN control (n = 1), all other samples have similarly small sample sizes (n = 2) for the acid solubility assay.

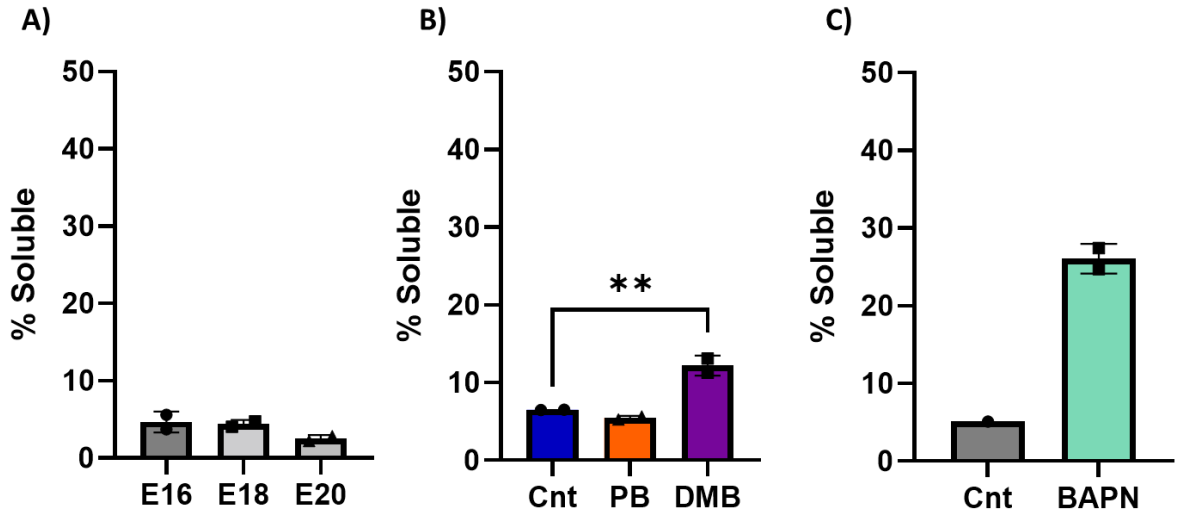

Figure 4.5: Acid solubility assay. A) Free soluble collagen as a funciton of development (n = 2). No significant change observed with maturation. B) Freely soluble collagen following flaccid (n=2) and rigid (n = 2) paralysis. A significant increase in freely soluble collagen found followign rigid immobilization ($p < 0.01$). C) Souble collagen following inhibition of LOX-mediated crosslinking. No signifance found between control (n =1) and BAPN treatment (n = 2), but testing power is limited due to sample size. ** $p < 0.01$

4.4 Discussion:

This study aimed to provide insight into how intermolecular crosslinks contribute to the mechanical capabilities of tendon during development and how it's affected following immobilization. An investigation of the thermodynamic parameters during physiological development indicates that two unique thermodynamic populations are present, as shown by the distinctive "Peak 1" and "Peak 2" curves (**Fig. 4.3A**). These findings contrast prior DSC data in mature tendon tissues, which presented a unimodal endotherm with a denaturation temperature around ~65^{o}C [21, 23]. The presence of the more readily denatured protein within the Peak 1 population is unique to embryonic tendon tissue, likely to pro-collagen or immature un-crosslinked collagen, which are less thermodynamically stable. Following crosslink inhibition with BAPN a bimodal response is still produced (**Fig. 4.4A**), however the specific enthalpy of the Peak 1 population is significantly increased, indicative that the Peak 1 population is indeed representative of un-crosslinked collagen. The relative proportion of collagen in this "immature" state can be captured via the Peak 1 Enthalpy/ Total Enthalpy plot. With maturation, the proportion of 'immature' collagen undergoes minimal changes, only significantly decreasing prior to hatching (E18 to E20, $p < 0.05$). These findings agree with acid solubility behavior (**Fig. 4.5A**), where minimal changes in freely liable collagen are observed during development. Collectively, these data indicate that collagen is rapidly crosslinked following deposition into the ECM. These findings are similar to prior studies which have demonstrated consistent crosslinking activity during development when normalized to collagen content [24].

Importantly, there is a significant increase in the denaturation temperature of both collagen populations with increasing maturation (**Table 4.1**; $p < 0.05$). This behavior is indicative of an increase in the kinetic barrier required to denature the triple helix [16, 21]. This may be due to an increase in gross crosslinking density or the establishment of trivalent pyridinolines crosslinks from less stable divalent precursors [15], decreasing lateral tropocollagen spacing [16]. However, this mechanism doesn't explain the increase in denaturation temperature observed within the immature Peak 1 population ($p < 0.05$) (Table 4.1). Alternatively, it is possible that this shift may be mediated by fusion events within the collagenous ultrastructure [25]. More precisely, the fusion of adjacent fibrils minimizes fibril surface area, functionally enabling more tropocollagen interactions, resulting in an increase in the collagenous thermal stability independent of crosslink formation [25]. This theory is consistent with prior findings that have demonstrated minimal shifts in thermal properties (~ $0.5^{o}C$) between tissues with significant differences in relative crosslinking [21]. However, additional work is required to explore the role of these distinctive protein populations and their dependence on crosslinking & secondary structure interactions.

This study further demonstrated that LOX-mediate crosslinking is essential to the development of the functional loading capabilities during late stages of tendon development. More specifically, there is a significant reduction in the macroscale loading capabilities of the tissue following LOX inhibition via BAPN treatments (**Fig. 4.2C**). These findings are consistent with macroscale mechanical effects observed in other systems following impaired crosslink formation. Nevertheless, we demonstrated that the fibril:tissue strain ratio was significantly reduced following crosslink inhibition, indicative

of a reduction in local fibril deformations [2, 12]. These findings are inconsistent with small angle x-ray scattering (SAXS) studies in mature rat tail tendons, which demonstrated an *increase* in local fibril strains relative to the macroscale tissue deformation following BAPN treatments [11, 26]. This discrepancy is potentially due to an impairment in the hierarchical organization of the collagen during fibrillogenesis following BAPN treatment. Indeed, recent studies have shown that tendon constructs treated with BAPN during their maturation form irregular fibrillar aggregates with increased interfibrillar spacing [13]. This change in fibril morphology and arrangement may impede interfibrillar load transmission [2], contributing to the reduced fibril strains observed in our system. Nevertheless, it is still unclear if the rapid increase in fibril lengthening is sensitive to crosslinking behavior and additional characterization is required to understand how crosslinking is altering the multiscale mechanical response during development. These preliminary finding have interesting implications on crosslinking as both a mechanical element and as a molecular regulator of fibril assembly [13]. However, no study to date (to my knowledge) has directly investigated *in vivo* effects on the collagenous ultrastructure following LOX inhibition during development and requires further study.

Interestingly, while the denaturation temperature of the Peak 1 population was unchanged following crosslink inhibition there was a significant increase in its relative width (**Fig. 4.4A, Table 4.1**). These findings are consistent with the abnormal fibril morphology observed following BAPN treatment [13]. More specifically, while fibril fusion events are allowed to occur, they fail to form a geometry that effectively minimizes the surface area (i.e., they poorly maximize local tropocollagen interactions). While these observations suggest that LOX-inhibited tissues are still able to fuse, it still largely unclear

if this has ramifications on the fibril lengthening behavior later in development. Additional work needs to be conducted to evaluate the collagenous ultrastructure following BAPN treatment to better elucidate the biological role of crosslinks in fibrillogenesis.

Perhaps of most interest, we found that muscle immobilization presented a unique thermodynamic response that is distinct from developmental changes and crosslink inhibition. More specifically, we found that immobilized embryos still underwent this primary shift from the Peak 1 to Peak 2 regions, suggestive that the collagen underwent an initial crosslink stabilization (**Fig. 4.4C**). The relative amount of "immature" crosslinks, observed via the Peak 1 Enthalpy/ Total Enthalpy, showed that only the flaccid paralysis (PB) displayed an impairment in this crosslink transformation (**Fig. 4.4D**). In contrast, the acid solubility assay showed that only the rigid paralysis (DMB) displayed any significant uptick in, suggestive of a reduction in crosslinking (**Fig. 4.5B**). Collectively, these findings indicate that immobilization decreased the relative crosslinking populations, consistent with prior studies [14].However, it's important to note that the effects appear mild in comparison to the severity of phenotype, suggestive that crosslinking may not be highly dependent on muscle activity.

Furthermore, it is still unclear if a reduction in crosslink formation alone is sufficient to explain the impaired increase in denaturation temperature observed with maturation. That is, following immobilization the Peak 2 populations of both DMB and PB failed to shift towards higher temperatures (**Table 4.1, Fig.4.4C**). It's currently unknown whether this is due to an impaired densification of crosslink population or impeded fibril fusion events *in vivo*. Crosslinking trends in Achilles tendon indicate no significant changes in crosslinking density during normal development between HH38 (E12) – HH43 (E17) [24], suggesting

that shift in denaturation behavior is not mediated by crosslink densification. Alternatively, prior work in collagenous gels (void of LOX-mediated crosslinks) have indicated that relatively small changes in fibril diameters (~5 nm) can drastically shift denaturation temperatures (~2-3 ^{o}C) [25]. Together, these findings indicate that fibril fusion behavior is driving the impaired denaturation behavior following paralysis, not a retardation in crosslinking. If fibril fusion events (i.e., fibril lengthening) are indeed impaired following paralysis, are findings would match the multiscale mechanical data reported in Chapter 3. However, at this time, additional work needs to be conducted to differentiate the role of crosslinks and fibril lengthening *in vivo* and validate these hypotheses.

A primary limitation to this study is that we were unable to quantify crosslinks directly. Initial characterization via liquid-chromatography mass spectroscopy (LC-MS) was conducted following previously reported protocols [24]. However, at the prepared sample concentrations (10 mg/mL), we were unable to detect mature trivalent hydroxylysl-pyridinoline (HP) or lysyl-pyridinoline (LP) crosslinks above the detectable limit (0.5 pmol). These findings contrast with prior literature, which demonstrated over ~ 5 – 25 pmol/mol of HP+LP crosslinks in embryonic chick tendons [24], despite using using identical sample preparations. Notably, this study in question utilized calcaneal (Achilles) tendons in comparison to our flexor tendons. High energy storing tendons (i.e., Achilles) are well documented to have high concentrations of mature HP/LP crosslinks [15, 22]. It's possible that our flexor tendons simply have lower concentrations [27] and thus are not detectable during development at the prepared concentration. Alternatively, it is possible that our samples are dominated by immature crosslinks [3], avoiding detection during HPLC-MS. Future work aims to re-conduct HPLC-MS analysis at higher sample concentrations and

include internal standards for immature crosslink populations to quantify crosslinking populations more conclusively during development and following treatment conditions.

Furthermore, while this thermodynamic characterization provided insight into the structural arrangement of these protein populations, a more detailed ultrastructural characterization is required to validate these hypotheses. Additionally, more work is required to investigate the relationship between fibril fusion behavior and denaturation temperature within our tissue systems. This is required to provide more conclusive evidence on the role of crosslinking and musculoskeletal stimulation on transformation within the structure-function relationship during late stages of tendon development.

4.5 Conclusions

This study has demonstrated that crosslinking plays a key role in fibrillogenesis and the structure-function relationship during development. Furthermore, our data indicates that while immobilization is displaying impair crosslinking capabilities the majority of collagen is undergoing initial crosslink stabilization. Regardless, it’s unclear the impaired shifts to higher denaturation temperatures following paralysis are truly due to impeded fibril fusion behavior (i.e., fibril lengthening) or retardation of additional crosslinking. Additional ultrastructural characterization is required to validate these hypotheses and more conclusively establish the primary elements that facilitate transformations in the structure-function relationship during late stages of tenogenesis.

4.6 References

1. Szczesny SE, Elliott DM (2014) Interfibrillar shear stress is the loading mechanism of collagen fibrils in tendon. Acta Biomaterialia 10:2582–2590. https://doi.org/10.1016/j.actbio.2014.01.032

2. Szczesny SE, Elliott DM (2014) Incorporating plasticity of the interfibrillar matrix in shear lag models is necessary to replicate the multiscale mechanics of tendon fascicles. Journal of the Mechanical Behavior of Biomedical Materials 40:325–338. https://doi.org/10.1016/j.jmbbm.2014.09.005

3. Bailey AJ, Paul RG, Knott L (1998) Mechanisms of maturation and ageing of collagen. Mechanisms of Ageing and Development 106:1–56. https://doi.org/10.1016/S0047-6374(98)00119-5

4. Ellingson A, Pancheri N, Schiele N (2022) Regulators of collagen crosslinking in developing and adult tendons. eCM 43:130–152. https://doi.org/10.22203/eCM.v043a11

5. Lee JM, Veres SP (2019) Advanced glycation end-product cross-linking inhibits biomechanical plasticity and characteristic failure morphology of native tendon. Journal of Applied Physiology 126:832–841. https://doi.org/10.1152/japplphysiol.00430.2018

6. Quigley AS, Bancelin S, Deska-Gauthier D, et al (2018) In tendons, differing physiological requirements lead to functionally distinct nanostructures. Sci Rep 8:4409. https://doi.org/10.1038/s41598-018-22741-8

7. Silver FH, Freeman JW, Seehra GP (2003) Collagen self-assembly and the development of tendon mechanical properties. Journal of Biomechanics 36:1529–1553. https://doi.org/10.1016/S0021-9290(03)00135-0

8. Thorpe CT, Stark RJF, Goodship AE, Birch HL (2010) Mechanical properties of the equine superficial digital flexor tendon relate to specific collagen cross-link levels: Tendon mechanical properties and collagen cross-links. Equine Veterinary Journal 42:538–543. https://doi.org/10.1111/j.2042-3306.2010.00175.x

9. Eyre DR, Paz MA, Gallop PM (1984) CROSS-LINKING IN COLLAGEN AND ELASTIN. Ann Rev Biochem 53:717–48

10. Haut RC (1985) The Effect of a Lathyritic Diet on the Sensitivity of Tendon to Strain Rate. Journal of Biomechanical Engineering 107:166–174. https://doi.org/10.1115/1.3138537

11. Puxkandl R, Zizak I, Paris O, et al (2002) Viscoelastic properties of collagen: synchrotron radiation investigations and structural model. Phil Trans R Soc Lond B 357:191–197. https://doi.org/10.1098/rstb.2001.1033

12. Eekhoff JD, Fang F, Lake SP (2018) Multiscale mechanical effects of native collagen cross-linking in tendon. Connective Tissue Research 59:410–422. https://doi.org/10.1080/03008207.2018.1449837

13. Herchenhan A, Uhlenbrock F, Eliasson P, et al (2015) Lysyl Oxidase Activity Is Required for Ordered Collagen Fibrillogenesis by Tendon Cells. Journal of Biological Chemistry 290:16440–16450. https://doi.org/10.1074/jbc.M115.641670

14. Pan XS, Li J, Brown EB, Kuo CK (2018) Embryo movements regulate tendon mechanical property development. Phil Trans R Soc B 373:20170325. https://doi.org/10.1098/rstb.2017.0325

15. Horgan DJ, King NL, Kurth LB, Kuypers R (1990) Collagen crosslinks and their relationship to the thermal properties of calf tendons. Archives of Biochemistry and Biophysics 281:21–26. https://doi.org/10.1016/0003-9861(90)90407-P

16. Miles CA, Ghelashvili M (1999) Polymer-in-a-Box Mechanism for the Thermal Stabilization of Collagen Molecules in Fibers. Biophysical Journal 76:3243–3252. https://doi.org/10.1016/S0006-3495(99)77476-X

17. Canty EG, Kadler KE (2005) Procollagen trafficking, processing and fibrillogenesis. Journal of Cell Science 118:1341–1353. https://doi.org/10.1242/jcs.01731

18. Tang SS, Trackman PC, Kagan HM (1983) Reaction of aortic lysyl oxidase with beta-aminopropionitrile. J Biol Chem 258:4331–4338

19. Hajdú I, Kardos J, Major B, et al (2018) Inhibition of the LOX enzyme family members with old and new ligands. Selectivity analysis revisited. Bioorg Med Chem Lett 28:3113–3118. https://doi.org/10.1016/j.bmcl.2018.07.001

20. Hamburger V, Hamilton HL (1951) A series of normal stages in the development of the chick embryo. J Morphol 88:49–92. https://doi.org/10.1002/jmor.1050880104

21. Herod TW, Chambers NC, Veres SP (2016) Collagen fibrils in functionally distinct tendons have differing structural responses to tendon rupture and fatigue loading. Acta Biomaterialia 42:296–307. https://doi.org/10.1016/j.actbio.2016.06.017

22. Svensson RB, Mulder H, Kovanen V, Magnusson SP (2013) Fracture Mechanics of Collagen Fibrils: Influence of Natural Cross-Links. Biophysical Journal 104:2476–2484. https://doi.org/10.1016/j.bpj.2013.04.033

23. Lin AH, Allan AN, Zitnay JL, et al (2020) Collagen denaturation is initiated upon tissue yield in both positional and energy-storing tendons. Acta Biomaterialia 118:153–160. https://doi.org/10.1016/j.actbio.2020.09.056

24. Marturano JE, Xylas JF, Sridharan GV, et al (2014) Lysyl oxidase-mediated collagen crosslinks may be assessed as markers of functional properties of tendon tissue formation. Acta Biomaterialia 10:1370–1379. https://doi.org/10.1016/j.actbio.2013.11.024

25. Godard P, Biebuyck JJ, Daumerie M, et al (1978) Crystallization and melting of aqueous gelatin. J Polym Sci Polym Phys Ed 16:1817–1828. https://doi.org/10.1002/pol.1978.180161009

26. Bianchi F, Hofmann F, Smith AJ, Thompson MS (2016) Probing multi-scale mechanical damage in connective tissues using X-ray diffraction. Acta Biomaterialia 45:321–327. https://doi.org/10.1016/j.actbio.2016.08.027

27. Birch HL, Thorpe CT, Rumian AP (2013) Specialisation of extracellular matrix for function in tendons and ligaments. Muscles, Ligaments and Tendons Journal 3:12–22. https://doi.org/10.11138/mltj/2013.3.1.012

Chapter 5 – Ultrastructural Characterization of Tendons Using Serial-Block Face Imaging & Deep Learning Tools

5.1 Introduction:

Our finding in Chapter 3 suggests that the load-bearing capabilities within tendons are derived from changes in collagen fibril lengths during development. Subsequent work has indicated that this structure-functional transformation is impeded via musculoskeletal immobilization, highlighting the importance of mechanobiological activity during development. However, work presented in Chapter 4 has suggested that impaired crosslinking activity may be contributing to the phenotypic behavior observed following muscle paralysis [1, 2]. It's still possible that the impaired thermodynamic behavior observed in immobilized tendons is reflective of impeded fibril lengthening events, but additional work is required to validate these findings. To investigate these hypotheses and conclusively establish the primary elements that facilitate the structure-function transformation in development we aimed to conduct a detailed ultrastructural characterization of the developing collagenous network.

Prior attempts to measure collagen fibrils during development have proven difficult due to their small diameter (12 to 100 nm) [3], high packing density [4, 5], and relatively long length (30 µm – 1+ mm) [6, 7]. Conventional light microscopy lacks the necessary optical resolution, requiring electron microscopy to distinguish individual collagen fibrils. Characterization of two-dimensional (2D) cross-sections is relatively straightforward and well-documented in literature [3, 8–10]. Briefly, tendons are dehydrated, embedded in resin, and then cut into ultra-thin sections (~100 nm). These sections are subsequently

stained with heavy metal salts to provide the contrast necessary to differentiate the collagen fibrils from the adjacent interfibrillar matrix and surrounding cells. Using these techniques, 2D characteristics such as fibril diameter and volume fraction can be directly measured. However, these strategies don't enable definitive assessments of three-dimensional (3D) parameters such as fibril lengths. Longitudinal sections have attempted to address this gap but fail to distinctively track fibrils due to movement in/out of the slicing plane [1, 2]. While these strategies have provided critical insight into the ultrastructural changes during embryonic development, additional work is required to investigate 3D changes within the collagenous fibril network during tenogenesis. This information is essential to understanding the dynamic structure-function changes that occur during tenogenesis.

To this end, recent advancements in serial block-face scanning electron microcopy (SBF-SEM) have enabled detailed 3D ultrastructural characterization of tendon networks [5, 11–15]. SBF-SEM is a commercially available electron microscopy technique that incorporates an ultramicrotome into the imaging chamber, enabling the collection of sequential SEM images in a highly regulated environment. These images can be combined to provide a 3D reconstruction of the microstructure to track objects (nuclei, membrane, cells, and fibrils) [16]. Prior studies have leveraged these techniques to track changes in cellular and fibrillary morphology during tenogenesis in mice [5], but none have focused on the developmental transformation that occurs during late stages of chicken development. This represents a critical gap in knowledge that needs to be explored to correlate changes in the collagenous network with the multiscale mechanical capabilities.

While powerful, the large amount of data generated from SBF-SEM presents a daunting task. More specifically, processing SBF-SEM data sets requires a combination of image processing, object segmentation, and volumetric quantification to extract useful information. Segmentation, the process which identifies specific objects of interest, is especially challenging as most studies still rely on manual segmentation. While this allows for detailed accuracy, it vastly limits the quantity of structures that can be tracked. For example, a standard 4096 x 4096 px image (2 nm/px resolution) of an E20 chicken tendon contains roughly ~8000 distinctive fibrils. Conservatively, an experienced user needs an estimated ~1.5 hour to manually isolate these structures on a single slice. Assuming the image stack has 500 images (not uncommon), it will take nearly 750 hours of continuous labor to volumetrically isolate all these structures of interests. When combined with multiple ROIs, developmental timepoints, and/or treatment conditions the laborious concerns are amplified. Current practices in the field compensate for this by reducing the quantify of objects tracked. However, this reduces the ability to capture heterogeneity in the sample population and weakens estimates that rely on probabilistic occurrence of specific events (i.e., finding fibril ends or branching).

To address these concerns, scientists have turned to machine learning strategies to automate the processing pipeline for extensive SBF-SEM dataset. Excitingly, a convolutional neural network called a “U-Net” was developed in 2015 [17], which demonstrated the ability to conduct fast and precise segmentation on biological images. Convolutional neural networks can distinguish anomalies and distinctive features while still tolerating variations in complex patterns, offering an advantage over traditional machine learning approaches [17, 18]. Furthermore, U-Net semantic segmentation

requires limited training data and can be run on modern computers, vastly enabling accessibility. More recently, open-source and commercially available software such as Python, MATLAB, and Dragonfly have begun to integrate U-Net neural architectures into their toolsets, further reducing the barrier of entry. However, deep learning tools have yet to be integrated into the tendon field for EM image processing, representing a critically untapped potential for ultrastructural characterization.

The primary objective of this chapter was to develop an analysis pipeline for the volumetric quantification of the collagenous ultrastructure during development and under treatment conditions. Using these strategies, we aimed to validate the structure-function relationships predicted by prior multiscale mechanical and thermodynamic characterization. More specifically, we aimed to isolate out several key 2D and 3D features of interest by leveraging deep learning neural networks. In 2D, we aimed to characterize the distribution of fibril diameters and calculate a representative fibril volume fraction. In 3D, we aimed to produce a robust pipeline to produce volumetric reconstructions of collagenous structures and identify terminated fibril ends. Prior work has shown that fibril ends can be used in a probabilistic analysis to estimate in vivo fibril length. However, this analysis scheme requires the tracking of a large quantity of unique fibril objects and presents a critical barrier. While still on-going, this chapter will outline the exciting progress made thus far in integrating deep learning neural networks for SBF-SEM characterization.

5.2 Materials & Methods:

5.2.1 Serial Block-Face SEM

Sample Preparations

Limbs were obtained from E16, E18, and E20 chickens to quantify developmental changes with the collagenous ultrastructure. All samples were obtained from freshly sacrificed animals and staged to ensure adequate comparisons. Limbs were kept whole to maintain native tension on the tissue during the fixation. To ensure proper penetration of the fixative, fresh hindlimbs had their skin and Achille's tendon removed to ensure that flexor tendons had direct contact with fixative solution. Limbs were immersed in a fresh fixative solution of 2% Paraformaldehyde/2.5% Glutaraldehyde with 2mM calcium chloride in 0.15 cacodylate buffer (pH 7.4). After 3 days samples were removed from the fixative solution, FDB digit II tendons isolated, and stained/resin embedded utilizing standard protocols within the field [13, 16].

Image Acquisition

Transverse cross-sections were scanned in series (**Fig. 5.1**) under 2.5 kV in low-vacuum pressure (35 - 40 Pa) using an Apreo VolumeScope (Thermo Fisher Scientific, Waltham, MA). Embryonic day 16 & 18 tissue samples were imaged under a 3072 x 2048 px field with a pixel size of 4nm/px. To account for higher packing densities, E20 tissue samples were imaged under a 4096 x 4096 px field with a pixel size of 2 nm/px. A total of 400 unique slices were collected for the E16 timepoint (~ 12 µm x 8 µm x 20 µm) to establish the volumetric reconstruction analysis pipeline. All subsequent imaging conditions collected ~30-50 slices for pilot assessments and 2D characterization.

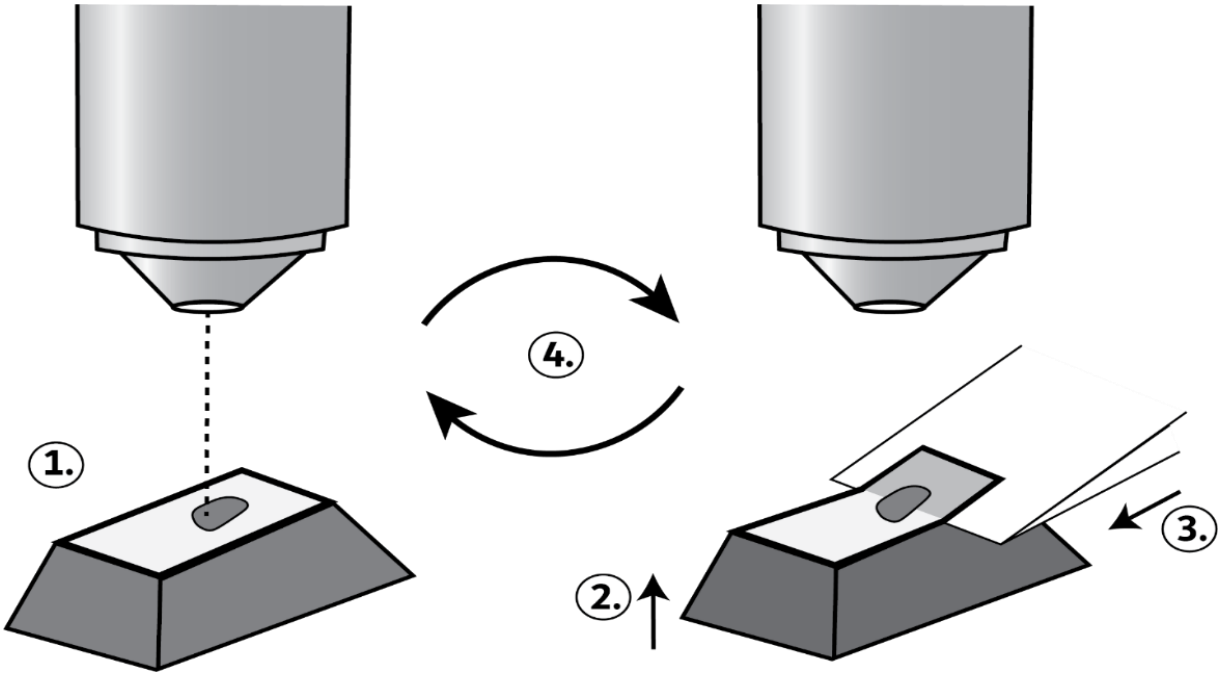

Figure 5.1:. Diagram on the principles of serial block-face scanning electron microscopy (SBF-SEM). (1) The surface of the sample is scanned using an electron beam and backscattered electrons are collected via a detector. (2) The block is moved up in the z-direction. This vertical translation in the z-direction dictates the thickness of the slices. (3) An ultramicrotome, incorporated into the chamber, removes an ultra-thin slice (~30 – 200 nm). (4) The ultramicrotome retracts and the process is repeated. [13]

5.2.2 Semantic Segmentation with Deep Learning

Image Pre-Processing

Initial image enhancing was conducted to accentuate collagen fibrils prior to model training (**Fig. 5.2**) and is critical to enhancing feature detection. Briefly, raw images were put through the “Enhance Contrast” function in Fiji (ImageJ), saturating the pixels by 5%. Output images were then passed through a FFT bandpass filter, reducing noise from objects smaller than 4 px or larger than 40 px. Images were brightness/contrast adjusted, saved as an image sequence, and then exported for semantic segmentation.

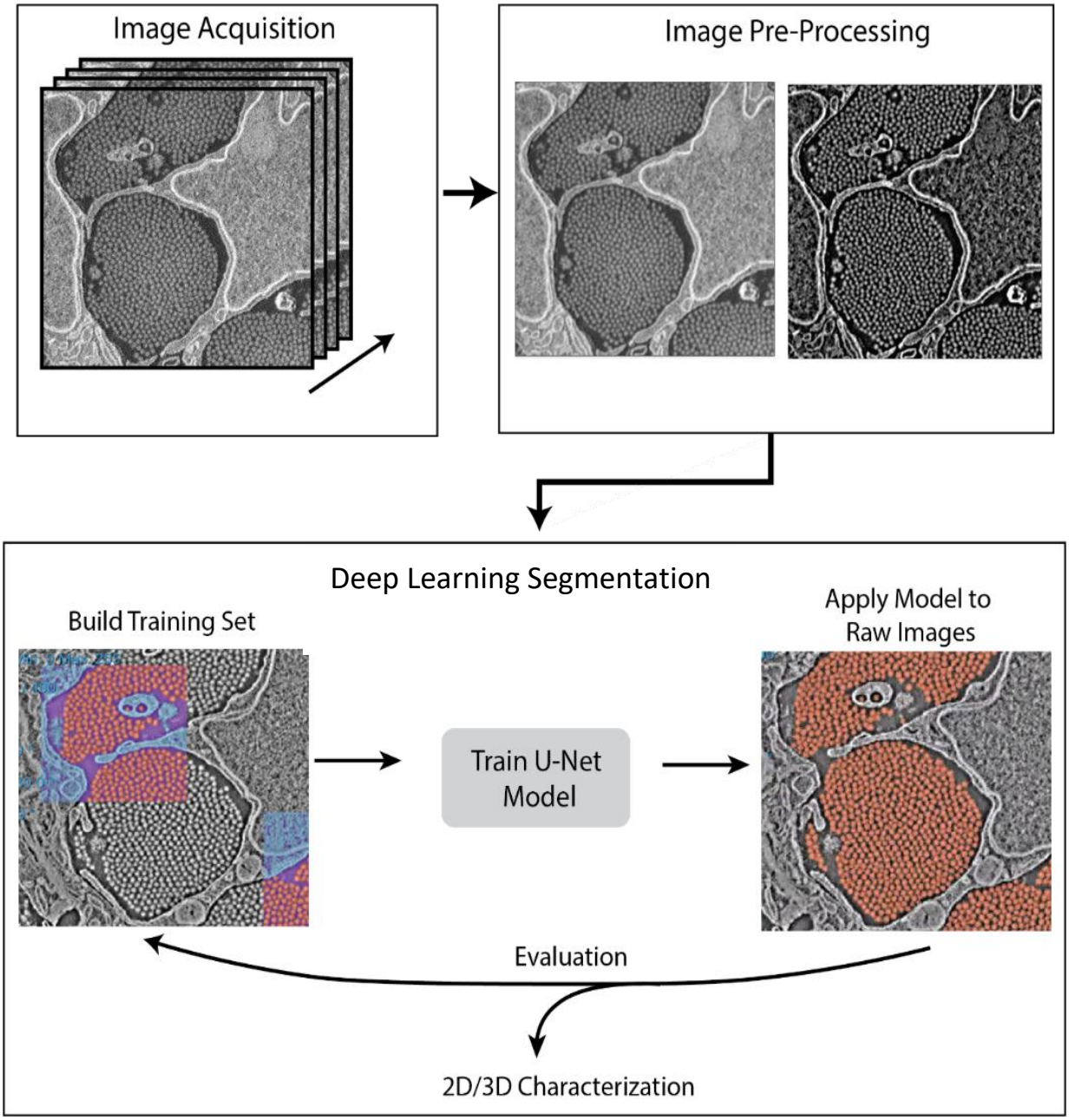

Figure 5.2: General outline of processing pipeline for automated segmentation.

Manual Training Set Generation

Manually segmented regions of interest (ROIs) are required to train the Deep Learning U-Net for automated segmentation. The U-Net convolution architecture requires relatively small amounts of training data (< 1-2%), as multiple comparisons across the various convolution levels amplifies the input training data. However, the final model accuracy is highly dependent on the image quality, contrast, and consistency of the data set [16, 17]. Furthermore, U-Net models progressively evolve over time with the continuous addition of training data. This enables the accuracy of the model to improve over time but is highly dependent on consistency of the input data. As such, models were individually trained for each specific developmental group to account for slight variability in image/stain quality across each condition of interest.

All training sets were manually segmented using Dragonfly (Version 2022.1, Object Research Systems, Montreal, Canada). Briefly, individual ROI “patches” were first identified within the image stack (**Fig. 5.3**). The size and number of training ROIs varied but aimed to accurately capture native variability within the data and provide sufficient examples of different ultrastructural morphology. Furthermore, this was conducted at various locations within the z-stack to capture potential variability through the bulk tissue. All objects within the training ROIs were segmented with a unique classification as background, cellular material, or collagen fibrils.

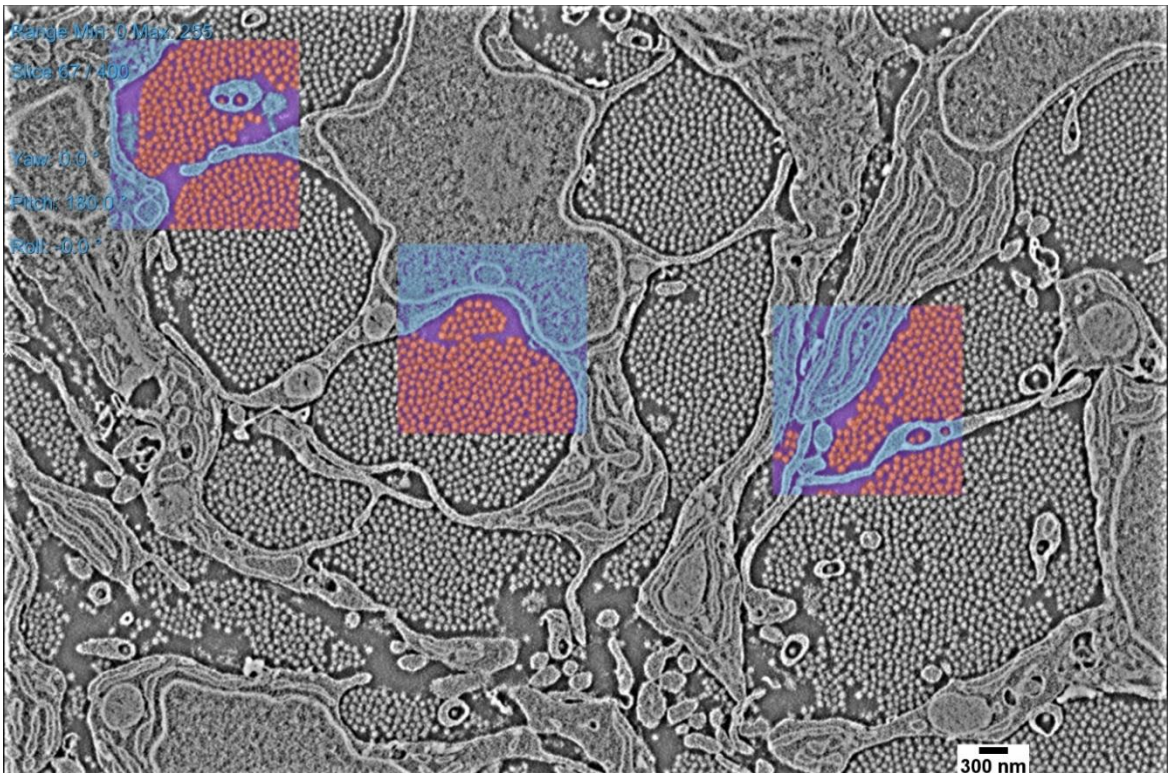

Figure 5.3: Example of manual segmentation for model training. Three distinct region of interest “patches” were selected above, attempting to capture examples of variable fibril and cellular morphologies. Cells (Blue), Fibrils (Red), and Background (Purple).

U-Net Training

In brief, the U-Net architecture describes a string of convolutional encoder-decoder networks [17]. The encoding path uses convolutions and spatial pooling to decompose the input image into a multiscale collection of features. The decoding path uses the resulting decomposed image to synthesize an output image by up-sampling and convolving the encoded features. The features segmented by the network are then validated against the manually trained dataset and an accuracy measurement is calculated. The model can be iteratively improved via data augmentation in an effort to minimize the loss function (i.e., maximize accuracy). More specifically, data augmentation describes the process in which the user artificially increases the amount of training data

by modifying pre-existing inputs. This includes modifying the size, angle, intensity, or noise of the training set, enabling the network to search for unique relationships between features to improve the predictive power. However, by increasing the number of simultaneous data augmentations the processing time can increase exponentially (e.g., 15 minutes to 20+ hour run time). While powerful, it's important to note that excessive data augmentation can be detrimental to model accuracy if your objects of interest are highly regular. Typically, increasing the size of the manual training set is a more effective way to improve the accuracy of the model.

Since its creation in 2015, numerous adaptations on the original U-Net design have emerged, tailored to specific image processing objectives. In this processing pipeline, a 2D and 2.5D U-Net will be utilized to identify features in both two and three dimensions [17]. All model development/training was conducted in Dragonfly (v2022.1, Object Research Systems, Montreal, Canada), utilizing the default neural networks architecture. For each condition, a 2D U-Net model was first trained to identify fibril objects within each slice. Additional training data was generated via data augmentation. More specifically, the data was allowed to be flipped horizontally/vertically, rotated, sheared (2^{o}), scaled (90 – 110%), and intensity modified (0.90 – 1.10). After training (~10 – 13hr) the model was applied to the entire data set and manually inspected to ensure accuracy of the segmented objects of interest. Additional training sets and/or data augmentations were incorporated into the model as needed. For the volumetric reconstruction of the E16 tissue, a 2.5D U-Net was trained to further improve model accuracy. In brief, the model looks for feature persistence in 2D and 3D (± 1 image stack), improving segmentation accuracy for structures with regular three-dimensional persistence.

For 2D characterization, binary masks are watershed to separate adjacent fibril objects. Images are then processed via the “Analyze Particles” (Fiji, size: 30nm – Infinity) to remove small non-fibril artifacts and quantify object diameters. The measurements were recorded, and diameter distribution plotted as a histogram. Furthermore, the total fibril area was calculated and divided by the entire field to get the relative fibril volume fraction as a function of development.

Volumetric reconstructions were conducted using Amira (Version 2019.3, Thermo Scientific, Waltham, MA) with the primary goal to identify terminated fibrils. Briefly, binary masks were put through distance and 3D anisotropic diffusion map to conduct a space-variant transformation of the original image, enabling continuous fibril detection in the event a fibril was temporarily missed during segmentation. Labels were generated using nearest neighbor clustering (neighborhood = 18), resulting in a label field of unique fibril IDs. Fibril structures were then filtered by their z-length, removing fibrils that exceeded 10 µm in length (i.e., persisted through the entire stack size). This enabled the investigation of fibrils which terminated within the given z-stack. Outputs were then visually examined to confirm fibril termination and determine the gross effectiveness of the volumetric labeling.

5.2.3 Statistics

All data is presented is as mean ± standard deviation. A one-way ANOVA with a Tukey’s post-test was conducted to evaluate differences in fibril diameter as a function maturation.

5.3 Results:

5.3.1 2D Ultrastructural Characterization

We demonstrated that deep learning neural networks were able to train models to automatically segment/identify with high accuracy (>95%) when validated with manually segmented training sets. With development, a progressive increase in fibril volume fraction was observed (**Fig. 5.4**). A look at individual fibril morphologies reveals an increase in mean fibril diameter ($p < 0.001$) with maturation (**Fig. 5.5**). Notably, both the E16 and E18 timepoint present a tight unimodal distribution of fibril diameters. However, at E20 the fibrils begin to present a bimodal distribution with a distinctive population of both small and large diameter fibrils.

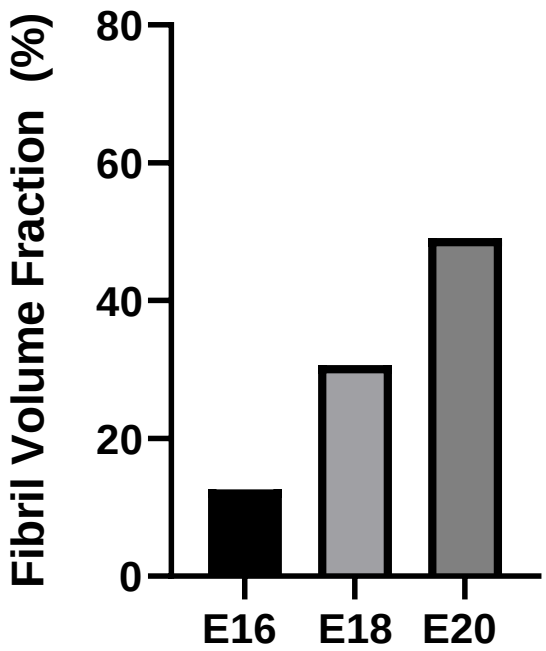

Figure 5.4: Fibril volume fraction as a function of maturation (n = 1).

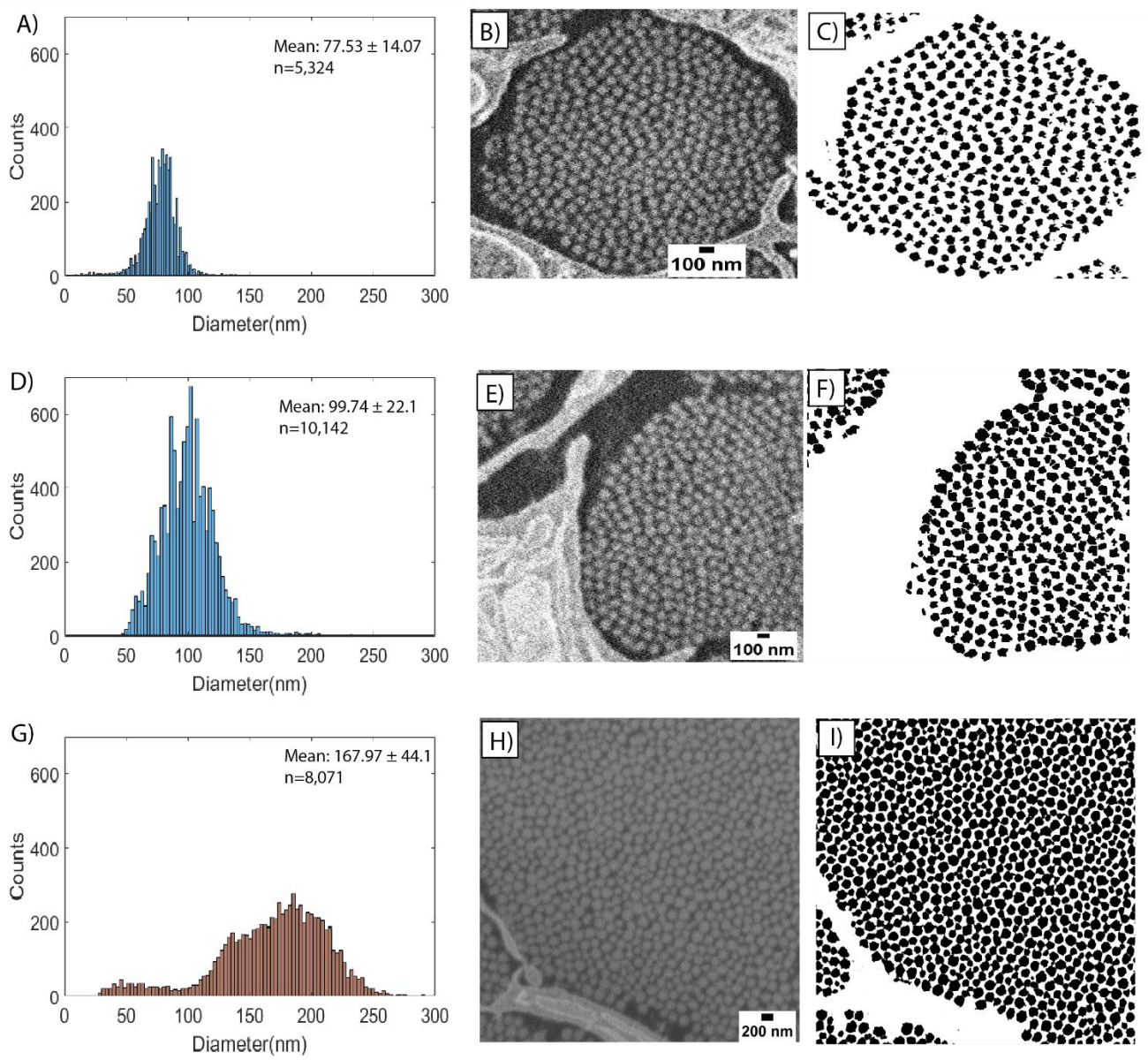

Figure 5.5: Collagen fibril diameter distributions (bins =100) as a function of development. **A)** E16 fibril diameter distribution (n = 5,324), with representative raw **B)** and **C)** masks generated via automatic segmentation. **D)** E18 fibril diameter distribution (n = 10,142), with representative raw **E)** and **F)** masks generated via automatic segmentation. **G)** E20 fibril diameter distribution (n = 8,071), with representative raw **H)** and **I)** masks generated via automatic segmentation.

5.3.2 3D Volumetric Reconstructions & Fiber Tracking

Volumetric reconstructions using Amira (Version 2019.3, Thermo Scientific, Waltham, MA) aimed to develop a method to accurately extract fibril objects and identify distinct fibril ends. The E16 timepoint was utilized as a pilot dataset to test the processing pipeline. Following segmentation, we demonstrated the capacity to identify, measure, and track individual fibril structures (**Fig. 5.6**). However, current reconstruction parameters struggled to accurately track highly mobile fibril units (**Fig. 5.6B**, Red arrow), resulting in a series of small, truncated fibril units. More specifically, fibers which had large translations in the x-y direction were difficult to uniquely differentiate through subsequent z-stacks. After filtering by z-length, over 2000 unique objects <10 µm were isolated and exceed what could be realistically manually validated (**Fig.5.6C**). Alterations in diffusion/anisotropic mapping increased the continuity of motile structures but typically resulted in fusion of adjacent fibril structures (data not shown).

Manual segmentation has shown that distinctive fibril ends do exist within the E16 samples (**Fig. 5.7**). However automated methods struggle to definitively distinguish fibril tips when in close contact with adjacent fibrils (**Fig. 5.7B-E**). Additional tools and/or manual validation is required to conclusively identify fibril ends within densely packed 3D data sets.

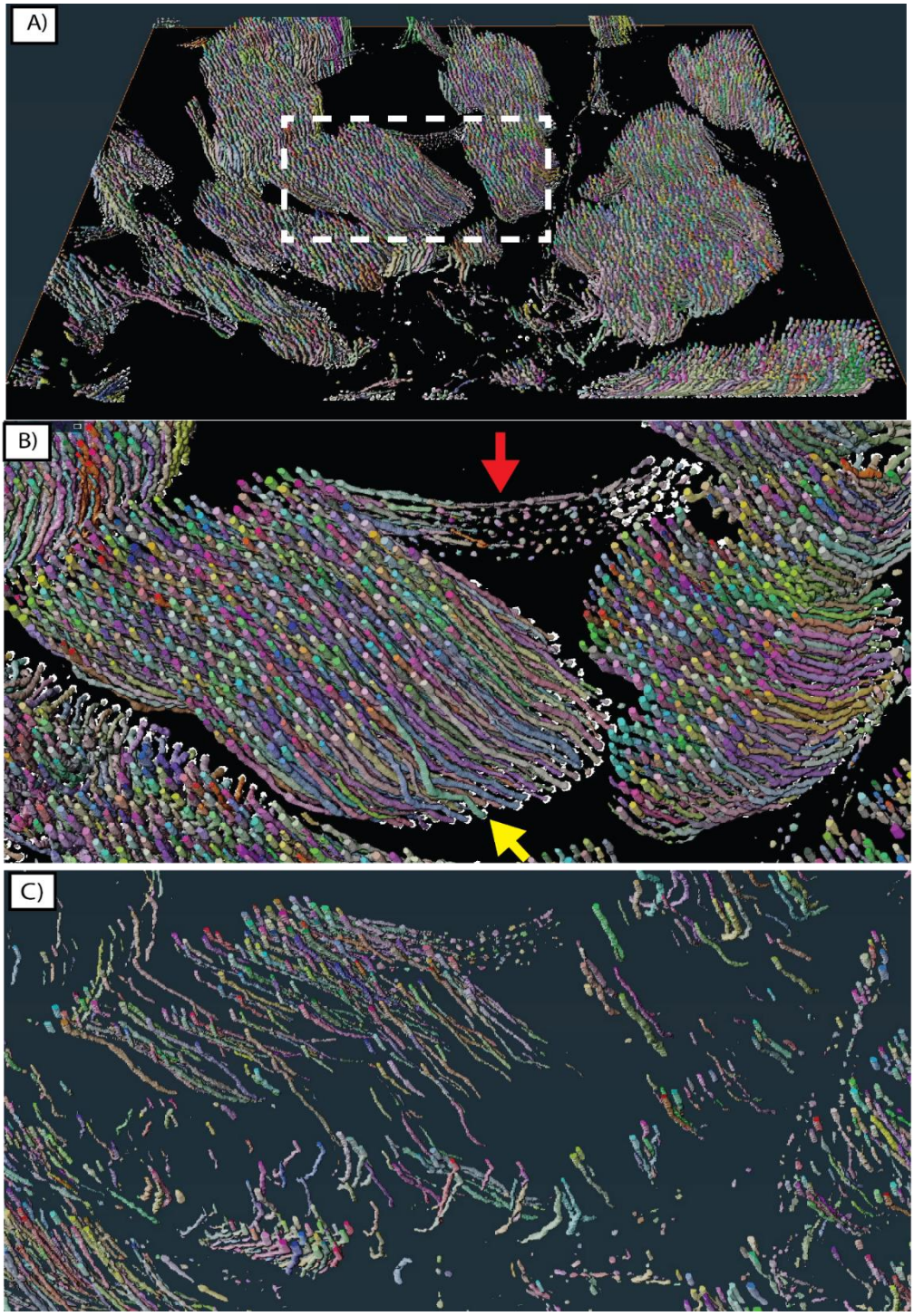

Figure 5.6: Volumetric rendering of E16 fibril network (200 stacks, 10 um). A) Full field and B) zoomed view of the fibril population following labeling. Unique fibril IDs represented by distinctive colors. Red arrow indicates highly motile region that was poorly tracked. Yellow arrow indicating a well tracked fibril structure. C) Representative region of interest after all structure greater than 10 µm were filtered out.

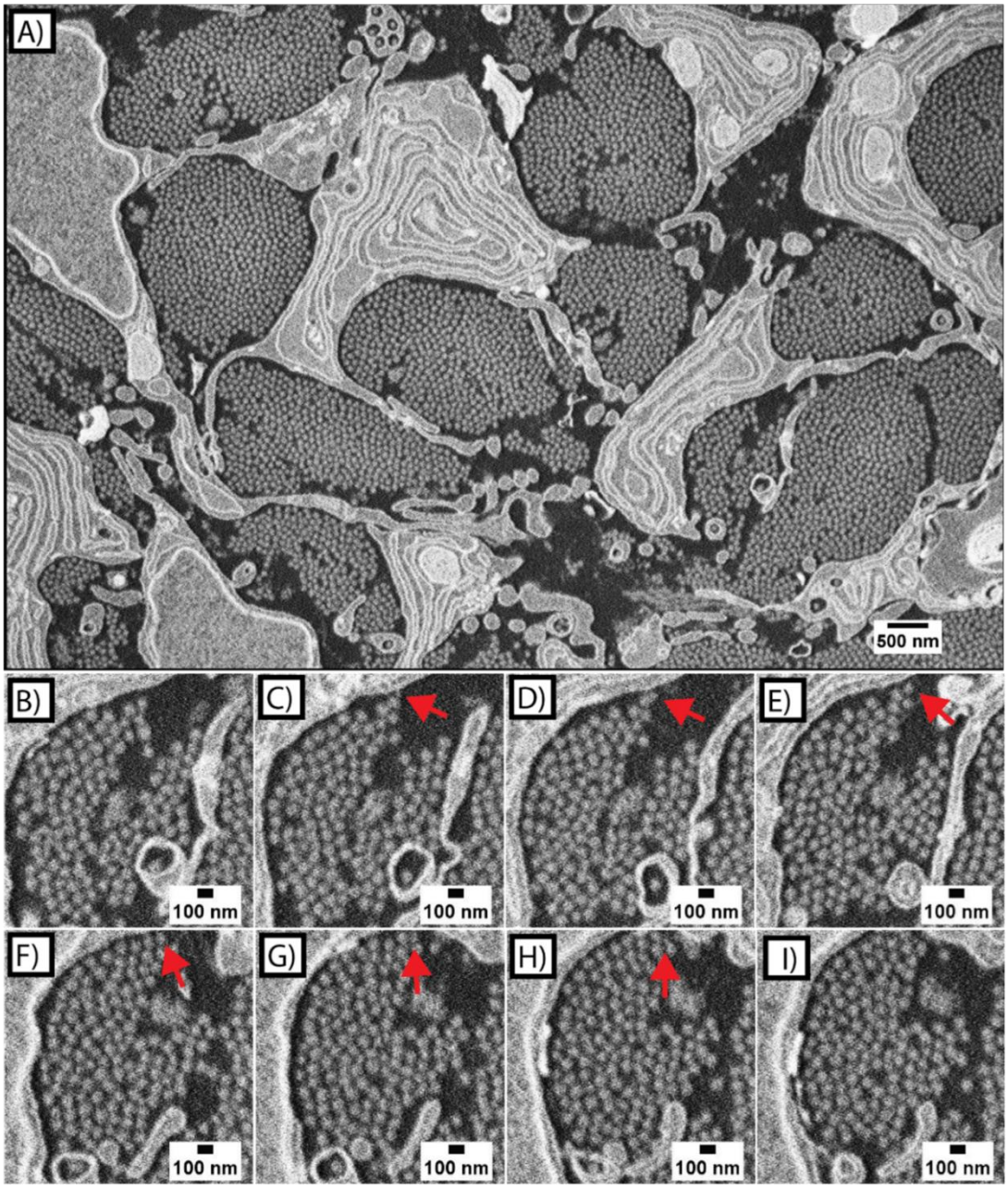

Figure 5.7: Example of fibrils coming into and leaving the imaging plane. **A)** Full field of view for E16 tendon. **B – E)** Fibril end coming into imaging plane as indicated by the red arrows. **F – I)** Example of a fibril terminating as indicated by the red arrows.

5.4 Discussion

During embryonic tendon development, there are a series of dynamic changes within the collagenous environment that drive the functional loading capabilities of the maturing tendon [3, 5, 10]. To study this, advanced electron microscopy tools are required to accurately investigate changes within collagenous ultrastructure. Conventional SEM/TEM cross-sectional imaging has provided useful insights into the progressive changes that occur within tendon during development [7, 19]. However, these tools are limited due to their reliance on manual segmentation and their inability to capture the three-dimensional nature of the collagenous ultrastructure. To address these challenges, we aimed to develop a processing pipeline for serial block-face images, integrating a deep learning neural network to automate fibril segmentation and minimize user labor. In particular, we aimed to quantify changes within 2D (diameters and fibril volume fraction) and 3D (fibril lengths) characteristics during development.

Utilizing a deep learning neural networks (U-Net) we've demonstrated the capability to accurately identify collagen fibril structures with an accuracy of 95% or greater, even in more densely packed collagenous environments (E20). However, it's important to note that model accuracy was evaluated by comparing model predictions with the manually segmented training data. While training ROIs were selected to be representative of the bulk data sets, model accuracy measurements are highly sensitive to the quality and quantity of in-put data. While not strictly regulated, the quantity and representative nature of the training ROIs tried to be consistent across all data sets.

Notably, fibril identification at E20 required an improvement in the imaging resolution (2nm/px) in comparison to the E16 and E18 timepoints (4nm/px) (data not shown). This resulted in a reduction in the field of view from ~12 µm x 8 µm (E16/18) to ~ 8 µm x 8 µm (E20). Despite this reduction, the increase in fibril volume fraction with maturation (**Fig. 5.4**) enabled fibril counts to stay above 5000. Furthermore, this relative change in fibril volume fraction with maturation is consistent with prior trends in literature [9]. While the change in imaging resolution may cause small discrepancies in measurement precision, we're confident that more distinctive contrast observed in the E16 & E18 samples still enables accurate fibril diameter measurements despite the change in imaging resolution. Importantly, we demonstrated the capacity to measure 5 – 10 times more objects than in prior studies [3, 5, 12] by deep learning strategies, improving our measurement of system heterogeneity and minimizing human bias.

Quantification of the fibril diameter showed a progressive increase in fibril cross-section with maturation, consistent with prior work in developing/neonatal mice [5]. These findings are consistent with an increase in lateral fibril fusion, driving an increase in diameter. This conclusion is consistent with prior studies which has shown a significant reduction in decorin, a SLRP that impairs lateral fibril interactions, during the E16 – E20 timepoints [3]. Future work could probe lateral fibril fusion behavior more closely to evaluate how fibril counts vary during fusion behavior. Notably, all samples presented a unimodal distribution, characteristic of developing tendons [3]. However, there appears to be a small increase in small-diameter fibrils at the E20 timepoint, suggestive of a shift towards a bimodal distribution and consistent with observations in neonatal mice [5]. The increase in small diameter fibril populations has additionally been implicated in

interfibrillar load transmission [11], potentially contributing to the increase in fibril:tissue strain ratio at E20 previously reported in Chapter 3.

The primary goal of the volumetric reconstruction was to track and identify distinctive fibril ends to allow for estimates of in vivo fibril lengths. Indeed, examples of fibrils appearing and terminating within the E16 image stacks can be manually identified (**Fig. 5.7**). Despite this, the current processing pipeline has demonstrated mixed results and struggle to isolate out these events. More specifically, while generally accurate, manual validation has indicated that automatic segmentation methods struggles to differentiate fibrils that encounter the cell membrane, compromising the continuity of the object through the imaging stack. To account for this, we utilized a combination of distance maps and 3D anisotropic diffusion maps to interpolate through these areas of interest. While these approaches aided in restoring fibril continuity, it was insufficient to capture highly motile fibril that drastically shift between stacks. This resulted in numerous small-length fibril structures to litter the image (**Fig. 5.6**, red arrow) which were difficult to differentiate from truly terminated fibrils (**Fig. 5.7**). Furthermore, if the diffusion parameters are too lax adjacent fibrils may fuse together to create larger collagenous aggregates. Attempts to extract truncated fibrils by their relative angle, volume, or length is possible but risks removing our primary objects of interest and poses a critical challenge.

Current on-going work is attempting to enhance confidence in our volumetric reconstructions and fibril tracking. Initial attempts focused on decreasing the slice thickness (50 nm to 40 nm). However, a reduction in slice thickness resulted in an increase in imaging distortion due to poor cutting and overcharging of the resin surface. Subsequent efforts have focused on improving the imaging resolution (4 nm/px to 2

nm/px) in aid in fibril identification. This has proven to aid imaging quality in E20 data sets (**Fig. 5.5H**) and future work aims to apply it to the E16 data sets for volumetric reconstructions. Improving the imaging resolution any further (1 nm/px) has proven to be ineffective, as it increased charge dispersions on the surface and decreased overall image quality.

We aim to couple improvements in imaging quality with more enhanced neural network models. More specifically, the current U-Net model for the volumetric reconstruction utilized a 2D and 2.5D U-Net, enabling feature detection in both dimensions [17]. The goal was to improve fibril detection by leveraging its persistent cylindrical geometry through the image stack and distinguish it from cellular features. However, the 2.5D U-Net only registers objects ± 1 stack, weakly accounting for persistent features in the z-direction. Future work aims to leverage a full 3D U-Net [18] to further improve U-Net detection for fibrils and enhance the volumetric reconstructions of fibril structures to validate prior hypotheses.

5.6 References

1. Herod TW, Chambers NC, Veres SP (2016) Collagen fibrils in functionally distinct tendons have differing structural responses to tendon rupture and fatigue loading. Acta Biomaterialia 42:296–307. https://doi.org/10.1016/j.actbio.2016.06.017

2. Quigley AS, Bancelin S, Deska-Gauthier D, et al (2018) In tendons, differing physiological requirements lead to functionally distinct nanostructures. Sci Rep 8:4409. https://doi.org/10.1038/s41598-018-22741-8

3. McBride DJ, Trelstad RL, Silver FH (1988) Structural and mechanical assessment of developing chick tendon. International Journal of Biological Macromolecules 10:194–200. https://doi.org/10.1016/0141-8130(88)90048-7

4. Chen S, Birk DE (2013) The regulatory roles of small leucine-rich proteoglycans in extracellular matrix assembly. FEBS J 280:2120–2137. https://doi.org/10.1111/febs.12136

5. Kalson NS, Lu Y, Taylor SH, et al (2015) A structure-based extracellular matrix expansion mechanism of fibrous tissue growth. eLife 4:e05958. https://doi.org/10.7554/eLife.05958

6. Craig AS, Birtles MJ, Conway JF, Parry DAD (1989) An Estimate of the Mean Length of Collagen Fibrils in Rat Tail-Tendon as a Function of age. Connective Tissue Research 19:51–62. https://doi.org/10.3109/03008208909016814

7. Birk DE, Nurminskaya MV, Zycband EI (1995) Collagen fibrillogenesis in situ: Fibril segments undergo post-depositional modifications resulting in linear and lateral growth during matrix development. Dev Dyn 202:229–243. https://doi.org/10.1002/aja.1002020303

8. Watanabe T, Hosaka Y, Yamamoto E, et al (2005) Control of the Collagen Fibril Diameter in the Equine Superficial Digital Flexor Tendon in Horses by Decorin. Journal of Veterinary Medical Science 67:855–860. https://doi.org/10.1292/jvms.67.855

9. Goh KL, Holmes DF, Lu H-Y, et al (2008) Ageing Changes in the Tensile Properties of Tendons: Influence of Collagen Fibril Volume Fraction. Journal of Biomechanical Engineering 130:. https://doi.org/10.1115/1.2898732

10. Birk DE, Zycband EI, Winkelmann DA, Trelstad RL (1989) Collagen fibrillogenesis in situ: fibril segments are intermediates in matrix assembly. Proceedings of the National Academy of Sciences 86:4549–4553. https://doi.org/10.1073/pnas.86.12.4549

11. Szczesny SE, Fetchko KL, Dodge GR, Elliott DM (2017) Evidence that interfibrillar load transfer in tendon is supported by small diameter fibrils and not extrafibrillar tissue components: INTERFIBRILLAR LOAD TRANSFER IN TENDON. J Orthop Res 35:2127–2134. https://doi.org/10.1002/jor.23517

12. Svensson RB, Herchenhan A, Starborg T, et al (2017) Evidence of structurally continuous collagen fibrils in tendons. Acta Biomaterialia 50:293–301. https://doi.org/10.1016/j.actbio.2017.01.006

13. Starborg T, Kalson NS, Lu Y, et al (2013) Using transmission electron microscopy and 3View to determine collagen fibril size and three-dimensional organization. Nat Protoc 8:1433–1448. https://doi.org/10.1038/nprot.2013.086

14. Holmes DF, Lu Y, Starborg T, Kadler KE (2018) Collagen Fibril Assembly and Function. In: Current Topics in Developmental Biology. Elsevier, pp 107–142

15. Canty EG, Lu Y, Meadows RS, et al (2004) Coalignment of plasma membrane channels and protrusions (fibripositors) specifies the parallelism of tendon. Journal of Cell Biology 165:553–563. https://doi.org/10.1083/jcb.200312071

16. Hua Y, Laserstein P, Helmstaedter M (2015) Large-volume en-bloc staining for electron microscopy-based connectomics. Nat Commun 6:7923. https://doi.org/10.1038/ncomms8923

17. Ronneberger O, Fischer P, Brox T (2015) U-Net: Convolutional Networks for Biomedical Image Segmentation. In: Navab N, Hornegger J, Wells WM, Frangi AF (eds) Medical Image Computing and Computer-Assisted Intervention – MICCAI 2015. Springer International Publishing, Cham, pp 234–241

18. Huang H, Lin L, Tong R, et al (2020) UNet 3+: A Full-Scale Connected UNet for Medical Image Segmentation. In: ICASSP 2020 - 2020 IEEE International Conference on Acoustics, Speech and Signal Processing (ICASSP). pp 1055–1059

19. Zhang G, Young BB, Ezura Y, et al (2005) Development of tendon structure and function: Regulation of collagen fibrillogenesis. J Musculoskelet Neuronal Interact 5:5–21

Chapter 6: Conclusions & Future Work

6.1 Conclusions

Tendon and ligament injuries account for roughly 25% of all musculoskeletal injuries [1, 2], making it one of the leading causes of disability in the United States [3]. These concerns are compounded by tendon's poor innate healing capacity and the limited efficacy of clinical interventions. Scaffold-free tissue engineering tendon constructs have emerged as a promising alternative to current regenerative strategies, mimicking developmental conditions to create tendon tissue in an in vitro environment [4, 5]. While these constructs successfully replicate the structure-function relationships in early stages of tendon development, they fail to reach full maturity and acquire load-bearing capabilities. The reason for this failed maturation is not clear, as the dynamic variables required to recapitulate the formation of functional tendon tissue are still largely unknown and represents a critical gap in knowledge.

Prior work has suggested that changes in collagen fibril lengths may mediate the transformation in the developing tendon [6]. However, no study has directly examined how progressive changes in fibril length contribute to the multiscale loading capabilities during tendon development. Recent findings have further suggested that muscle activity (e.g., kicking) is essential to the transformation in tendon's structure-function capabilities and may impact crosslinking activity [4, 7, 8]. Indeed, immobilized embryos have demonstrated a reduction in compressive modulus and collagenous crosslinking[8]. However, no study has directly reported how developmental paralysis effects the maturation in tensile multiscale mechanical properties. Collectively, there is a severe lack

of understanding concerning the multiscale loading environment during late stages of tendon development. Establishing these fundamental structure-function relationships throughout tenogenesis is essential to elucidating the mechanisms that govern the formation of load-bearing tendons.

As such, the primary objective of this dissertation was to evaluate how changes within the collagenous ultrastructure contribute to the multiscale loading capabilities during late stages of tendon development. To evaluate this, we first needed to establish how the multiscale mechanical response is influenced by changes in collagen fibril continuity. In Chapter 2, we demonstrated that we could increase the multiscale mechanical loading behavior in rat tail tendons by inducing continuity within the fibril network with short gauge-length testing conditions. In doing so, we estimated that rat tail tendons have fibril lengths between 5 and 10mm. These findings are consistent with prior findings in literature [9, 10] and establish how relative changes in fibril continuity can be examined via multiscale mechanical testing. We further validated our mechanical testing apparatus for small tissue biomechanical testing, enabling subsequent studies in developmental tendons.

In Chapter 3, we aimed to evaluate how the tendon multiscale mechanical behavior changes as a function of maturation and investigate its sensitivity to musculoskeletal activity. We demonstrated that there is a significant increase in the macroscale mechanics and fibril loading behavior during late-stages of tendon development. These results were indicative of an increase in interfibrillar load transmission and a reduction in interfibrillar sliding within the collagenous matrix [11–13], consistent with an increase in fibril lengths. This structure-function transformation was shown to occur between the embryonic days

16 & 18, in agreement with prior literature estimates[6, 14]. Subsequent work aimed to investigate how this maturation in biomechanical capabilities is dependent on muscle activity utilizing a combination of rigid (DMB) and flaccid (PB) paralysis models. We demonstrated that both drug treatments significantly (and equally) impaired embryonic mobility *in ovo*. Following paralysis, the macroscale mechanical capabilities of the tissues were significantly reduced, clearly establishing the role of muscle activity in the functional development of tendon. Multiscale mechanical testing further revealed that both forms of immobilization significantly impaired the fibril loading of the tissue. These findings are consistent with a reduction in interfibrillar loading capabilities and an impairment in fibril lengthening events during development. However, prior work postulated that changes in collagenous crosslinking may be contributing to the multiscale mechanical capabilities acquired during development [15, 16] and be sensitive to musculoskeletal activity [8]. Additional work needed to be conducted to evaluate the role of crosslinking during late-stages of tendon development. Nevertheless, this study provides valuable insight into the multiscale structure-function relationships of developing tendons and the importance of mechanical stimulation in producing a robust tensile load-bearing soft tissue

In Chapter 4, we aimed to investigate how collagenous crosslinks contribute to the development of tendon multiscale mechanical behavior and its sensitivity to musculoskeletal activity. Utilizing a LOX inhibitor (BAPN) we showed that crosslink maturation has a critical role in the developmental of the biomechanical capabilities. More specifically, we showed crosslink inhibition significantly reduced the macroscale and multiscale mechanical capabilities of the tissue. Interestingly, the absence of crosslinking significantly decreased interfibrillar loading, contradicting prior work in mature tendon

systems [17]. In vitro culture systems have suggested that fibril assembly may be perturbed following BAPN treatment [18, 19], potentially contributing to the impaired micro and macroscale mechanical behavior observed. Interestingly, these finding implicate that crosslinking may play an important role in tendon development as both a mechanical element and a molecular regulator of fibrillogenesis, however additional work is needed to investigate these hypotheses.

We further demonstrated that muscle immobilization presents a thermodynamic response distinctive from standard development and BAPN treated tissues. More precisely, immobilized tissues presented an initial elevation in denaturation temperature consistent with crosslink formation during fibrillogenesis. Enthalpy and acid solubility measurements do indicate some retardation in relative crosslinking; however the effects appear minor relative to the severity of the phenotype. Further shift towards higher denaturation behavior may indicate that downstream crosslinking may have been impaired. However, current data suggests that an impaired fibril fusion response is more likely and would be consistent the multiscale mechanical behavior exhibited in Chapter 3. Nonetheless, additional work is required to evaluate crosslinking populations and their effects more conclusively on the fibril ultrastructure.

Finally, in Chapter 5 we outlined on-going work with serial block-face scanning electron microcopy (SBF-SEM) to directly characterize the three-dimensional collagenous ultrastructure during development in an effort to validate findings outlined in Chapters 3 & 4. Notably, we investigated the use of deep learning neural networks to automatic segmentation of the collagen fibrils [20]. These tools enable volumetric reconstruction of the collagen network without excessive manual segmentation and

minimizes user bias. We've demonstrated that our neural network models can identify fibrils with a 95 – 99% accuracy at our E16, E18, and E20 timepoints, despite progressive changes in collagen packing density. Utilizing trained neural networks, we were able to automatically segment 5000 – 10,000+ fibrils, increasing sampling sizes 5 - 10x in comparison to prior studies that rely on manual object segmentation. Notably, we showed a progressive increase in collagen fibril diameter with maturation, indicative of a fibril fusion events.

Subsequent work aimed to develop a pipeline for 3D reconstructions of the collagenous ultrastructure to quantify fibril properties in vivo. More specifically, we aimed to conclusively identify distinctive fibril ends to enable a probabilistic analysis of fibril lengths in vivo. Unfortunately, while we've developed a robust pipeline for the volumetric reconstruction, current strategies struggle to accurately track fibrils which are highly mobile or make excessive contact with the cell plasma membrane. These events appear as terminated fibrils within the reconstruction and exceed what can be manually validated (2000+). On-going work is focused on enhancing the raw data and neural networks to improve tracking capabilities and provide more conclusive insight into the 3D ultrastructural changes mediate the functional capabilities of developmental tissues.

6.2 Future Work:

While this work has provided critical insights into understanding the structure-function relationships in developing tendon, there are several studies that could extend its significance and impact in the field. Primary amongst these is finalizing the volumetric fibril tracking capabilities in our SBF-SEM images. Initial pilot work has demonstrated the potential of neural networks to automate the segmentation of fibrils within large volumetric data sets [20]. Indeed, current strategies are capable of accurately extracting collagen fibrils within E16 chick tendons with high accuracy. However, numerous challenges still need to be overcome to extract meaningful volumetric data.

First, we need to establish a more robust pipeline for volumetric fibril tracking. While we demonstrated impressively accurate fibril segmentation, the neural network still struggles in consistently identifying fibrils in contact with the plasma membrane. To address this, improvements are being made across the entire processing pipeline. Recent imaging trials have demonstrated that our imaging resolution (4nm/px) can be doubled (2nm/px) without excessive charge accumulation on the sample, vastly improving image clarity. These improvements aim to be coupled with more advanced 3D U-Net neural networks. In contrast to 2D and 2.5D U-Net networks outlined in Chapter 5, a full 3D U-Net identifies persistent features in all directions throughout multiple stacks[20, 21]. While more computationally intensive, this should vastly improve the tracking and identification of column-like fibril structures, which present highly distinguishable 3D features. Furthermore, this network should be more robust and address prior concern with fibril track at the cell membrane. In the event this is insufficient, we're currently collaborating with Dr. Jeff Caplan, Director of the BioImaging Center at the University of Delaware.

Recent work by Dr. Caplan and his team demonstrated the capability to isolate fibrils from SBF-SEM images of plantaris tendons in mature rats, which are larger and more densely packed. If their networks are accessible, we should be able to improve our segmentation and tracking capabilities.

Utilizing these improvements, we aim to get a direct estimate of in vivo fibril lengths. However, in vivo fibril length (~120 µm – 13 mm) [6, 9, 10] greatly exceed the z-depth that can be reasonably collected by the SBF-SEM (~20 – 30 µm). Prior work by Starborg et al., has demonstrated that that measurements of fibril ends be used in a probabilistic estimate to calculate fibril lengths [21]. However, due to the small probability of identifying a fibril end, this approach requires a high quantity of fibril to be tracked (i.e., 10,000 +). While daunting for manually segmented data sets, this approach is highly accessible using our automated neural networks approach. With these estimates, we aim to validate how fibril lengths change as a function of maturation and its sensitivity to musculoskeletal immobilization.

Subsequent work aims to integrate these system measurements to model the multiscale mechanical capabilities of developmental tendons. More precisely, prior findings by Szczesny et al., [11, 12] demonstrated that shear lag modeling is uniquely capable of fitting the macroscale tendon mechanics and predict fibril deformation behavior in vivo. However, the shear-lag model requires numerous material parameters [12], such as fibril volume fraction, fibril radius, length, and modulus, which are dynamically changing during development [6, 14, 23]. By coupling our SBF-SEM ultrastructural imaging with the previously developed shear-lag model, future work aims to identify key structural elements that facilitate the transformation in load-bearing capabilities observed

during tenogenesis. These findings will aid in establishing key structure-function benchmarks required for tissue engineered tendon constructs and regenerative medicine strategies that aim to restore load-bearing capabilities.

Outside of the immediate project aims, our findings provided key insight into several other mechanisms, notably the role crosslinking during fibrillogenesis. While the formation of enzymatic crosslinks is understood to contribute to the mechanical capabilities of tendon [15, 16, 24], little is known about their role in mediating fibril formation/assembly. Indeed, in vitro work suggests that decorin co-localizes with LOX to enhance crosslink formation and fibril fusion behavior [25]. More specifically, when decorin is added to decorin-deficient fibroblast there is an increase in crosslink formation and average fibril diameter [25], despite decorin's classification as an inhibitor of lateral fibril interactions[26–29]. These findings present interesting questions regarding the crosstalk between enzymatic crosslinkers and the ECM proteoglycans, such as…

1) How does variable spatial/temporal distribution of decorin influence crosslinking capabilities & fibril fusion behavior in vivo.
2) Does this co-localization include other SLRPS (i.e., biglycan)?
3) How does tendon-specific crosslinking capabilities alter LOX - decorin co-localization? Does this contribute to the unique fibril diameter distributions seen across energy-storing & positional tendons?
4) Does co-localization vary between LOX and LOX-L isoforms?
5) Does LOX co-localization stabilize decorin's presence over time and aid in fibril stabilization?

These questions have interesting implications in how tissue-specific structural relationships are established during tendon development. Furthermore, the presence of SLRPs is known to vary with maturation throughout adolescence and adulthood [30–34]. Suggesting that LOX-SLRP interactions may have critical implications the long-term homeostatic relationship of tendons. Indeed, this relationship may explain why LOX inhibition in adult rats presented such drastic impairments in their multiscale loading capabilities [17], despite having an established (and crosslinked) fibril network. More specifically, LOX inhibition may have impaired the fibrillogenesis of new small-diameter fibrils, which are progressively deposited during homeostatic remodeling [35]. Thus, resulting in the progressive loss in small-diameter fibrils over time [26, 36], impairing interfibrillar load-transfer capabilities mediated by small-diameter fibrils [21, 22]. However, additional work is required to investigate these relationships more thoroughly.

There is additionally interesting potential in expanding our findings to other animal models. While prior work has shown that similar events occur within other animal models (i.e., mice) [38], the timescale in which they occur are not well understood. More specifically, our findings indicate that this structural transformation in chick embryos occurs over 1-2 days, between E16 – E18. If the temporal sensitive of this transformation is retained in other models, it could provide interesting insights into the biological inputs that are instigating these changes. Furthermore, if these observations can be confirmed in mice, it may allow more sophisticated studies with the use of more widely available transgenic animals. Conducting multiscale mechanical testing of mice is highly difficult due to their small size and motivated our use of chick embryos. However, recent advancements in tensile equipment have demonstrated enhanced testing capabilities for

small samples as small as 2mm, enabling future work conducting advanced mechanical testing in developing mice [39] .

Similarly, it could be interesting to expand to other chick tendons. In the presented studiies work, we utilized the flexor digitorium long/brevis digit II tendons across all tests in an effort to reduce cross-sample variability. However, it's unclear if this structure-function transformation is constant across all tendons in the chick. Within vertebrate models, tendons can be broadly identified according to their embryonic origins as either craniofacial, axial, or limb tendons. Where craniofacial tendons are derived from the neural crest [40], axial tendons from the somites [41], and limb tendons from the limb lateral plate [42]. Interestingly, despite achieving the same functional end-product, these tendon groups have variable dependence on the co-development of skeletal muscle [43]. More specifically, axial tendons fail to initiate Scx expression (a robust marker for tendon identify) in the absence of muscle during early stages of development [44]. In contrast, craniofacial and limb tendons have unperturbed Scx expression during early stages [40, 45], but lose Scx expression at later developmental timepoints [46–48]. Suggesting that while muscle activity is required for the long-term retention of tendon identity, its role in early stages of tendon development is dependent on their embryonic origin. The exact biological mechanisms by which muscle modulates tendon induction and development is unclear but believed to be linked to the mechanical stimulation generated by muscle contractions. This variable behavior across tendons generates interesting questions regarding tendon-specific tissue fate. Future work is required to investigate these relationships but could generate critical implications into current regenerative medicine and tissue engineering tendon strategies.

6.3 References:

1. Badley EM, Tennant A (1993) Impact of disablement due to rheumatic disorders in a British population: estimates of severity and prevalence from the Calderdale Rheumatic Disablement Survey. Ann Rheum Dis 52:6–13. https://doi.org/10.1136/ard.52.1.6

2. Fleming DM, Cross KW, Barley MA (2005) Recent changes in the prevalence of diseases presenting for health care. Br J Gen Pract 7

3. NONFATAL OCCUPATIONAL INJURIES AND ILLNESSES REQUIRING DAYS AWAY FROM WORK, 2015. Bureau of Labor Statistics, U.S. Department of Labor

4. Kalson NS, Holmes DF, Herchenhan A, et al (2011) Slow stretching that mimics embryonic growth rate stimulates structural and mechanical development of tendon-like tissue in vitro. Dev Dyn 240:2520–2528. https://doi.org/10.1002/dvdy.22760

5. Kalson NS, Holmes DF, Kapacee Z, et al (2010) An experimental model for studying the biomechanics of embryonic tendon: Evidence that the development of mechanical properties depends on the actinomyosin machinery. Matrix Biol 29:678–689. https://doi.org/10.1016/j.matbio.2010.08.009

6. Birk DE, Zycband EI, Winkelmann DA, Trelstad RL (1989) Collagen fibrillogenesis in situ: fibril segments are intermediates in matrix assembly. Proc Natl Acad Sci 86:4549–4553. https://doi.org/10.1073/pnas.86.12.4549

7. Wu K-C, Streicher J, Lee ML, et al (2001) Role of motility in embryonic development I: Embryo movements and amnion contractions in the chick and the influence of illumination: Embryonic Motility of the Chick. J Exp Zool 291:186–194. https://doi.org/10.1002/jez.1068

8. Pan XS, Li J, Brown EB, Kuo CK (2018) Embryo movements regulate tendon mechanical property development. Philos Trans R Soc B Biol Sci 373:20170325. https://doi.org/10.1098/rstb.2017.0325

9. Craig AS, Birtles MJ, Conway JF, Parry DAD (1989) An Estimate of the Mean Length of Collagen Fibrils in Rat Tail-Tendon as a Function of age. Connect Tissue Res 19:51–62. https://doi.org/10.3109/03008208909016814

10. Provenzano PP, Vanderby R (2006) Collagen fibril morphology and organization: Implications for force transmission in ligament and tendon. Matrix Biol 25:71–84. https://doi.org/10.1016/j.matbio.2005.09.005

11. Szczesny SE, Elliott DM (2014) Interfibrillar shear stress is the loading mechanism of collagen fibrils in tendon. Acta Biomater 10:2582–2590. https://doi.org/10.1016/j.actbio.2014.01.032

12. Szczesny SE, Elliott DM (2014) Incorporating plasticity of the interfibrillar matrix in shear lag models is necessary to replicate the multiscale mechanics of tendon fascicles. J Mech Behav Biomed Mater 40:325–338. https://doi.org/10.1016/j.jmbbm.2014.09.005

13. Szczesny SE, Fetchko KL, Dodge GR, Elliott DM (2017) Evidence that interfibrillar load transfer in tendon is supported by small diameter fibrils and not extrafibrillar tissue

components: INTERFIBRILLAR LOAD TRANSFER IN TENDON. J Orthop Res 35:2127–2134. https://doi.org/10.1002/jor.23517

14. McBride DJ, Trelstad RL, Silver FH (1988) Structural and mechanical assessment of developing chick tendon. Int J Biol Macromol 10:194–200. https://doi.org/10.1016/0141-8130(88)90048-7

15. Eekhoff JD, Fang F, Lake SP (2018) Multiscale mechanical effects of native collagen cross-linking in tendon. Connect Tissue Res 59:410–422. https://doi.org/10.1080/03008207.2018.1449837

16. Marturano JE, Arena JD, Schiller ZA, et al (2013) Characterization of mechanical and biochemical properties of developing embryonic tendon. Proc Natl Acad Sci 110:6370–6375. https://doi.org/10.1073/pnas.1300135110

17. Puxkandl R, Zizak I, Paris O, et al (2002) Viscoelastic properties of collagen: synchrotron radiation investigations and structural model. Philos Trans R Soc Lond B Biol Sci 357:191–197. https://doi.org/10.1098/rstb.2001.1033

18. Herchenhan A, Uhlenbrock F, Eliasson P, et al (2015) Lysyl Oxidase Activity Is Required for Ordered Collagen Fibrillogenesis by Tendon Cells. J Biol Chem 290:16440–16450. https://doi.org/10.1074/jbc.M115.641670

19. Ellingson A, Pancheri N, Schiele N (2022) Regulators of collagen crosslinking in developing and adult tendons. Eur Cell Mater 43:130–152. https://doi.org/10.22203/eCM.v043a11

20. Ronneberger O, Fischer P, Brox T (2015) U-Net: Convolutional Networks for Biomedical Image Segmentation. In: Navab N, Hornegger J, Wells WM, Frangi AF (eds) Medical Image Computing and Computer-Assisted Intervention – MICCAI 2015. Springer International Publishing, Cham, pp 234–241

21. Huang H, Lin L, Tong R, et al (2020) UNet 3+: A Full-Scale Connected UNet for Medical Image Segmentation. In: ICASSP 2020 - 2020 IEEE International Conference on Acoustics, Speech and Signal Processing (ICASSP). pp 1055–1059

22. Starborg T, Kalson NS, Lu Y, et al (2013) Using transmission electron microscopy and 3View to determine collagen fibril size and three-dimensional organization. Nat Protoc 8:1433–1448. https://doi.org/10.1038/nprot.2013.086

23. Canty EG, Kadler KE (2005) Procollagen trafficking, processing and fibrillogenesis. J Cell Sci 118:1341–1353. https://doi.org/10.1242/jcs.01731

24. Snedeker JG, Gautieri A (2014) The role of collagen crosslinks in ageing and diabetes - the good, the bad, and the ugly. Muscles Ligaments Tendons J 4:303–308

25. Seidler DG, Schaefer L, Robenek H, et al (2005) A physiologic three-dimensional cell culture system to investigate the role of decorin in matrix organisation and cell survival. Biochem Biophys Res Commun 332:1162–1170. https://doi.org/10.1016/j.bbrc.2005.04.175

26. Robinson KA, Sun M, Barnum CE, et al (2017) Decorin and biglycan are necessary for maintaining collagen fibril structure, fiber realignment, and mechanical properties of mature tendons. Matrix Biol 64:81–93. https://doi.org/10.1016/j.matbio.2017.08.004

27. Corsi A, Xu T, Chen X-D, et al (2002) Phenotypic Effects of Biglycan Deficiency Are Linked to Collagen Fibril Abnormalities, Are Synergized by Decorin Deficiency, and Mimic Ehlers-Danlos-Like Changes in Bone and Other Connective Tissues. J Bone Miner Res 17:1180–1189. https://doi.org/10.1359/jbmr.2002.17.7.1180

28. Douglas T, Heinemann S, Bierbaum S, et al (2006) Fibrillogenesis of Collagen Types I, II, and III with Small Leucine-Rich Proteoglycans Decorin and Biglycan. Biomacromolecules 7:2388–2393. https://doi.org/10.1021/bm0603746

29. Dunkman AA, Buckley MR, Mienaltowski MJ, et al (2014) The Tendon Injury Response is Influenced by Decorin and Biglycan. Ann Biomed Eng 42:619–630. https://doi.org/10.1007/s10439-013-0915-2

30. Chen S, Birk DE (2013) The regulatory roles of small leucine-rich proteoglycans in extracellular matrix assembly. FEBS J 280:2120–2137. https://doi.org/10.1111/febs.12136

31. Rigozzi S, Müller R, Stemmer A, Snedeker JG (2013) Tendon glycosaminoglycan proteoglycan sidechains promote collagen fibril sliding—AFM observations at the nanoscale. J Biomech 46:813–818. https://doi.org/10.1016/j.jbiomech.2012.11.017

32. Scott JE, Orford CR, Hughes EW (1981) Proteoglycan-collagen arrangements in developing rat tail tendon. Biochem J 195:573–581

33. Iozzo RV, Murdoch AD (1996) Proteoglycans of the extracellular environment: clues from the gene and protein side offer novel perspectives in molecular diversity and function. FASEB J 10:598–614. https://doi.org/10.1096/fasebj.10.5.8621059

34. Kuo CK, Petersen BC, Tuan RS (2008) Spatiotemporal protein distribution of TGF-betas, their receptors, and extracellular matrix molecules during embryonic tendon development. Dev Dyn Off Publ Am Assoc Anat 237:1477–1489. https://doi.org/10.1002/dvdy.21547

35. Chang J, Garva R, Pickard A, et al (2020) Circadian control of the secretory pathway maintains collagen homeostasis. Nat Cell Biol 22:74–86. https://doi.org/10.1038/s41556-019-0441-z

36. Geng Y, McQuillan D, Roughley PJ (2006) SLRP interaction can protect collagen fibrils from cleavage by collagenases. Matrix Biol 25:484–491. https://doi.org/10.1016/j.matbio.2006.08.259

37. Peterson BE, Szczesny SE (2020) Dependence of tendon multiscale mechanics on sample gauge length is consistent with discontinuous collagen fibrils. Acta Biomater 117:302–309. https://doi.org/10.1016/j.actbio.2020.09.046

38. Kalson NS, Lu Y, Taylor SH, et al (2015) A structure-based extracellular matrix expansion mechanism of fibrous tissue growth. eLife 4:e05958. https://doi.org/10.7554/eLife.05958

39. Acuna A, Jimenez JM, Deneke N, et al (2021) Design and validation of a modular micro-robotic system for the mechanical characterization of soft tissues. Acta Biomater 134:466–476. https://doi.org/10.1016/j.actbio.2021.07.035

40. Chen JW, Galloway JL (2014) The development of zebrafish tendon and ligament progenitors. Development 141:2035–2045. https://doi.org/10.1242/dev.104067

41. Brent AE, Schweitzer R, Tabin CJ (2003) A Somitic Compartment of Tendon Progenitors. Cell 113:235–248. https://doi.org/10.1016/S0092-8674(03)00268-X

42. Kieny M, Chevallier A (1979) Autonomy of tendon development in the embryonic chick wing. Development 49:153–165. https://doi.org/10.1242/dev.49.1.153

43. Gaut L, Duprez D (2016) Tendon development and diseases. WIREs Dev Biol 5:5–23. https://doi.org/10.1002/wdev.201

44. Brent AE, Braun T, Tabin CJ (2005) Genetic analysis of interactions between the somitic muscle, cartilage and tendon cell lineages during mouse development. Development 132:515–528. https://doi.org/10.1242/dev.01605

45. Grenier J, Teillet M-A, Grifone R, et al (2009) Relationship between Neural Crest Cells and Cranial Mesoderm during Head Muscle Development. PLOS ONE 4:e4381. https://doi.org/10.1371/journal.pone.0004381

46. Schweitzer R, Chyung JH, Murtaugh LC, et al (2001) Analysis of the tendon cell fate using Scleraxis, a specific marker for tendons and ligaments. Development 128:3855–3866. https://doi.org/10.1242/dev.128.19.3855

47. Edom-Vovard F, Schuler B, Bonnin M-A, et al (2002) Fgf4 Positively Regulates scleraxis and Tenascin Expression in Chick Limb Tendons. Dev Biol 247:351–366. https://doi.org/10.1006/dbio.2002.0707

48. Edom-Vovard F, Duprez D (2004) Signals regulating tendon formation during chick embryonic development. Dev Dyn 229:449–457. https://doi.org/10.1002/dvdy.10481

Vita

Benjamin E. Peterson

Education

Pennsylvania State University, University Park, PA
Ph.D - Bioengineering Engineering — Dec. 2022

North Carolina State University (NCSU), Raleigh, NC
B.S Materials Science & Engineering – Biomaterials Concentration — May 2017
Minors: Biotechnology, Tissue Engineering

Peer-Reviewed Publications

Sep. 3rd, 2021	**Peterson, Benjamin E.,** Rebecca A. Rolfe, Allen Kunselman, Paula Murphy, and Spencer E. Szczesny. "Mechanical Stimulation via Muscle Activity Is Necessary for the Maturation of Tendon Multiscale Mechanics During Embryonic Development." Frontiers in cell and developmental biology (2021): 2471.2.
Sep. 30th, 2020	**Peterson, Benjamin E**., and Spencer E. Szczesny. "Dependence of Tendon Multiscale Mechanics on Sample Gauge Length is Consistent with Discontinuous Collagen Fibrils." Acta Biomaterialia (2020); **Publication**
April 17th, 2019	Abune, L., Zhao, N., Lai, J., **Peterson, B**., Szczesny, S., & Wang, Y. Macroporous hydrogels for stable sequestration and sustained release of vascular endothelial growth factor and basic fibroblast growth factor using nucleic acid aptamers. ACS biomaterials science & engineering, 5(5), 2382-2390 (2019); **Publication**
Oct.25th 2018	McGoorty, M. M., Singh, A., Deaton, T. A., **Peterson, B**., Taliaferro, C. M., Yingling, Y. G., & Castellano, F. N. (2018). Bathophenanthroline Disulfonate Ligand-Induced Self-Assembly of Ir (III) Complexes in Water: An Intriguing Class of Photoluminescent Soft Materials. ACS omega, 3(10), 14027-14038; **Publication**